AD-A105 995 TELEDYNE GEOTECH ALEXANDRIA VA SEISMIC DATA LAB F/G 17/10
AN INVESTIGATION OF ATTENUATION, SCATTERING AND SITE EFFECTS ON--ETC(U)
MAR 81 Z A DER, A O'DONNELL, P J KLOUDA F08606-79-C-0007
UNCLASSIFIED SDAC-TR-81-4 VSC-TR-81-11 NL

1 OF 2
AD A
105995

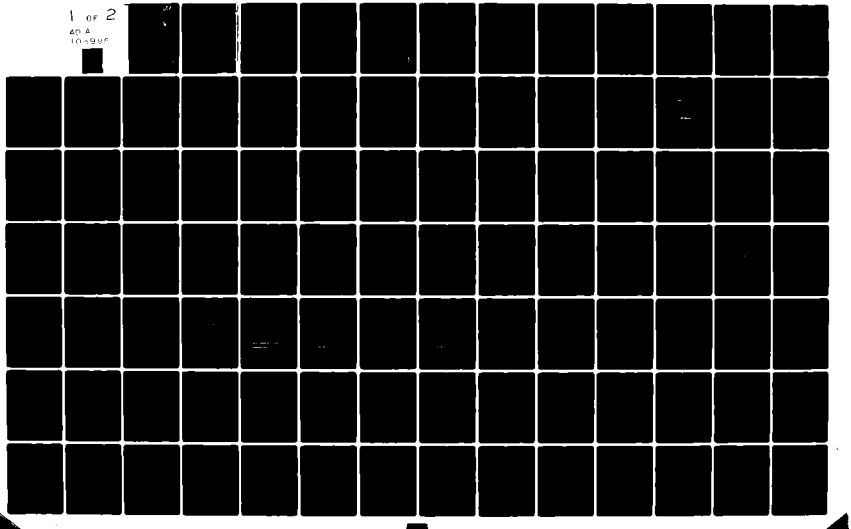

12

VSC-TR-81-11

AN INVESTIGATION OF ATTENUATION, SCATTERING AND SITE EFFECTS ON REGIONAL PHASES

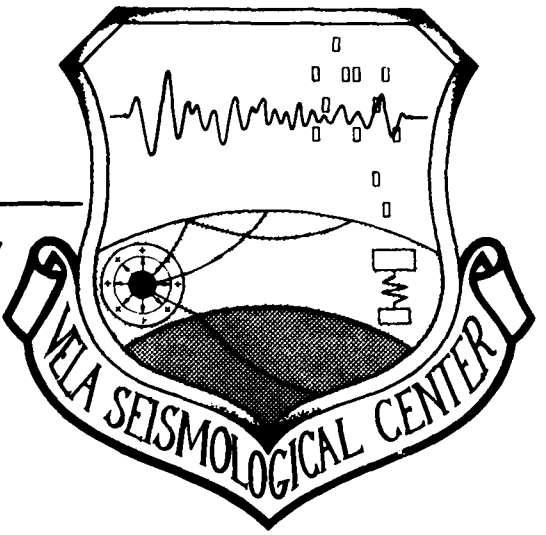

Z. A. Der, A. O'Donnell, P. J. Klouda
Seismic Data Analysis Center
Teledyne Geotech
314 Montgomery Street
Alexandria Virginia 22314

14 JULY 81

APPROVED FOR PUBLIC RELEASE; DISTRIBUTION UNLIMITED.

Monitored By:
VELA Seismological Center
312 Montgomery Street
Alexandria, VA 22314

Sponsored by

The Defense Advanced Research Projects Agency (DARPA)

DARPA Order No. 2551

Unclassified

SECURITY CLASSIFICATION OF THIS PAGE (When Data Entered)

REPORT DOCUMENTATION PAGE

READ INSTRUCTIONS BEFORE COMPLETING FORM

1. REPORT NUMBER: VSC-TR-81-11	2. GOVT ACCESSION NO.: AD-A105 995
3. RECIPIENT'S CATALOG NUMBER:	
4. TITLE (and Subtitle): AN INVESTIGATION OF ATTENUATION, SCATTERING AND SITE EFFECTS ON REGIONAL PHASES	5. TYPE OF REPORT & PERIOD COVERED: Technical
	6. PERFORMING ORG. REPORT NUMBER: SDAC-TR-81-4
7. AUTHOR(s): Zoltan A. Der, Anne O'Donnell, Pamela J. Klouda	8. CONTRACT OR GRANT NUMBER(s): F08606-79-C-0007
9. PERFORMING ORGANIZATION NAME AND ADDRESS: Teledyne Geotech, 314 Montgomery Street, Alexandria, Virginia 22314	10. PROGRAM ELEMENT, PROJECT, TASK AREA & WORK UNIT NUMBERS: VT/0709
11. CONTROLLING OFFICE NAME AND ADDRESS: Defense Advanced Research Projects Agency, 1400 Wilson Boulevard, Arlington, Virginia 22209	12. REPORT DATE: 23 Mar 1981
	13. NUMBER OF PAGES: 97
14. MONITORING AGENCY NAME & ADDRESS (if different from Controlling Office): VELA Seismological Center, 312 Montgomery Street, Alexandria, Virginia 22314	15. SECURITY CLASS. (of this report): Unclassified
	15a. DECLASSIFICATION/DOWNGRADING SCHEDULE

16. DISTRIBUTION STATEMENT (of this Report)

APPROVED FOR PUBLIC RELEASE; DISTRIBUTION UNLIMITED.

17. DISTRIBUTION STATEMENT (of the abstract entered in Block 20, if different from Report)

18. SUPPLEMENTARY NOTES

19. KEY WORDS (Continue on reverse side if necessary and identify by block number)

Seismic Waves
P_g, L_g
Attenuation
Scattering

20. ABSTRACT (Continue on reverse side if necessary and identify by block number)

Investigation of regional phase amplitudes at a large number of LRSM sites showed a pronounced increase of P_n, P_g, and L_g amplitudes at sedimentary structures relative to hard rock. In the early part of the coda and the main part of the wavetrain for L_g, lower order modes generated by mode conversion at local inhomogeneities must be present to explain the site variations and the coherence structure of L_g. A modification of Aki's scattering theory is presented to explain such observations. Analysis of the late coda of L_g showed

DD FORM 1 JAN 73 1473 EDITION OF 1 NOV 65 IS OBSOLETE

Unclassified

SECURITY CLASSIFICATION OF THIS PAGE (When Data Entered)

high crustal Q values at RKON and much lower values at OB2NV. At OB2NV the crustal Q appears to be frequency dependent, increasing from 200 to about 600 in the 1-10 Hz band.

AN INVESTIGATION OF ATTENUATION, SCATTERING AND SITE EFFECTS ON REGIONAL PHASES

SEISMIC DATA ANALYSIS CENTER REPORT NO.: SDAC-TR-81-4

AFTAC Project Authorization No.:	VELA T/0709
Project Title:	Seismic Data Analysis Center
ARPA Order No.:	2551
Name of Contractor:	TELEDYNE GEOTECH
Contract No.:	F08606-79-C-0007
Date of Contract:	01 October 1980
Amount of Contract:	$1,493,393
Contract Expiration Date:	30 September 1981
Project Manager:	Robert R. Blandford (703) 836-3882

P. O. Box 334, Alexandria, Virginia 22313

APPROVED FOR PUBLIC RELEASE; DISTRIBUTION UNLIMITED.

ABSTRACT

Investigation of regional phase amplitudes at a large number of LRSM sites showed a pronounced increase of P_n, P_g, and L_g amplitudes at sedimentary structures relative to hard rock. In the early part of the coda and the main part of the wavetrain for L_g, lower order modes generated by mode conversion at local inhomogeneities must be present to explain the site variations and the coherence structure of L_g. A modification of Aki's scattering theory is presented to explain such observations. Analysis of of the late coda of L_g showed high crustal Q values at RKON and much lower values at OB2NV. At OB2NV the crustal Q appears to be frequency dependent, increasing from 200 to about 600 in the 1-10 Hz band.

TABLE OF CONTENTS

LIST OF FIGURES

LIST OF FIGURES (Continued)

LIST OF FIGURES (Continued)

LIST OF TABLES

INTRODUCTION

In order to use regional phase characteristics for detection and identification of nuclear explosions and the determination of source parameters, one must be able to separate propagation and local site effects from source related signal properties. Several recent research efforts attempted to utilize some gross properties of regional signals for discrimination without any corrections for path or site effects. Blandford and Hartenberger (1978) found that P_{max} to L_g amplitude ratios can be used to discriminate between earthquakes and explosions in the eastern U.S. Gupta et al (1980) and Gupta and Burnetti (1981) found that ratios of amplitudes measured in various time windows for southern Asian events can also be used for discrimination. Pomeroy (1978a,b), on the other hand, found that no discrimination potential existed in several of the amplitude ratios of regional phases he investigated. Clearly much more research needs to be done along these lines. It also appears that purely empirical approaches to this problem are doomed to failure unless a more basic understanding of the major factors determining the characteristics of regional phases is reached. For instance, time domain amplitudes in various time windows may be dominated by site effects (Barker et al, 1980). The frequency content of signals is affected by both Q along the path and site effects. The relative proportion of shear to compressional energy in the signals may be altered considerably by mode conversions along some paths.

In this report we shall compare several basic measurable properties of regional phases with various models of signal propagation, attenuation and scattering. We shall also present the results of some further investigation of site effects.

The signal characteristics to be matched to theoretical models are the following:

Time domain envelope shapes in various frequency bands;
Spatial coherence structure;
Apparent phase velocities across arrays; and
Amplitude ratios of various phases in several time windows.

Due to the wide scope of this research, no final answers are available to all the questions mentioned above and the investigation continues. Most of

the research was concentrated on the L_g phase, although some results are presented for other regional phases such as P_n, P_g and S_n.

The available theoretical framework for the analysis and interpretation of regional signals includes normal mode theory (Harkrider, 1964) and the recently developed scattering theory for slightly inhomogeneous media as presented by Aki (1969), Aki and Chouet (1975) and Malin (1978). Successful models of regional phase propagation should be able to reproduce and predict the observed properties of signals. In addition to the two models of laterally homogeneous or slightly inhomogeneous media used in normal mode or weak scattering theory, occasionally numerical, deterministic modeling of strong lateral heterogeneities may be necessary for predicting the properties of observed signals.

This report discusses several somewhat loosely related topics. The first section describes the results of a study of site effects on L_g, P_g and P_n at a set of stations in the north central part of the United States. These stations are located primarily on shield type crust with varying sedimentary covers. The second section discusses several limitations on the applicability of normal mode theory to explain the observed properties of L_g. In the third section, a modification of the first order simple coda theory that allows for mode conversions at near surface inhomogeneities is discussed. The last section presents some observations of site effects at NTS and the results of some studies of the shear wave Q in the crust using the band-pass filtered codas of L_g

Throughout this report, the Q values quoted are effective Q in the sense used by Aki (1980). Therefore, the Q values include the losses of the waves through scattering.

THE EFFECT OF SITE GEOLOGY ON THE REGIONAL PHASES P_n, P_g AND L_g AT SHIELD SITES

In our previous work at NTS, we have shown that at sites underlain by low velocity materials the amplitudes of the regional phases P_g and L_g were amplified by factors up to 10, and the envelope shapes of both phases also changed, resulting in a prolongation of wavetrains at those sites (Barker et al, 1980). The observed site effect for L_g and P_g appears, therefore, to be several times greater than that for teleseismic P and would seriously affect any yield estimates based on measurements on these phases. The sites at NTS were closely spaced such that differences in paths, as manifested in multipathing, source radiation patterns and varying geophysical properties along the paths, should not seriously affect the conclusions about site effects.

To further investigate site effects we have undertaken the analysis of regional phase amplitudes at LRSM stations located in the north-central region of the US and some adjoining regions of Canada. The stations analyzed thus far are shown in the enclosed map (Figure 1) along with the locations of the events used. The event parameters are listed in Table I. Amplitudes of all identifiable regional phases were read at each station. In addition, for L_g the envelope shapes were characterized by noting the time of the onset of the phase, the time at the maximum, and finally, where the envelope decreased to one-half of the maximum. The L_g amplitudes used in the estimation of site effects were at the maximum of the magnitude.

The L_g amplitudes were corrected to a common distance of 500 km using the Δ^{-2} fall-off rate appropriate to the eastern US (EUS). The station sites were subdivided into two groups: hardrock sites and sedimentary sites. Hardrock sites were defined as stations resting on granitic or consolidated lower Paleozoic rocks having no more than 50 m of overlying unconsolidated rock cover. All sites not satisfying these criteria were classified as sedimentary sites. This subdivision is indicated in Figure 1. The distance corrected amplitudes were also corrected for event magnitude by dividing them with the average of the hardrock site amplitudes. Histograms of these reduced amplitudes of L_g for the two types of sites (Figure 2), clearly show the effect of site amplification. The average of the sedimentary site amplitudes is larger by a factor of 1.55 (about .19 amplitude units). This contrast is considerably less than at NTS. This can be explained by the fact that the

TABLE I

Event List for Regional Phase Study

#	Date	Origin Time	Location	Latitude	Longitude	Magnitude	Depth (km)
1	15 Jul 62	11 59 21.9	Montana	45.0°N	110.2°W		25
2	23 Jul 62	06 05 18.4	New Madrid	36.1°N	89.8°W		18
3	22 Oct 62	05 05 05.9	Montana	45.2°N	111.3°W		33
4	04 Nov 62	06 18 31.5	Yellowstone	44.3°N	110.3°W		
5	04 Dec 62	17 49 59.4	Colorado	39.8°N	104.7°W		33
6	28 Dec 62	10 01 23.6	Montana	48.4°N	113.9°W		33
7	30 Jan 63	05 05 59.5	Montana	45.0°N	110.8°W		33
8	30 Jan 63	23 05 09.6	Colorado	39.8°N	104.6°W		33
9	16 Feb 63	03 01 41.0	Montana	46.1°N	111.0°W		33
10	25 Feb 63	18 45 16.5	Wyoming	42.6°N	109.2°W		33
11	08 Mar 63	00 14 15.6	Q. Eliza. Is.	76.7°N	94.9°W	3.9	33
12	20 Jul 63	00 11 35.0	N. Yukon	65.2°N	133.7°W	4.6	
13	03 Aug 63	00 37 50.3	S. Illinois	37.0°N	88.8°W		18
14	04 Sep 63	21 20 18.5	Baffin Is.	71.5°N	72.8°W	4.1	33
15	04 Sep 63	21 41 00.6	Baffin Is.	71.6°N	73.5°W	4.4	33
16	06 Sep 63	01 46 13.0	Baffin Is.	71.5°N	73.0°W	4.4	33
17	12 Oct 63	02 46 48.1	Baffin Is.	71.6°N	73.0°W	4.1	33
18	15 Oct 63	12 28 58.4	S. Quebec	46.6°N	77.6°W		18
19	15 Oct 63	13 59 49.7	S. Quebec	46.3°N	77.8°W	3.8	14
20	16 Oct 63	15 31 01.8	S. New Eng.	42.5°N	70.8°W		20
21	08 Jan 64	10 04 31.6	S. Quebec	46.1°N	77.7°W	3.8	33
22	18 Feb 64	09 31 10.5	Alabama	34.8°N	85.5°W		15
23	18 May 64	01 04 30.5	N. Eliza. Is.	74.3°N	97.4°W	4.1	15
24	27 Aug 64	09 53 51.1	N. Yukon	65.3°N	133.8°W	4.6	33
25	21 Oct 64	07 38 31.0	Hebgen Lake	44.8°N	111.6°W	5.8	33
26	22 Oct 64	16 00 00.0	SALMON	33.4°N	89.6°W	4.6	
27	25 Nov 64	02 50 05.0	W. Virginia	37.4°N	81.5°W	4.5	
28	06 Mar 65	21 08 49.9	Missouri	37.4°N	91.1°W	5.3	33
29	03 Jun 65	19 30 25.7	Wyoming	43.6°N	106.5°W	4.7	33
30	15 Jul 65	14 16 07.0	Off E. coast	37.3°N	74.4°W	5.1	

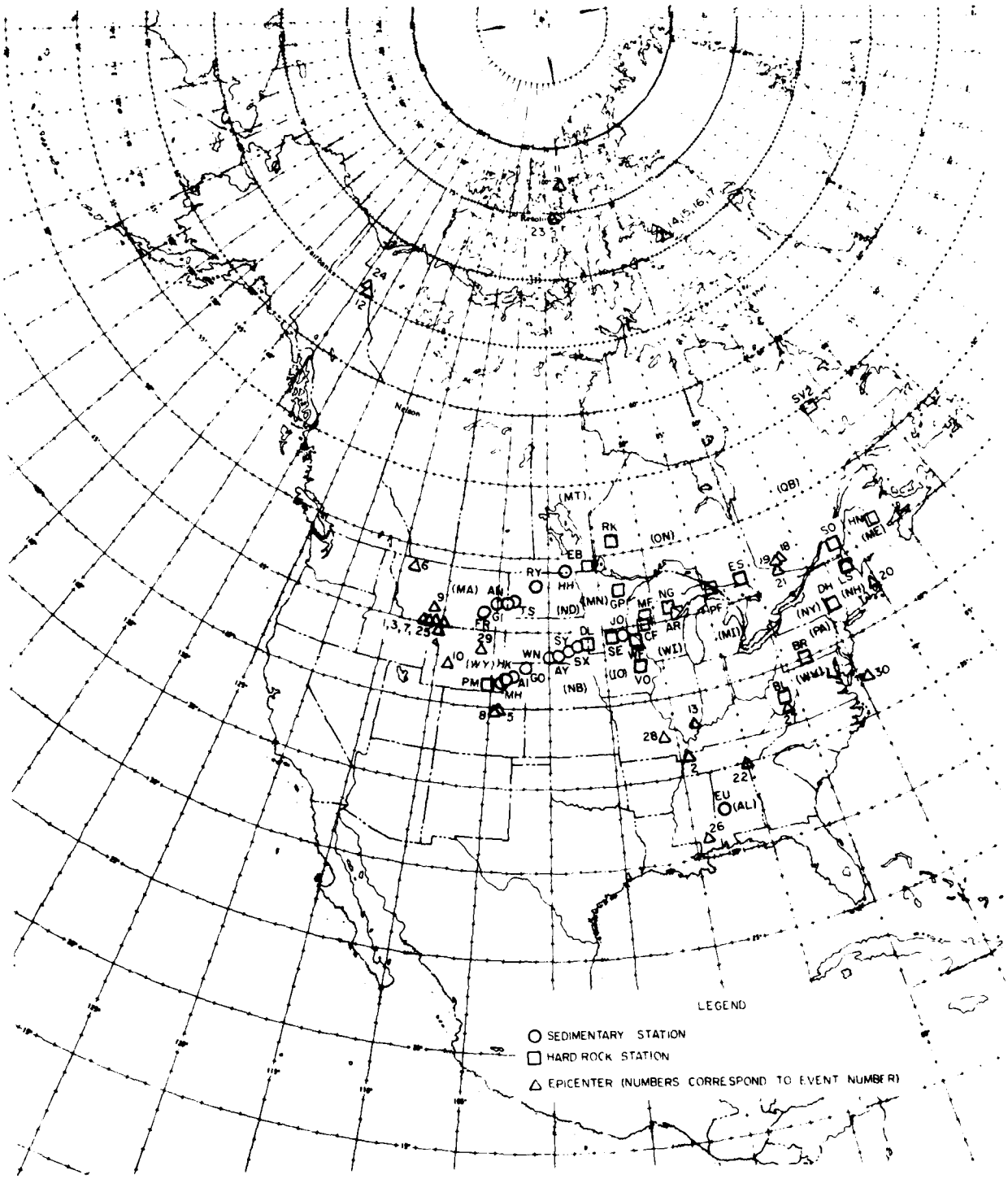

Figure 1 Stations used to investigate amplification of regional phases at sedimentary sites (circles) relative to hard rock sites (squares) located on the shield or stable platform region of North America. Triangles denote the locations of events studied.

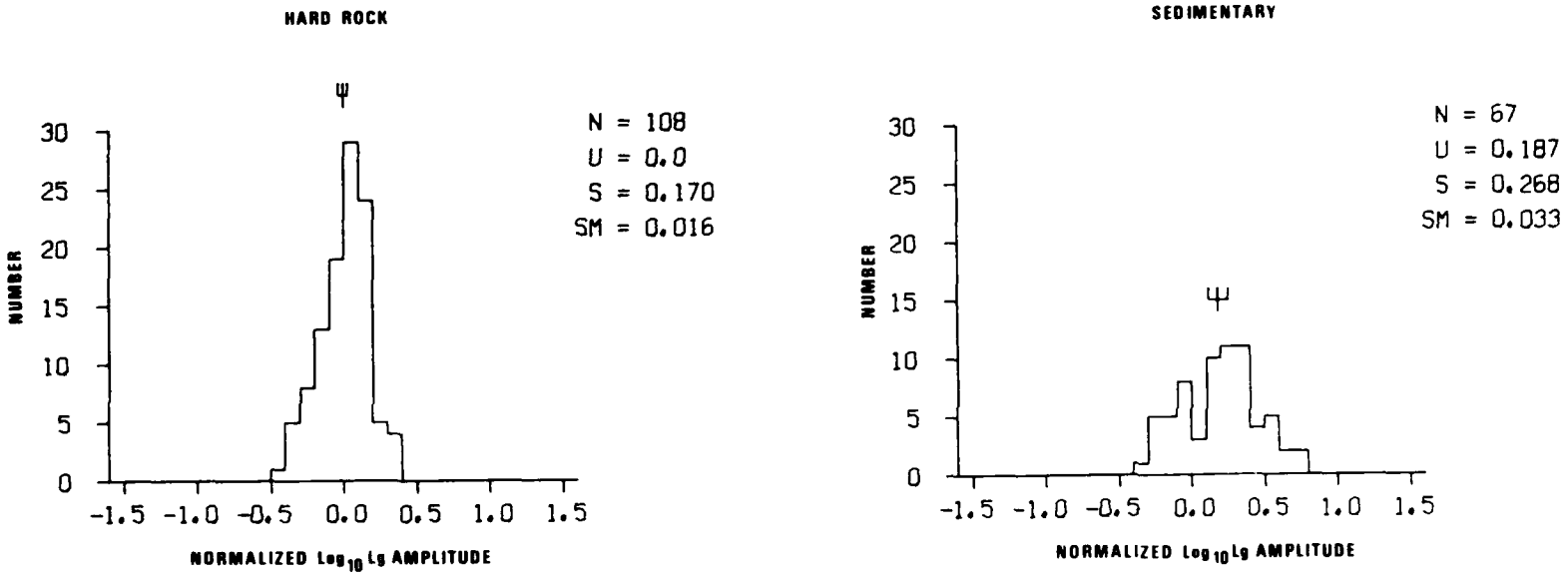

Figure 2 Histograms of reduced logarithmic amplitudes at hard rock and sedimentary sites for the L_g phase. Explanation of symbols: N = Number of data points, $\bar{U}$ = mean, S = standard deviation, SM = standard deviation of the mean. The locations of means and their 95% confidence limits are indicated above each histogram.

sedimentary sites we examined do not have the thick, extremely low-velocity sediments or volcanics present at Pahute Mesa and Yucca Flats. Also, many of the sedimentary sites actually rest on fairly well consolidated rocks.

The P_n and P_g amplitudes were reduced by the regional fall-off rate written as $\Delta^{-2} \exp(-\pi f(\Delta/8.1) \cdot (1/Q))$ where the values f = 3 Hz and 2.5 Hz and Q = 1000 (Alsup, 1972) were used respectively for P_n and P_g. The frequencies used were determined by measuring the records. After correcting for event magnitudes, we obtained histograms for the two types of sites; these are shown in Figures 3 and 4, respectively. The site effect due to sediments appears to be quite large, being 0.36 magnitude units larger for P_g and 0.27 magnitude units for P_n. The scatter in all histograms is less for the hardrock group. This may be explained by the more restrictive criteria applied to hardrock site selection, while sedimentary sites may vary widely in structure, lithology, and the thickness of strata. The amplitude differences between the "hardrock" and sedimentary groups at the 95% level is highly significant statistically speaking. The observed site amplifications for P_g and L_g being unequal would affect the P_g/L_g ratio to some degree as a discriminant. This is in conflict with observations at NTS where this ratio was not changed (Barker et al, 1980). It must be noted, however, that in this study lateral focusing can contribute considerably to the observed amplitudes due to the wide areal coverage at the stations. At NTS on the other hand all stations were closely spaced so this perturbing factor was effectively reduced. We are not sure, therefore, that our results presented above imply a significant change in the P_g/L_g amplitude ratio. The amplitude-distance formulas used also may be in some error.

In addition to effects on amplitudes, the envelope shapes of L_g are also changed by type of sediments and possible multipathing effects. The envelope shapes characterized by the arrival times of the L_g maxima and the 1/2 maxima points were examined by plotting these arrival times as functions of distance for all the events. The first observation one can make is that sedimentary sites tend to have longer codas and later arrivals for the maximum of the L_g. This tendency, however, is not clear on all the plots. Another observation that may be more important is the similarity in coda characteristics for events that come from the same source region. This

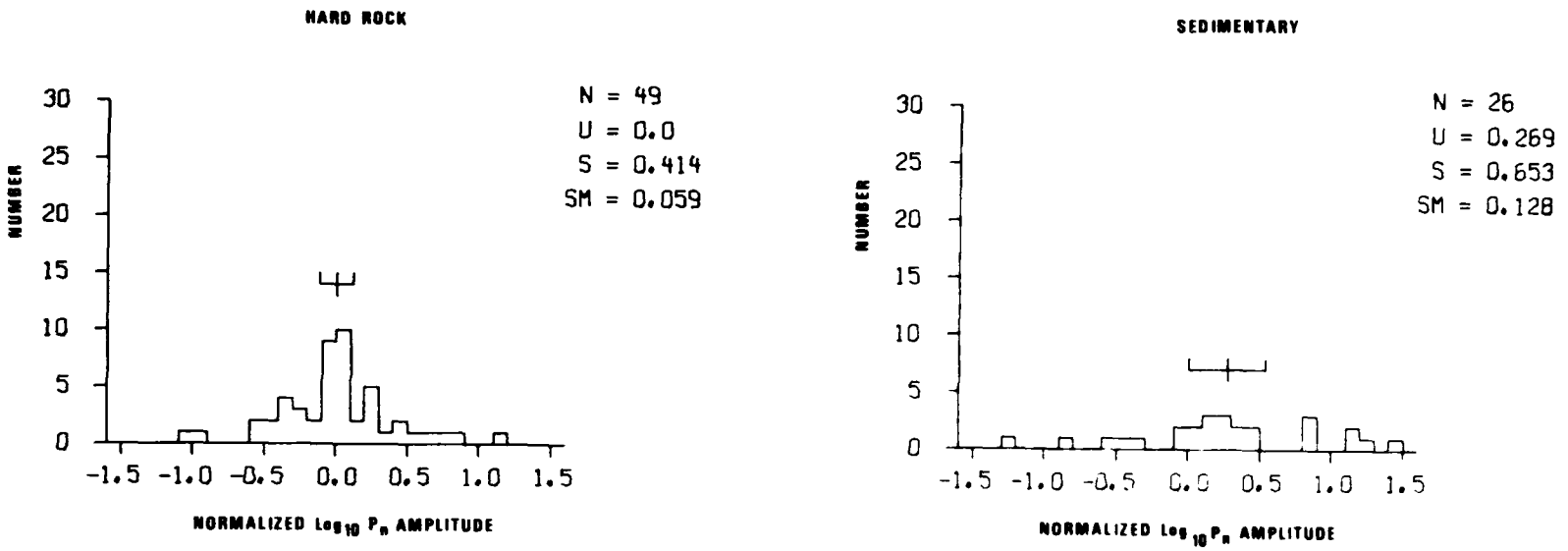

Figure 3 Histograms of reduced logarithmic amplitudes at hard rock and sedimentary sites for the P_n phase.

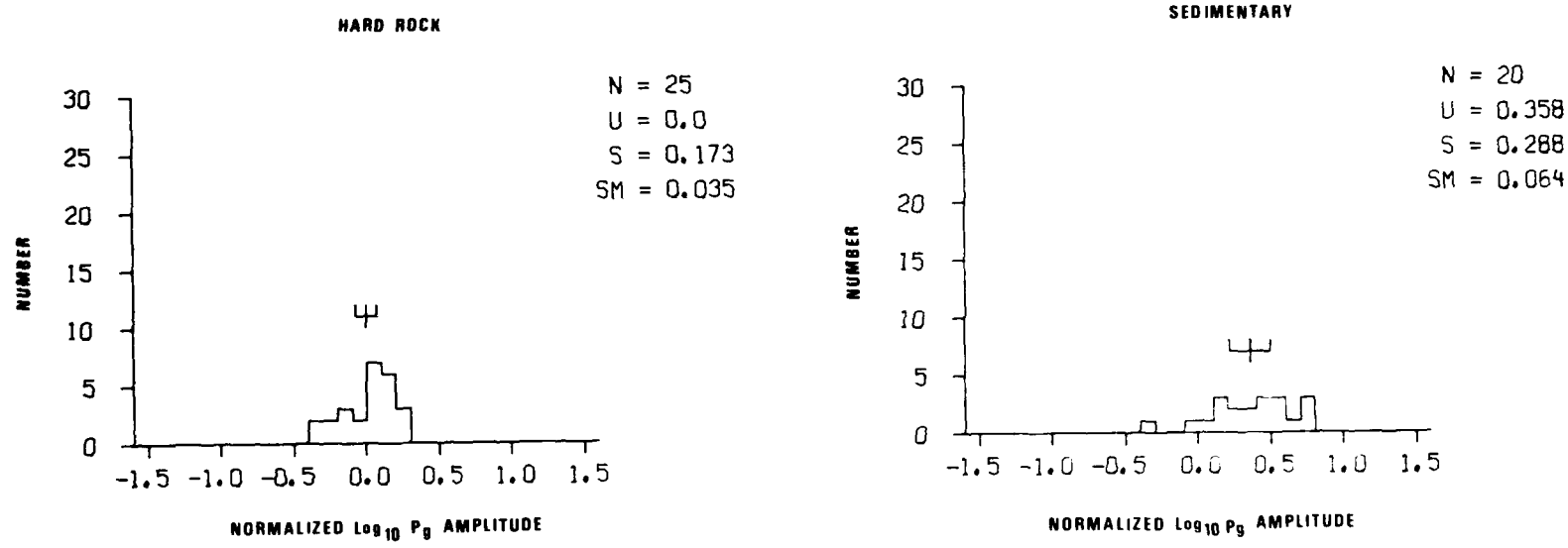

Figure 4 Histograms of reduced logarithmic amplitudes at hard rock and sedimentary sites for the P_g phase.

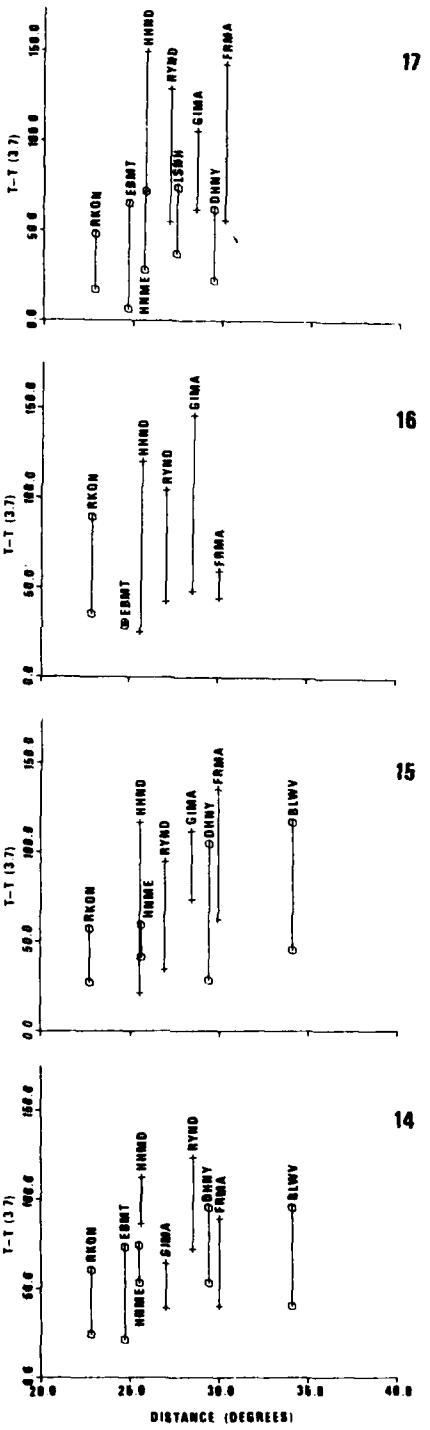

Figure 5 Length of coda as a function of distance and station for events 14, 15, 16, and 17 at Baffin Bay. Note the similarities in coda length patterns at common stations. (Coda lengths are characterized as the time between the trace maximum and the 1/2 maximum point on the trace envelope.)

effect often overshadows the site geology effect. For instance, for a group of events at Baffin Bay, there are some remarkable similarities in the coda characteristics at common stations (Figure 5). The most likely explanation for these similarities is that lateral focusing and multipathing patterns are likely to be similar for events coming from the same source region. The above findings indicate that time domain envelope shapes of L_g are quite fragile and cannot be used to derive details of source characteristics unless their behavior is better understood. The stations analyzed in this study cover a wide area, unlike those in the NTS study, and, therefore, lateral focusing plays a greater role. These findings are similar to those of von Seggern (1980).

More L_g coda shapes are shown in the appendix of this report. One thing that can be said about these envelopes is that there exists a tendency for the L_g maximum to arrive later at sedimentary sites; the length of the wave-train also tends to be longer at these sites. It may be necessary to make some site corrections to the group velocity of the L_g maximum that, according to Pomeroy and Chen (1980), has a potential for discrimination. Some of the coda analysis work may also need to be corrected for site effects, since some codas may consist more of locally excited waves than back-scattered energy from distant inhomogeneities.

LIMITATIONS OF NORMAL MODE THEORY

The most widely used model of regional phases involves normal mode theory. It was noted very early that the group velocity of L_g coincides with the group velocities of Airy phases in a large number of higher Love and Rayleigh modes (Oliver and Ewing, 1957; Press and Ewing, 1952; Knopoff et al, 1973; Panza and Calcagnile, 1975). Harvey (1980) succeeded in simulating regional seismograms containing P_n, P_g and L_g phases by superposing a large number of normal modes of the Rayleigh type. The success of normal mode theory for modeling regional phases is encouraging, since, although the computation of a large number of mode eigenfunctions and dispersion curves is extremely laborious, the excitation of normal modes can be readily described in terms of source mechanism and the properties of layered media. It is possible, in terms of mode theory, to identify crustal features determining the characteristics of the various regional phases and the effects of changes in the structure on the same. The absence of the $\overline{P}$ phase in the eastern US as opposed to the western US must be due to some yet unidentified crustal feature. The effect of source depth, and source mechanism can be easily simulated and compared to observations using mode theory.

In spite of the success of mode theory in describing the general characteristics of regional phases, data in several major aspects deviate from the predictions of mode theory. Time domain envelopes derived from mode theory do in general predict the beginning of the L_g envelope, but do not describe the (long) coda. Figure 6 shows such a comparison between the predicted and actual L_g shapes.

The coda shapes vary from station to station considerably even if they are closely spaced. There exists also an erratic behavior in the length of the L_g wavetrain with distance that mode theory does not predict. Superposition of a large number of normal modes would give a steady increase in the length of the wavetrain. It seems to be clear that local site effects simular to those observed at Yucca Flats and Pahute Mesa predominate (Barker et al, 1980) changing both the amplitudes and envelope characteristics of L_g. It is therefore not prudent to attach too much significance to the relative amplitudes in various time windows for discrimination purposes, unless some correction for site effects is made. Another major deviation from the predictions of mode theory is the spatial coherences of regional signals. Mode theory predicts high coherences over small arrays of a few km in diameter. For example, a typical L_g phase has most of its energy at frequencies below 2 Hz. Assuming that all possible modes are

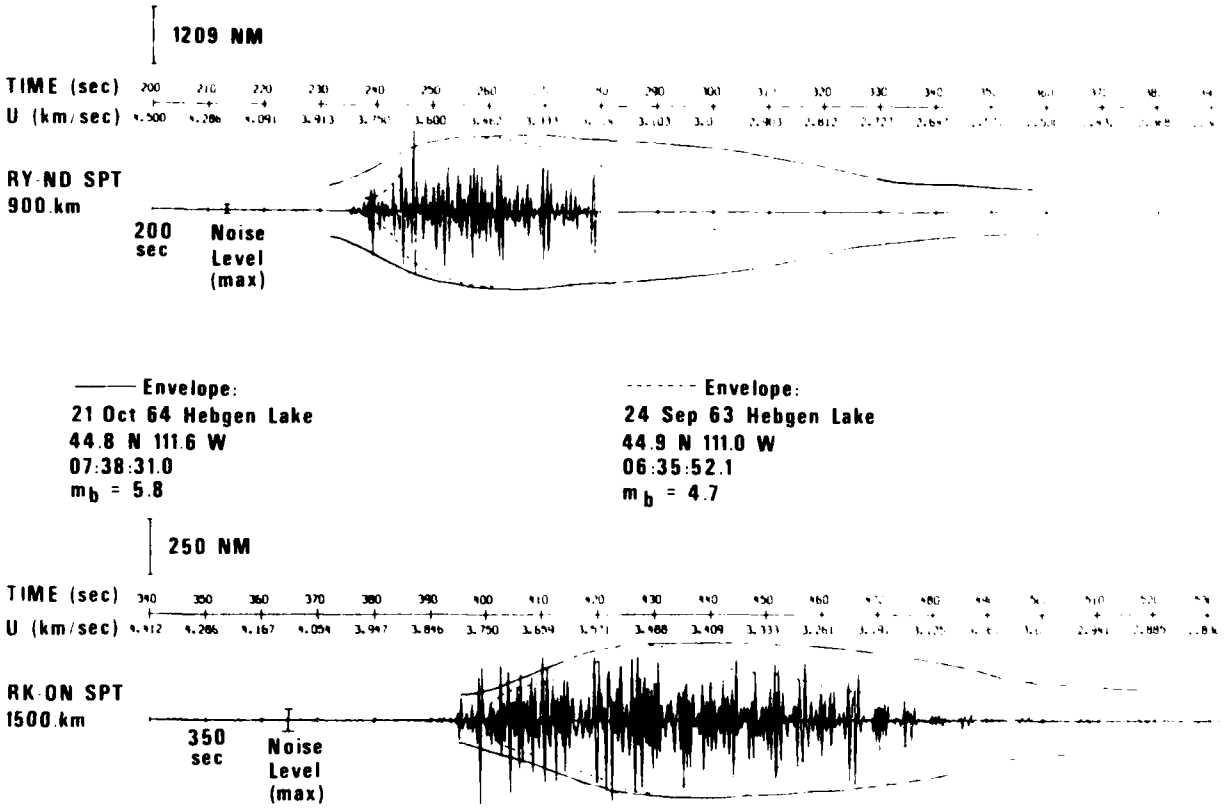

Figure 6 Comparison of L_g envelope shapes with signals derived from mode theory: Canadian shield, no sediments, 30 km depth. While the fit for one of the events is fairly good, the other event does not fit at all. The differences are too large to be explained by source mechanism or depth. The figure shows dramatically the capricious nature of some L_g envelope characteristics. The coda in each case cannot be explained by mode theory.

equally excited, the coherences predicted are still high, being 0.7 at 5 km spacing along the direction of propagation. For this example, 28 modes are possible, which we assumed to be equally excited. This is a worst case analysis, since for most real sources only a few modes would be present at significant energy levels and the predicted coherences would be even higher. Moreover, the mode theory predicts a coherence of unity between sensors spaced perpendicular to the direction of propagation. Observations of actual L_g phases show a considerably lower coherence perpendicular to the direction of propagation, in sharp contradiction with the predictions made assuming a set of coherently propagating modes. In any direction, parallel or perpendicular to the wave direction, the coherences are considerably lower than those predicted by mode theory. Finally, another strong indication that it is not permissible to propagate modes unchanged from the source to the receiver, is the presence of a large transverse component of motion in the L_g from the nuclear explosion SALMON. This explosion in salt exhibited an extremely symmetrical near source motion at ranges of a few km from the source with no appreciable transverse motion. At about 30 km from the source, a large transverse component appears (Werth and Randolph, 1966), indicating possible mode conversion along the path.

The most basic limitation on mode theory is that at the short wavelengths associated with 1 to 2 Hz L_g waves the very definition of modes is breaking down. If one considers modes as arising from the constructive interference of, say, SH waves multiply reflected within the crust one can use Brune's (1966) constructive interference criterion to derive the dispersion curves

$$2N = 2\left(t - \frac{\Delta}{c}\right)\frac{1}{T} + \frac{1}{2} \qquad (1)$$

where N is an integer, Δ is the epicentral distance, t is travel time along a diving ray, $c = \frac{d\Delta}{dt}$ is the apparent phase velocity of the ray and T is the wave period. Taking Δ, c, and t computed for various rays and solving (1) for T, the phase velocity curve of a certain mode can be traced out. Changing N changes the mode number. The 1/2 in the formula accounts for a $\pi/2$ phase shift at the turning point which should be true at the high frequency limit (Tolstoy and Clay, 1966).

Although this is a crude approximation that neglects internal reflections, it appears to describe the basic structure of dispersion curves fairly well.

Figure 7 shows a comparison of higher mode Love dispersion curves computed by Knopoff et al (1973) with those derived from equation (1). The agreement is remarkable considering the approximate nature of equation (1). Considering now that the average phase velocity difference between two adjacent modes is about 0.15 km/s at around 1 Hz, this corresponds to a difference in the angles of incidence for corresponding rays at the surface of about 1.5 degrees. A surface slope of half that amount at the point of reflection will deflect energy of one mode into the next. Surface slopes of that magnitude are quite common over distances comparable to the wave length of an L_g 1-Hz wave. As the various higher modes exchange energy, determining source depth using the nulls of excitation in a few modes becomes impossible, because all modes may have considerable energy after propagating to a certain distance.

Summarizing, this mode theory can be used to study the effects of crustal structure and source mechanism on the major time domain characteristics of regional phases. Mode theory, on the other hand, cannot predict some of the major observed characteristics of the signals, and the very concept of modes may not be valid for the laterally variable wave guides representative of the Earth's crust.

Figures 8 and 9 shows some measurements of signal coherence in L_g measured at LASA and CPO from Mrazek et al (1980). Despite the great scatter, these figures show a fast decrease of spatial coherence with increasing sensor separation. Comparing these with theoretical predictions using the superposition of all modes for a given model (Figures 10 and 11), it appears that even adding up about 28 equally excited modes does not produce the low coherences observed (Mrazek et al, 1980). Moreover, no matter how complicated the mode structure is, coherences should be near unity for sensor pairs oriented perpendicularly to the direction of propagation. In reality, however, the coherence for such sensor pairs is slightly less than that for pairs in the line of the direction of propagation (Mrazek et al, 1980) for the same event. This is not as evident as in Figures 8 and 9 as it is on pair by pair comparison because these figures show a compilation of coherence values from many events, some of which, for reasons unknown, appear to be more coherent than the others.

It must be noted, on the other hand, that there have been some reports of higher coherences at the C6 subarray of NORSAR and at the YKA array (Mykkeltveit et al, 1980; Pomeroy, 1980). From the above discussion, it is

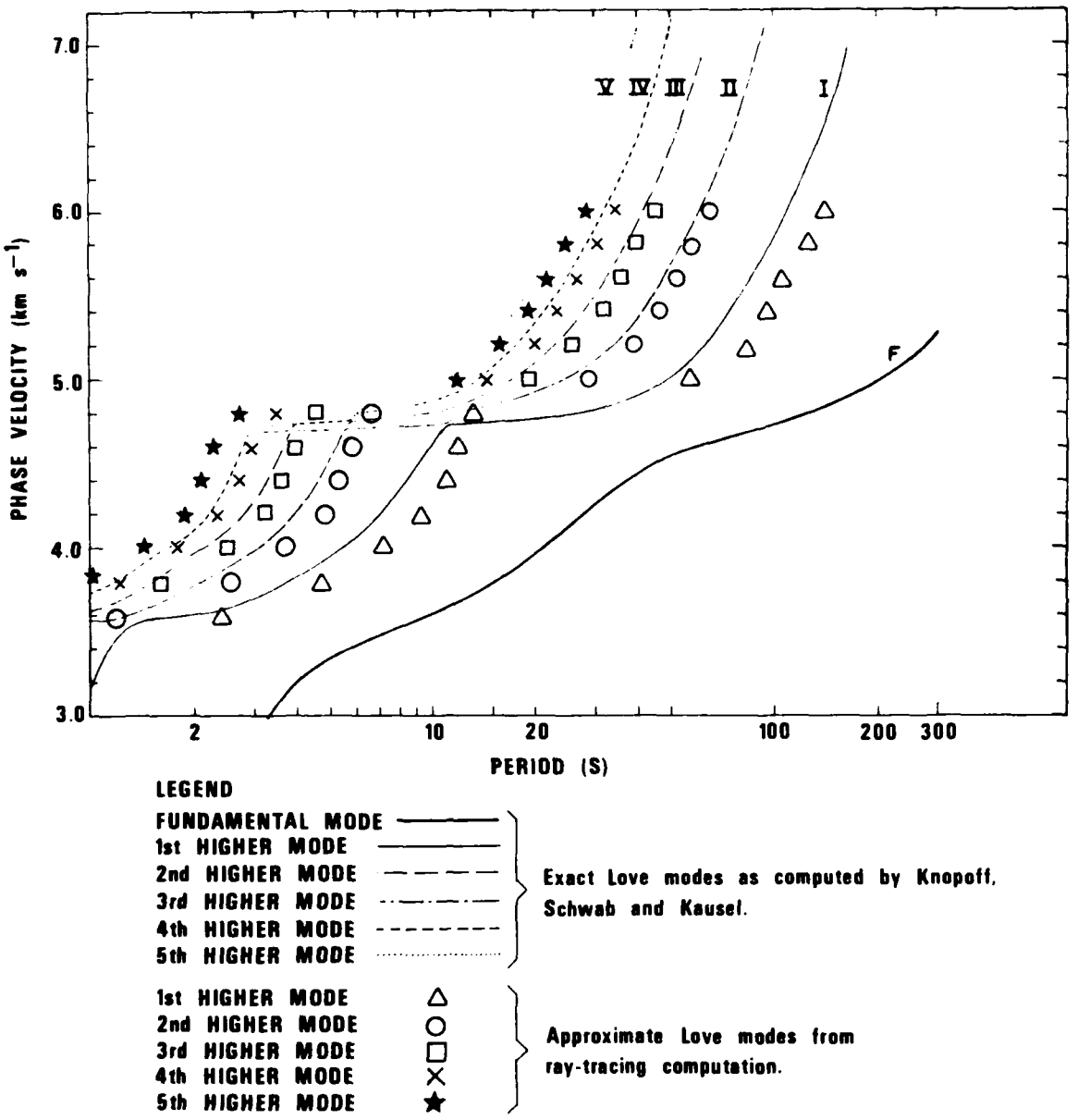

Figure 7 Comparison of exact Love model phase velocities with those derived from ray approximation (after Mrazek et al, 1980).

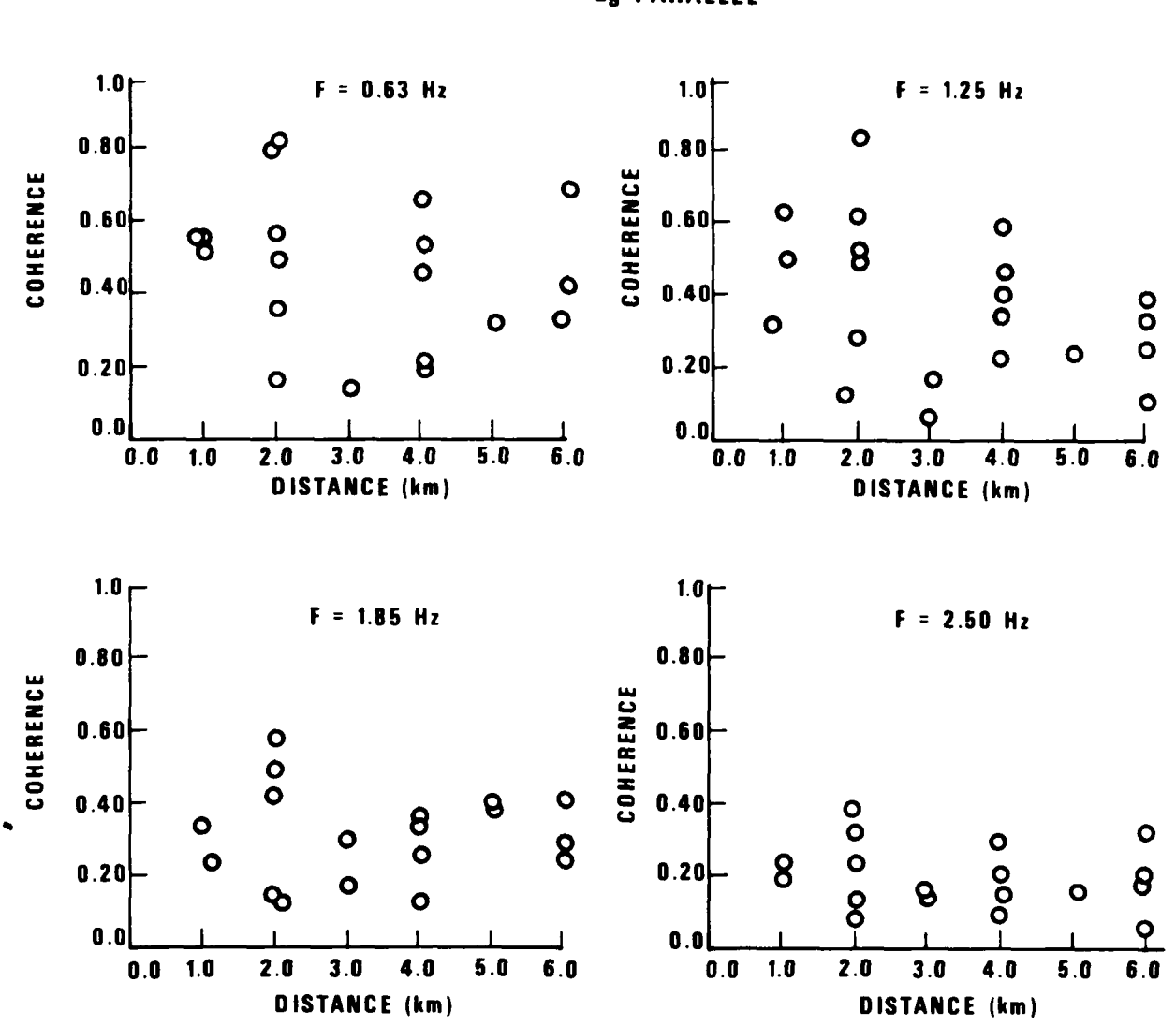

Figure 8 Observed L_g coherences as functions of frequency and inter-station spacing parallel to the direction of propagation (after Mrazek et al, 1980).

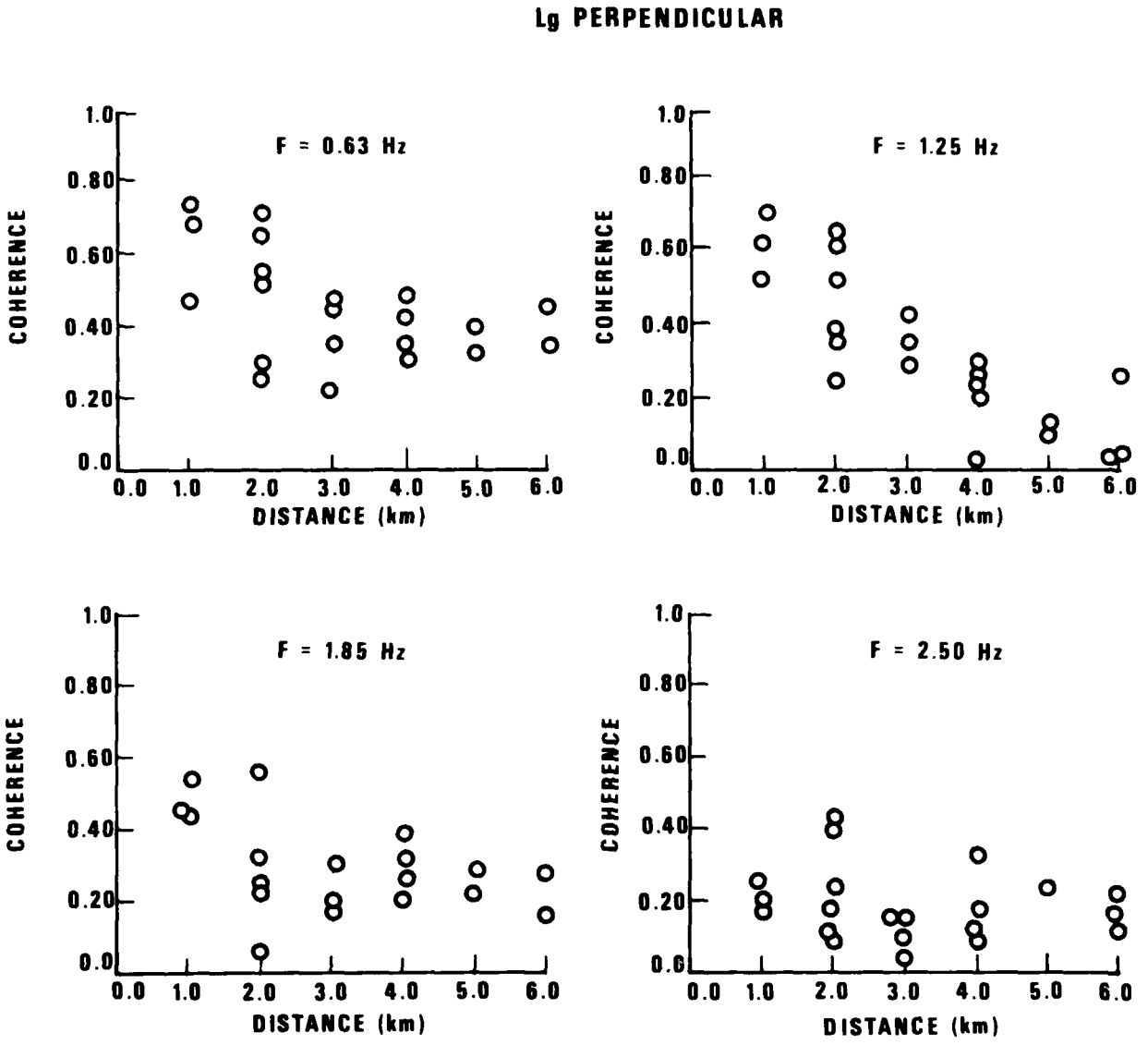

Figure 9 Observed L_g coherences as functions of frequency and inter-station spacing perpendicular to the direction of propagation (after Mrazek et al, 1980).

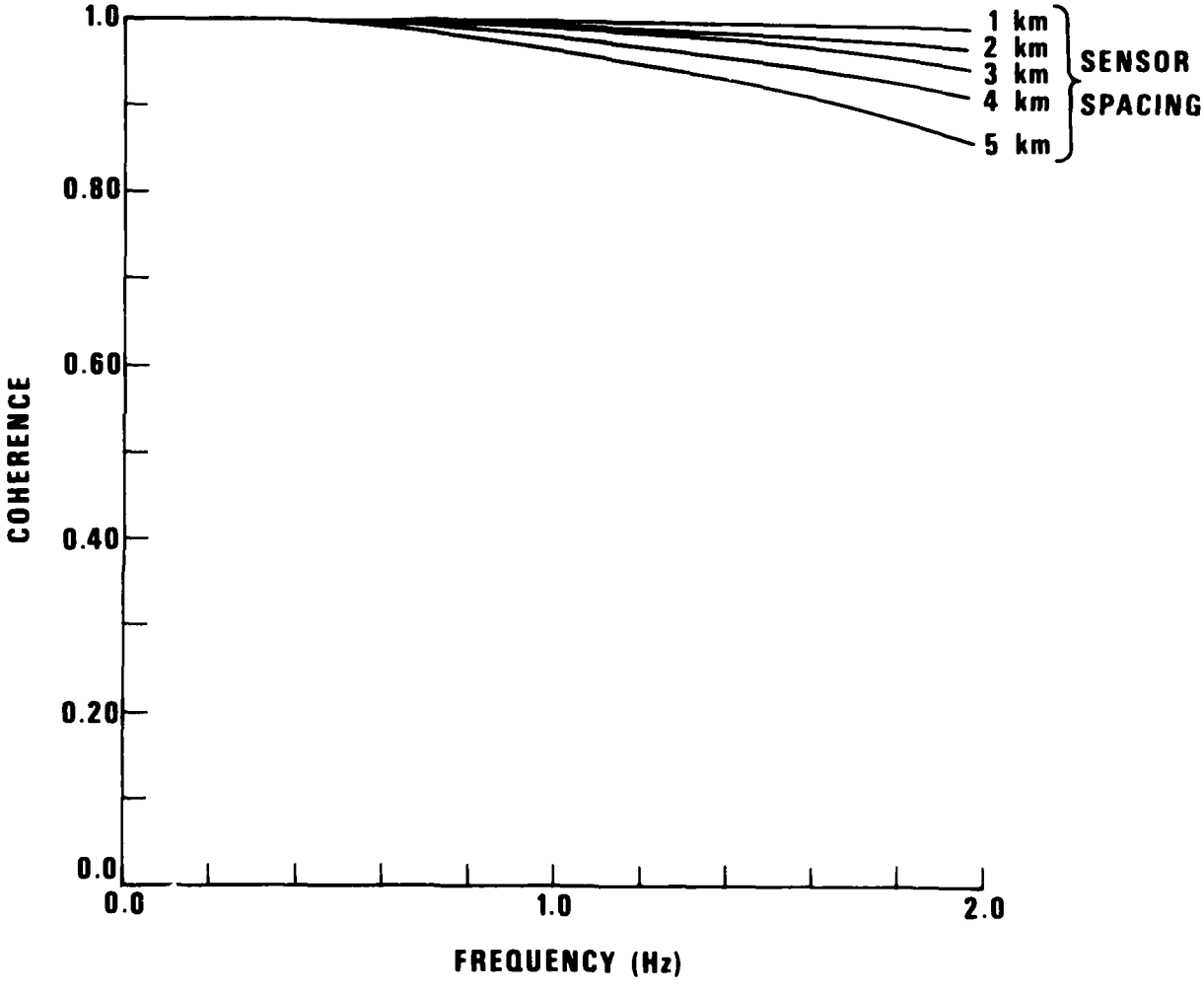

Figure 10 Theoretical L_g coherences using unequal excitation of modes (after Mrazek et al, 1980).

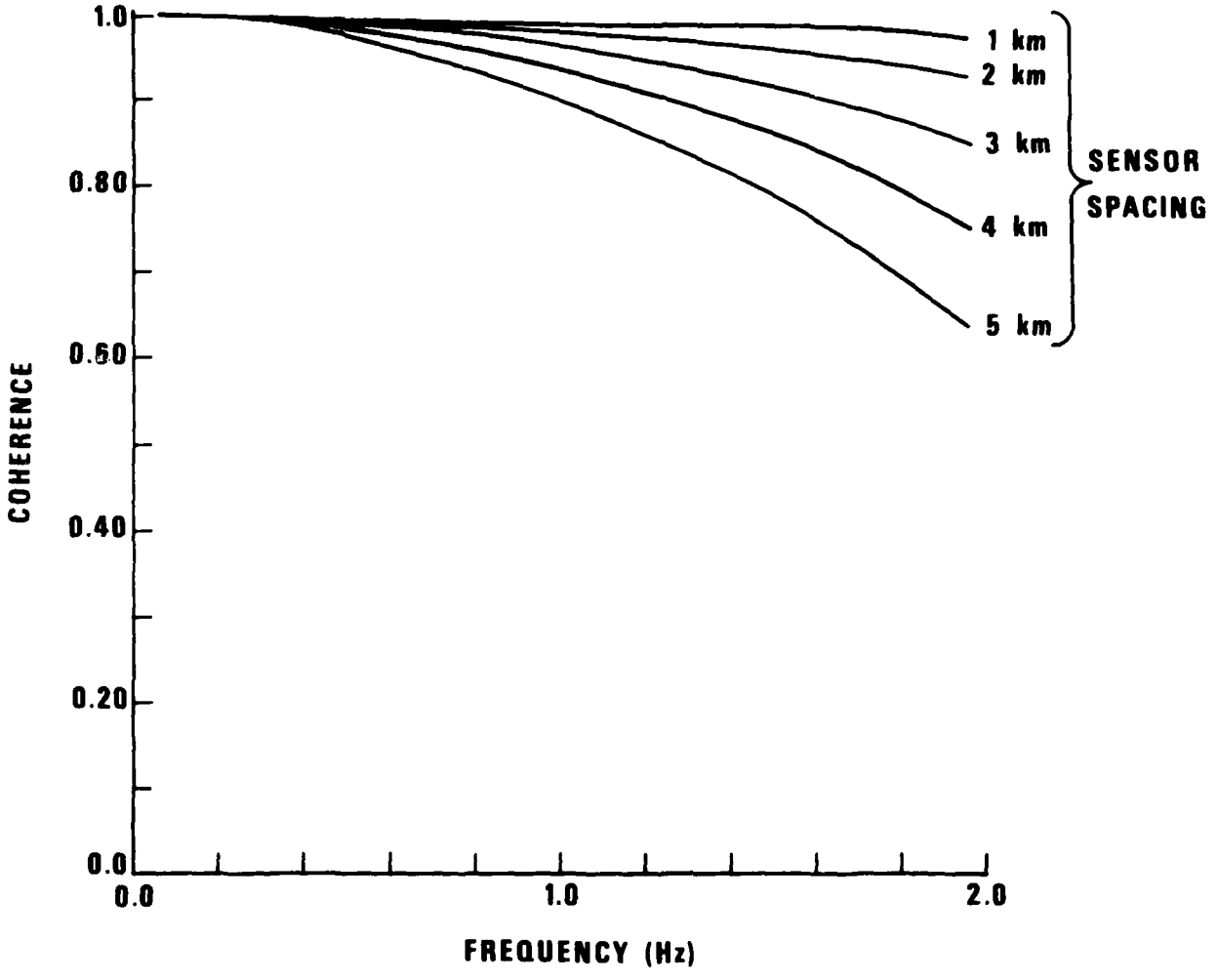

Figure 11 Theoretical L_g coherences derived by assuming equal excitation of all modes (after Mrazek et al, 1980).

evident that the degree of local scattering is strongly dependent on the topography and the geology in the vicinity of the sensor. All the effects are strongly site dependent. In surveying for suitable sites for regional detection and signal enhancement, sites with laterally homogeneous geology and high spatial signal coherence should be given preference.

CODA ANALYSIS OF THE L_g PHASE

General

Aki (1969) proposed a mechanism for the generation of the codas observed after local earthquakes. The mechanism he advocated was back scattering of seismic waves from inhomogeneities in the crust. The proposed model includes several basic assumptions. These are: a) The distance of the scatterers from the station is large compared to the distance between the local earthquake and the station. In other words, the coda is measured at times late enough that the geometry shown in Figure 12 exists to describe the locations of the scatterers, the event, and the station. b) The primary waves exciting the scatterers are of the same type as the scattered waves, i.e., high frequency surface waves of low mode number. This assumption is also implicit in the configuration in Figure 12. c) The scatterers are distributed two-dimensionally over the Earth's surface with uniform density.

From these starting assumptions, Aki derived some simple formulas to relate the change with time of the dominant period of waves in the coda to crustal Q. In later studies Herrmann (1980) and Nuttli (1980) applied these formulas to codas of earthquakes at regional distances. It is likely, however, that when Aki's method is applied to regional events, several of the fundamental assumptions above are violated and thus the theory may also need modification. Assuming that b) is true, the geometry, in most practical cases, is modified to that shown in Figure 13. The scattered waves come from a locus of an elongated ellipse, instead of a near circle.

To maintain condition a) with a source to station distance of, say, 1000 m, would require a coda measurement at times when the coda had already disappeared. The ellipse at such a distance would cover areas larger than continental dimensions. It is also improbable that condition b) can be maintained for such cases. For regional events, the coda on the short-period instrument usually means the coda of L_g. L_g consists of higher modes with particle motion encompassing the whole crust. The most drastic inhomogeneities, on the other hand, occur close to the surface. The common occurrence of sedimentary basins with large velocity contrasts compared to the surrounding rock and varying topographic relief are two prominent examples of this. Deeper in the crust lateral heterogeneities still exist, but the associated velocity contrasts are likely to be much smaller. Near surface

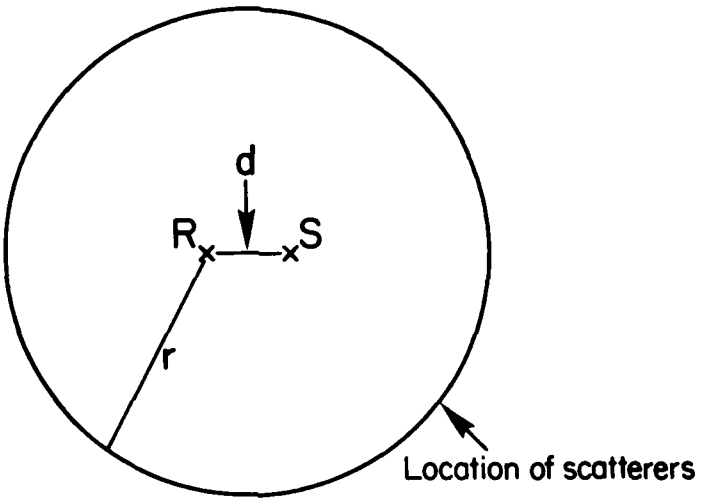

$$r \gg d$$
$$U_1 = U_2$$
$$Q_1 = Q_2$$

Figure 12 Geometry of sources, receivers and the location of scatters implied by Aki's (1969) theory.

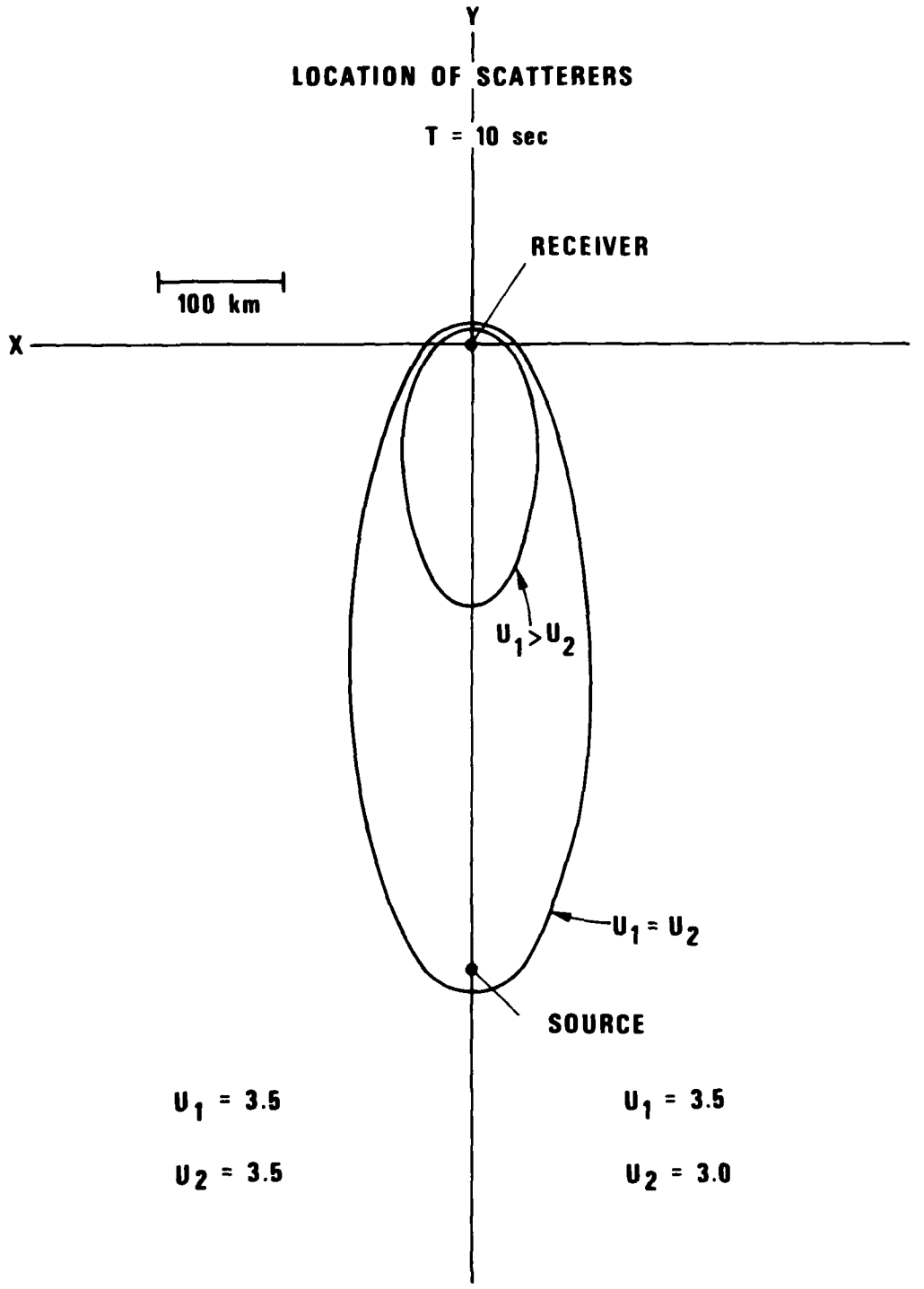

Figure 13 Location of the scatterers at T = 10 s after the passage of the primary wave for the cases $U_1 = U_2 = 3.5$ km/sec and $U_1 > U_2$ where $U_1 = 3.5$ km/sec and $U_2 = 3.0$ km/sec.

heterogeneities will tend to cause scattering into lower order modes, with the fundamental mode as prime candidate.

Moreover, some of the near surface heterogeneities are not weak perturbations, as most of the first order scattering theory assumes. Figure 14 illustrates this principle. The dominant inhomogeneities near the surface, sedimentary structures and topography, cause preferential conversion into fundamental or lower order modes for which the particle motion is primarily confined to shallow depths. Incidentally, the lower order modes thus generated may not have much energy associated with them, and thus the net energy loss of the primary high order modes may also be small. At the surface, however, the scattered low order modes can dominate the motion and completely obscure the source diagnostics sought in discrimination studies. An extreme example of such effects was furnished by the results of our study at NTS (Barker et al, 1980), where the motion was dominated by low order modes generated locally in near surface structures. There is no reason to believe, however, that such effects do not often occur, to a lesser degree, at other locations where the near surface inhomogeneities are not as pronounced.

This distribution of inhomogeneities also implies that the effective Q of lower order modes must be lower than those of the higher order modes. Since the particle motion of the fundamental mode, for instance, is confined to the top of the structure, it will encounter major inhomogeneities and will be severely attenuated. This has also been observed directly; direct fundamental mode waves from shallow sources attenuate quickly with distance and may entirely disappear in the short-period band, while higher modes, L_g for example, persist.

Malin (1978, 1979), using a model of an inhomogeneous layer overlaying a homogeneous halfspace, concluded that there is a preferential conversion of the primary waves into scattered waves of the same modal composition if all the modes are essentially confined to the inhomogeneous layer. For the reasons discussed above, this model and the conclusions drawn from it are not applicable to the model with uneven depth distribution of inhomogeneities proposed in this report.

We feel, therefore, that it is necessary to introduce some modifications, and unfortunately, some extra free parameters into Aki's theory for the analysis of L_g codas. In our approach, we allow different velocities and Q factors for the primary and scattered waves, but consider no cases where the scattered waves travel

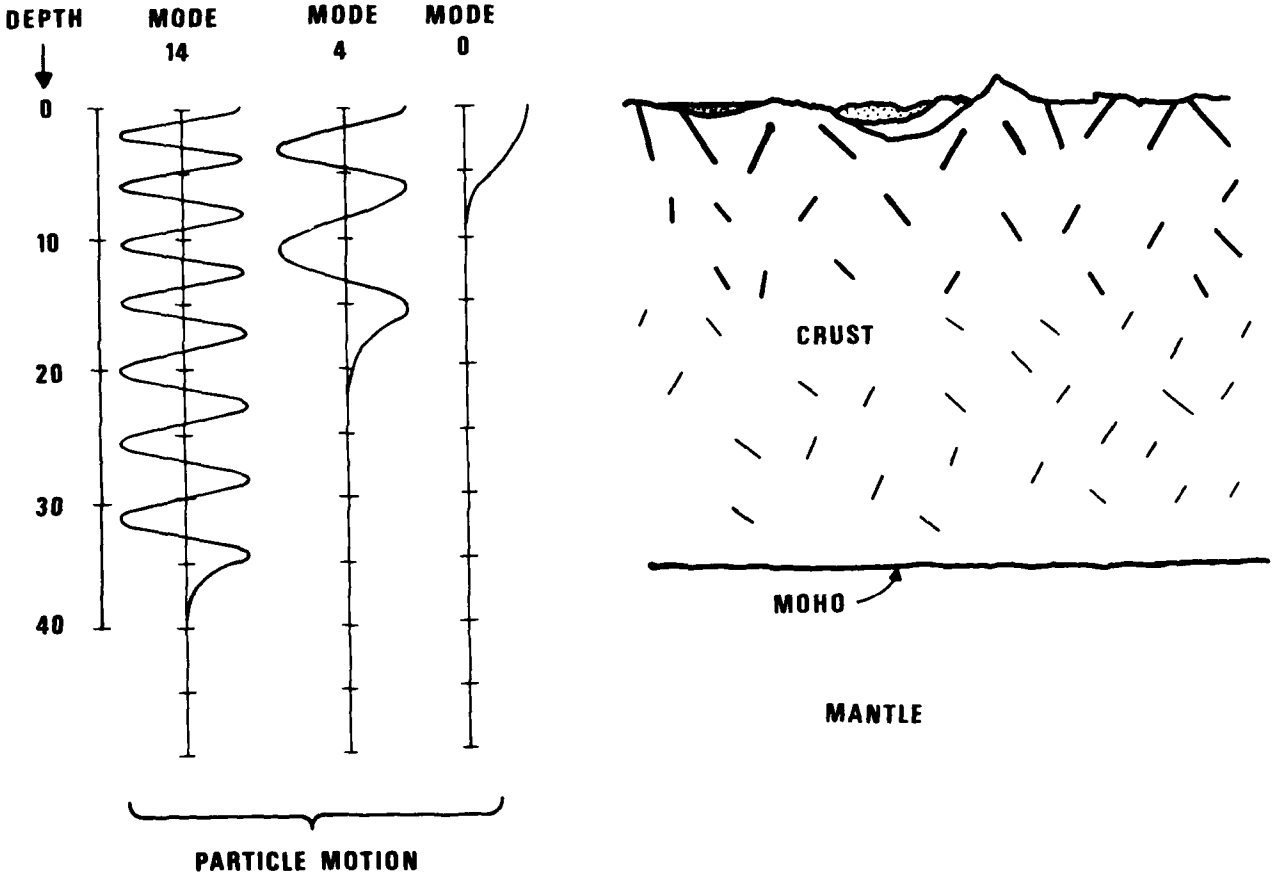

Figure 14 Figure illustrating the interrelationships among distribution of crustal inhomogeneities and the modal particle displacements in the crust.

faster than the primary wave. We also assume that the Q values for the scattered waves are lower than for the primary waves, to allow for greater scattering losses from the lower order modes at the near surface. These assumptions are reasonable in view of the physics of the problem we are attempting to tackle. To make up for the extra degrees of freedom of the problem, we shall also attempt to introduce new constraints. Instead of the time domain measurements of dominant periods, used by Herrmann (1980) we use band pass filtered codas, a more precise measurement. We shall also consider array measurements of spatial coherences in various directions with respect to the wave propagation direction and apparent phase velocities in the coda to define the problem.

We shall start out with the assumption that Aki's conditions b) and c) are true at the beginning and introduce modifications if the data require it. Investigation of the regional variations of the crustal Q is extremely important for determining the detectability of high frequency energy at regional distances from small events. Decoupled nuclear explosions that most efficiently generate high frequency seismic waves are of special interest in this context.

The Case for Mode Conversions

Since, as we mentioned above, most of the crustal inhomogeneities associated with large velocity contrasts are near the earth's surface, one must consider the possible effects of such inhomogeneities. Most of the theory developed to estimate the properties of scattered waves is based on first order perturbation theory presupposing weak inhomogeneities. Although most near surface velocity perturbations are quite drastic the results of past theoretical studies are still quite valuable to provide insight into the problem. Perturbation theory was used by Haddon (1978), Miles (1960), Knopoff and Hudson (1964, 1966), Hudson (1977) and many others to estimate scattering effects due to small inhomogeneities distributed throughout the elastic media. The effect of inhomogeneities can be described in terms of equivalent force systems distributed through the inhomogeneous region. Following Haddon (1978) the equation of motion in this region can be written as

$$\rho_0 \frac{\partial^2 u_i^1}{\partial t^2} - (k_0 + \frac{1}{3}\mu_0) \frac{\partial \Theta^1}{\partial x_i} - \mu_0 \nabla^2 u_i^1 = Q_i(\underset{\sim}{r},t),$$

where u_i^1 denotes the scattered wave displacement components, k_0 and μ_0 are the unperturbed elastic constants, ρ_0 is the unperturbed density, and Θ^1 is the volume dilatation of scattered waves. The term $Q_i(\underset{\sim}{r},t)$ on the right hand side is the equivalent force system that can be described in terms of the particle displacements of the primary wave and the elastic constant and density perturbations, along with their gradients as

$$Q_i(\underset{\sim}{r},t) = -\Delta\rho \frac{\partial^2 u_i^0}{\partial t^2} + (\Delta k + \frac{1}{3}\Delta\mu) \frac{\partial \Theta^0}{\partial x_i} + \Delta\mu \nabla^2 u_i^0$$

$$+ \frac{\partial}{\partial x_i}(\Delta k - \frac{2}{3}\Delta\mu)\Theta^0 + \frac{\partial}{\partial x_j}(\Delta\mu)\left[\frac{\partial u_i^0}{\partial x_j} + \frac{\partial u_j^0}{\partial x_i}\right]$$

In this formula, $\Delta\rho$, $\Delta\mu$ and Δk are the density and elastic constant perturbations and the quantities with the null superscripts pertain to the unperturbed primary wave displacement components. The equivalent force system given above can, with considerable labor, be described in a straightforward manner in terms of various types of inhomogeneities.

Using similar approaches, Hudson and Knopoff (1967), Hudson (1967), Gilbert and Knopoff (1960) and many others described the effects of topography and shallow near surface structures in terms of equivalent surface stress systems. Given any force or surface stress system, it is straightforward to compute the scattered wave field in terms of Green's functions of the unperturbed medium. For our purposes, the surface wave theory as given by Haskell (1964) and Harkrider (1964) is the most important.

For near surface sources the contributions to the lower order modes, especially the fundamental mode, are the most substantial. Higher modes are much less regardless of the nature of the primary waves. In the crust, lower order modes, in general, have lower group velocities and Q values in the same frequency ranges than do the higher modes. These considerations justify the proposed modifications to Aki's theory outlined above.

Contrary to scattering theories in random media, such as Chernov's (Chernov, 1960), radiation patterns of such equivalent sources do not have the strong forward scattering components, but rather would radiate with less directionality (Miles, 1960; Aki and Richards, 1980). This provides justification for assuming no directionality for the scattered radiation in this study.

Computation of Coda Characteristics

There are several approaches to the measurement of crustal Q using measurements on the L_g coda. The simplest is the method used by Herrmann (1980) that involves only time domain measurements on the recorded traces. This approach, although simple, is quite crude and cannot discern finer details such as possible frequency dependence of Q in the crust. It also depends on several limiting factors imposed by the instrument response and the location of the source corner frequency. Another method that involves the use of many sharply tuned band pass filters eliminates many of the above mentioned limitations. This method was used by Aki and Chouet (1975), Tsujiura (1966, 1978), Rautian and Khalturin (1978) and we are using the same method in this report. The application of this method does not pose any difficulties if digital data are available, as was the case in this study. In addition to the theory used by Aki (1969) and Herrmann (1980), we shall derive coda characteristics by allowing the velocities and Q of the scattered waves to be different from those of the primary waves.

Assuming that the group velocity of the primary waves is U1 and that of the scattered waves is U2, we designate the corresponding quality factors as Q_1 and Q_2. The distance from the source to the scatterer is R_1 and the scatterer to receiver distance is designated as R_2. The time after the passage of the primary wave in the coda Δt can then be written as

$$\Delta t = R_1/U_1 + R_2/U_2 - D/U_1 \qquad (1)$$

where D is the distance between the source and receiver. The loci defined by equation (1) for a constant Δt define an ellipse with foci at the source and the receiver for the case $U_1 = U_2$. If $U_1 > U_2$ the curve encloses the receiver but the source may lie outside. The contribution of scatterers located on a segment of length ds of this curve to the power in the coda at time t can be written as

$$dP \sim \exp\left(-2\pi f(R_1/U_1Q_1 + R_2/U_2Q_2)\right)ds/(R_1 \cdot R_2) \qquad (2)$$

assuming that the primary and scattered waves are surface wave modes that decrease as 1/r with increasing distance. f is the frequency.

The right hand side of equation (2) may also need to be multiplied by a directionally varying factor due to the directional properties of scattering. For the case not involving mode conversions, such a factor is not important because the dominant scattering is backwards relative to the direction of the primary waves, and the variation with azimuth in these directions is small (Aki, 1969, 1980; Aki and Chouet, 1975; Chernov 1960). For mode conversion models these factors should be reevaluated, although the extreme differences between the forward and backward scattering coefficients found for scattering of waves of the same kind are probably not valid. This is due to the mismatch in phase velocities in the primary and scattered wave fields and the constructive interference conditions from inhomogeneities with various scale sizes as given by Malin (1978).

The power in the coda can be obtained as a function of time after the arrival of primary waves Δt for various frequencies and can be compared directly to data after integrating along the curves describing the loci of scatterers

$$P = \int_C dP. \tag{3}$$

The trace amplitude is simply $\sqrt{P}$ on the band pass filtered traces. The above formulas can be readily modified to include frequency dependent Q. Normal mode dispersion was neglected in the above formulas since its effect is expected to be unimportant. The above algorithm allows one to compute the ranges of distances from the receiver that contribute to the observed coda energy. The spatial coherence of coda waves can also be easily estimated. While (3) gives the estimate of the coda power spectrum, cross power spectra between two sensors located along a vector $\vec{\Delta r}$ can be readily computed by the formula

$$P(f, \vec{\Delta r}) = \int_0^{2\pi} dP \cdot \exp(i \cdot \vec{k}_\phi \cdot \vec{\Delta r})\, d\phi$$

where ϕ is the azimuth angle, $\vec{k}_\phi$ is the appropriate wavenumber vector, and dP is the scattered wave power coming from the direction ϕ.

The intersensor coherence thus becomes

$$coh(f,\vec{\Delta r}) = P(f,\vec{\Delta r})/P(f).$$

The intersensor coherences computed can be directly compared to observations of ensemble average coherences such as those obtained by Mrazek et al (1980) for various orientations of intersensor spacing relative to the direction of the primary waves.

Let us investigate now some possible implications of such modifications of Aki's theory. Let us start with the properties implied in the original formulation and compare this with the results obtained from unequal wave velocities and Q.

Figure 13 shows the loci of scatterers for a source-sensor separation of 500 km at 10 sec after the primary wave has passed and a similar figure is displayed for T = 40 sec in Figure 15. The first of these figures shows a great difference in geometry at 10 sec that disappears pretty much at 40 sec. Since we are concerned with the late coda it would appear that the modification is unimportant. If one, on the other hand, examines the distance distribution of the scattered energy contributions, the presumed inequality of the associated Q values makes a great difference. In Figure 16 we show the cumulative energy plotted as a function of distance for the case of equal velocities and Q's. In such cases both sides of the scattering ellipses contribute evenly, resulting in a directional distribution focused along the large axis of the ellipse. Such directionality cannot explain the low coherence in the main part of L_g found by many researchers. On the other hand, for the case of unequal Q, most of the scattered energy comes from the near side of the ellipse and the directions the scattered waves come from are more broadly distributed. In addition, both the directional and the distance distributions are frequency dependent as shown in Figures 17a and 17b such that higher frequencies come from the closest part of the loci of scatterers. In most cases, the far end of the loci (they are no longer ellipses) contribute little. A frequency dependent effective Q in the crust can make this situation even more complex.

If one computes the intersensor coherences for the case of equal velocities and Q values for both primary and scattered waves, the coherences turn out to be considerably higher than those obtained from the case of unequal velocities and Q values. Figures 18 to 21 show some examples of this for the cases of T = 10 sec and T = 40 sec. These values of T of course are too

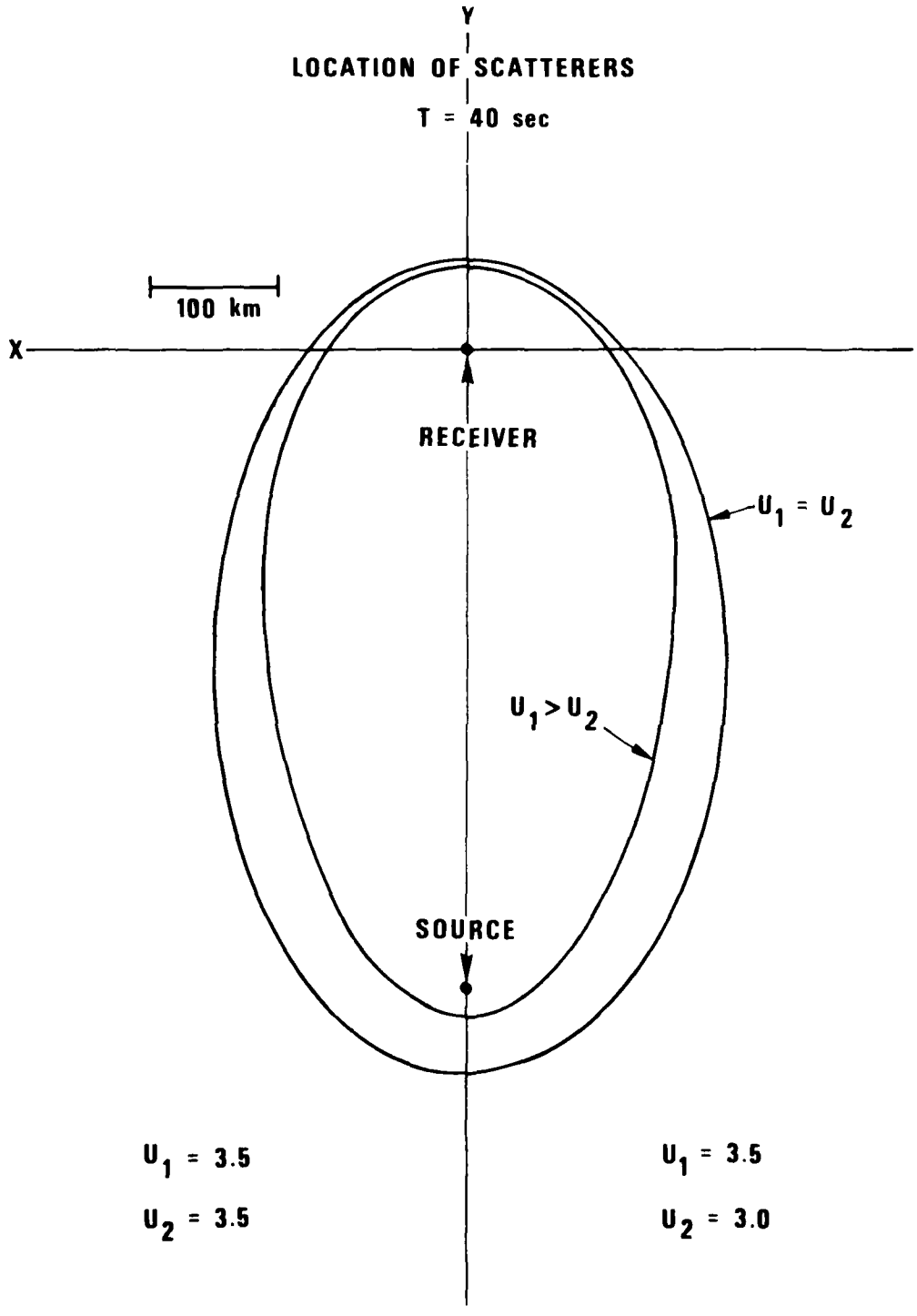

Figure 15 Location of the scatterers at T = 40 s after the passage of the primary wave for the cases $U_1 = U_2 = 3.5$ km/sec and $U_1 > U_2$ where $U_1 = 3.5$ km/sec and $U_2 = 3.0$ km/sec.

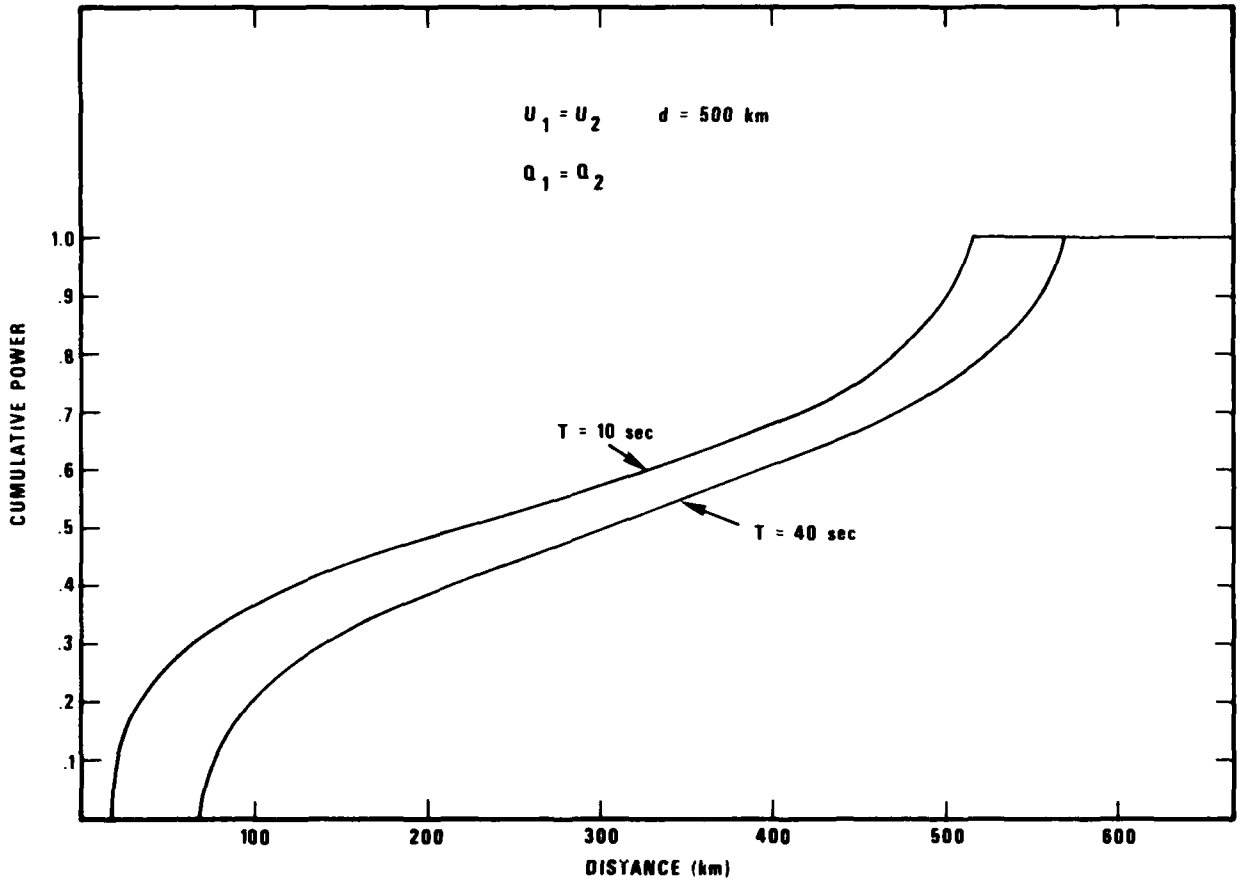

Figure 16 Cumulative energies as functions of distance from the receiver for the case involving equal velocities for the primary and scattered waves.

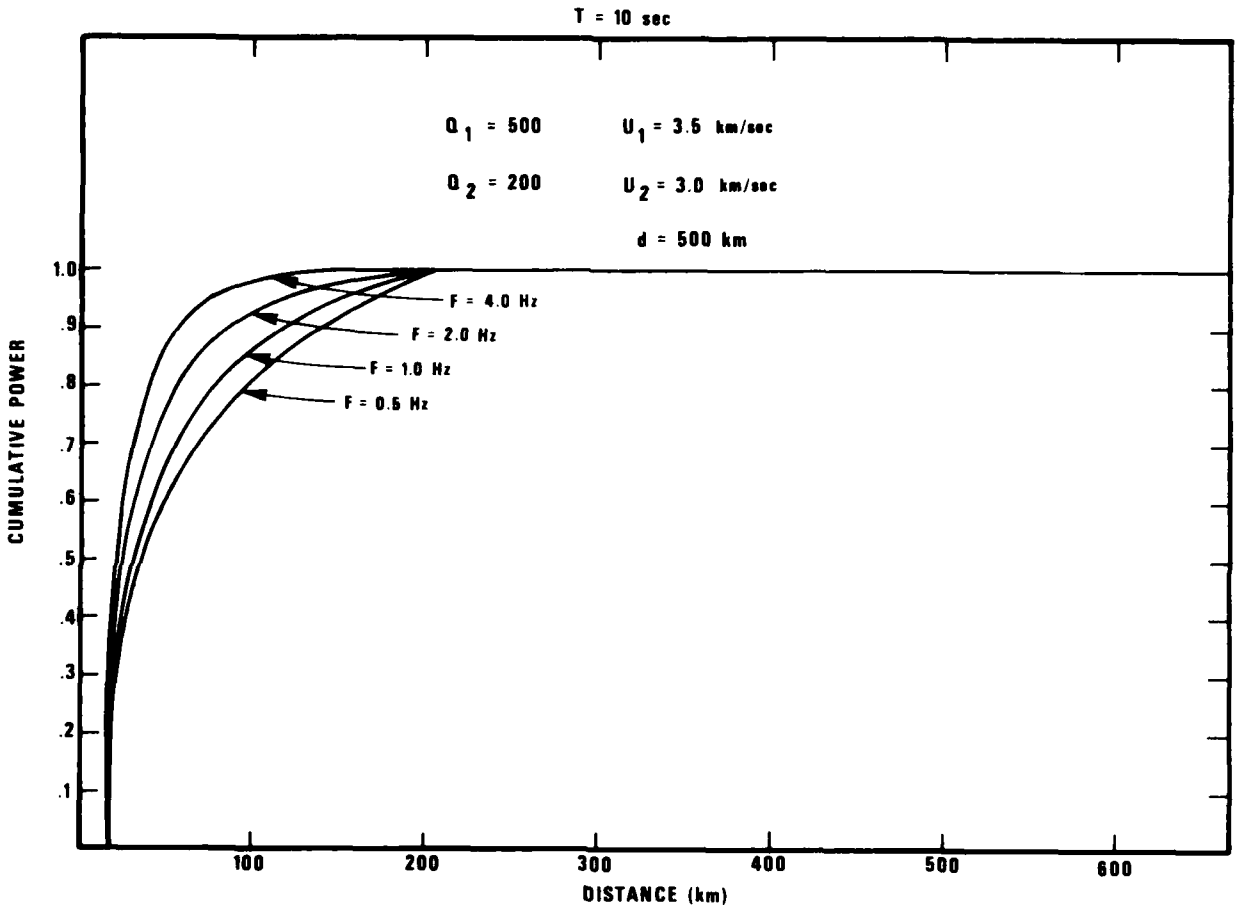

Figure 17a Cumulative energy in the scattered wavetrains as functions of frequency and distance for the case of unequal velocities and Q values in the scattered and primary waves. Most of the scattered energy comes from scatterers in the vicinity of the station.

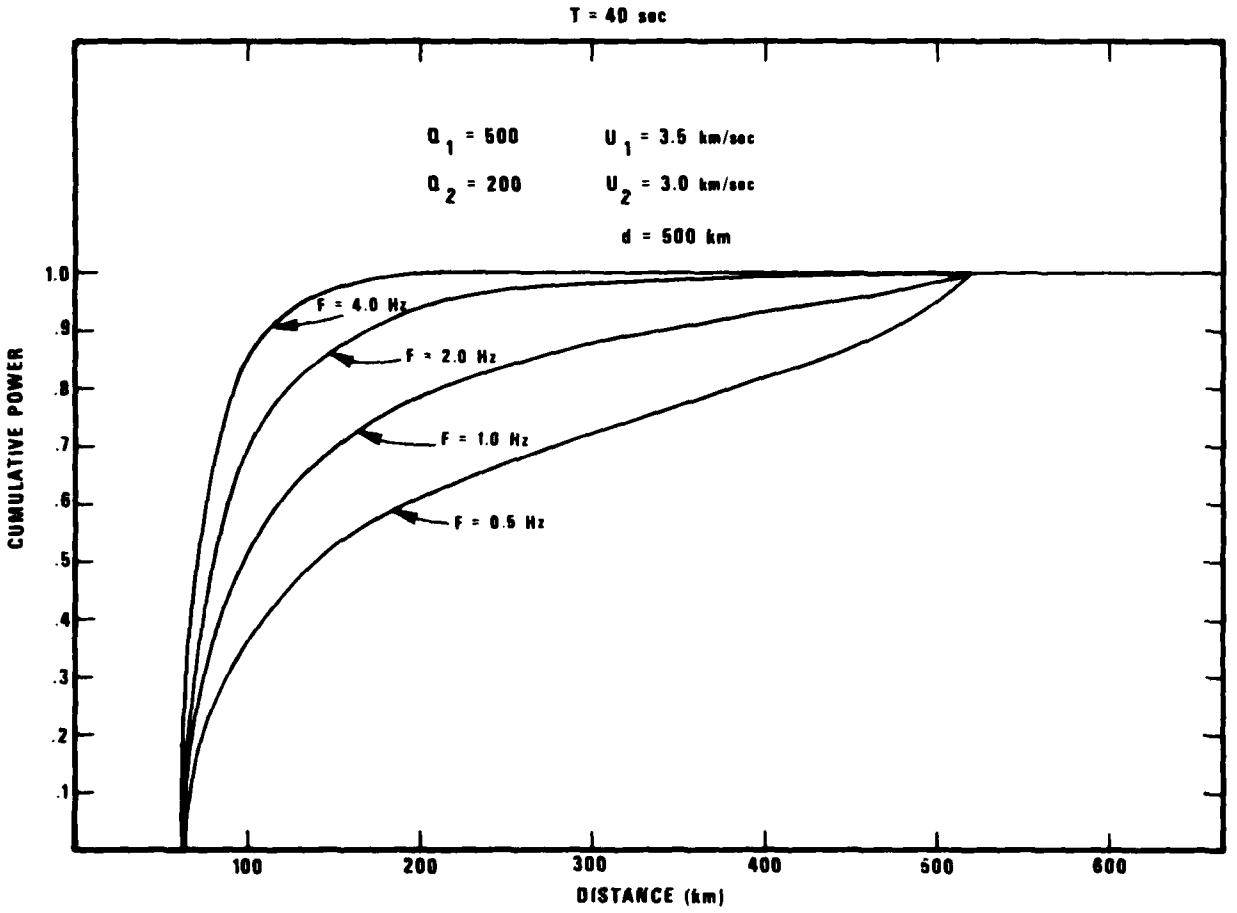

Figure 17b Cumulative energy in the scattered wavetrains as functions of frequency and distance for the case of unequal velocities and Q values in the scattered and primary waves. Most of the scattered energy comes from scatterers in the vicinity of the station.

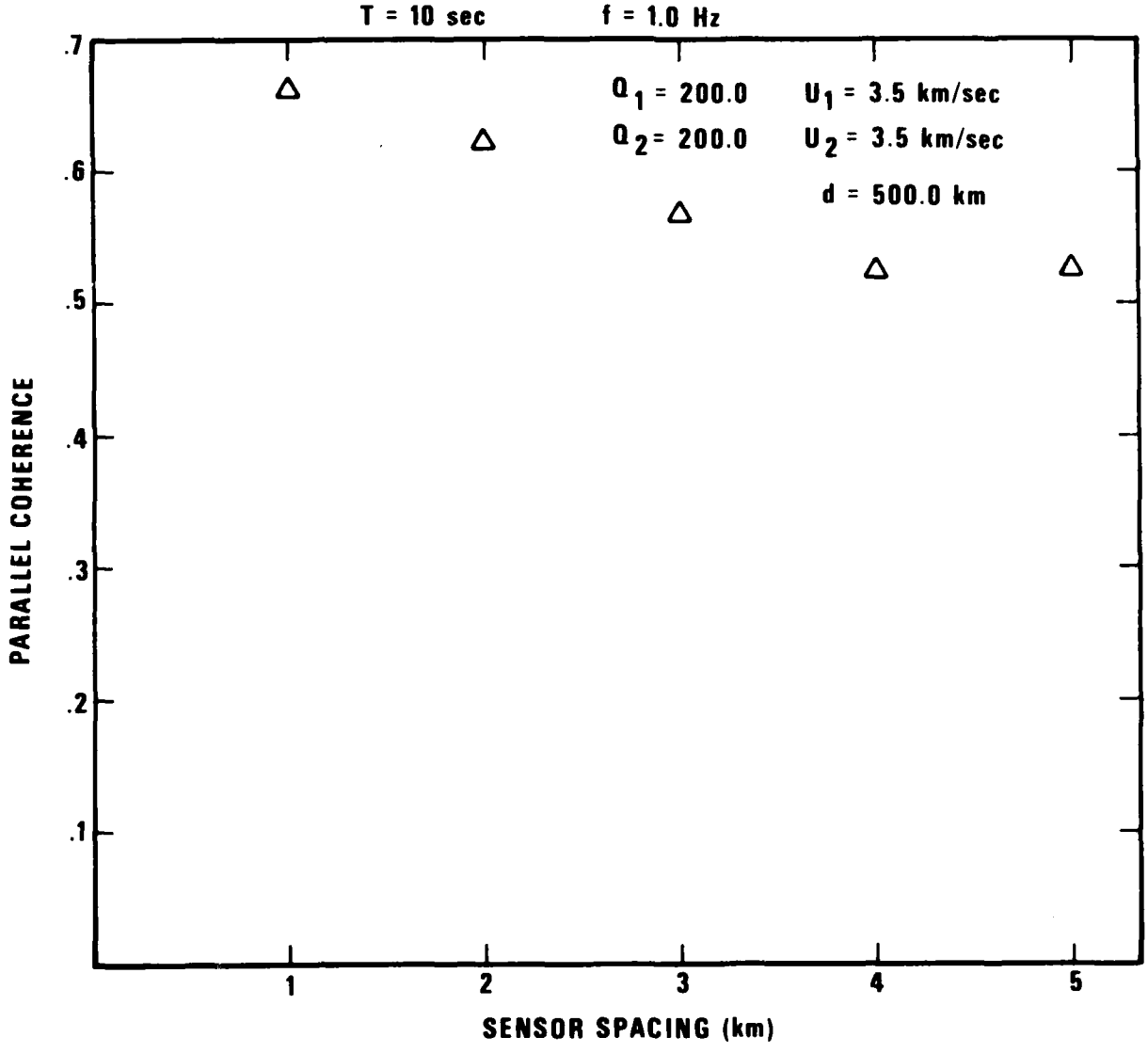

Figure 18 Intersensor coherences in the direction of propagation as functions of sensor spacing for the case of equal velocities and Q's at T = 10 sec.

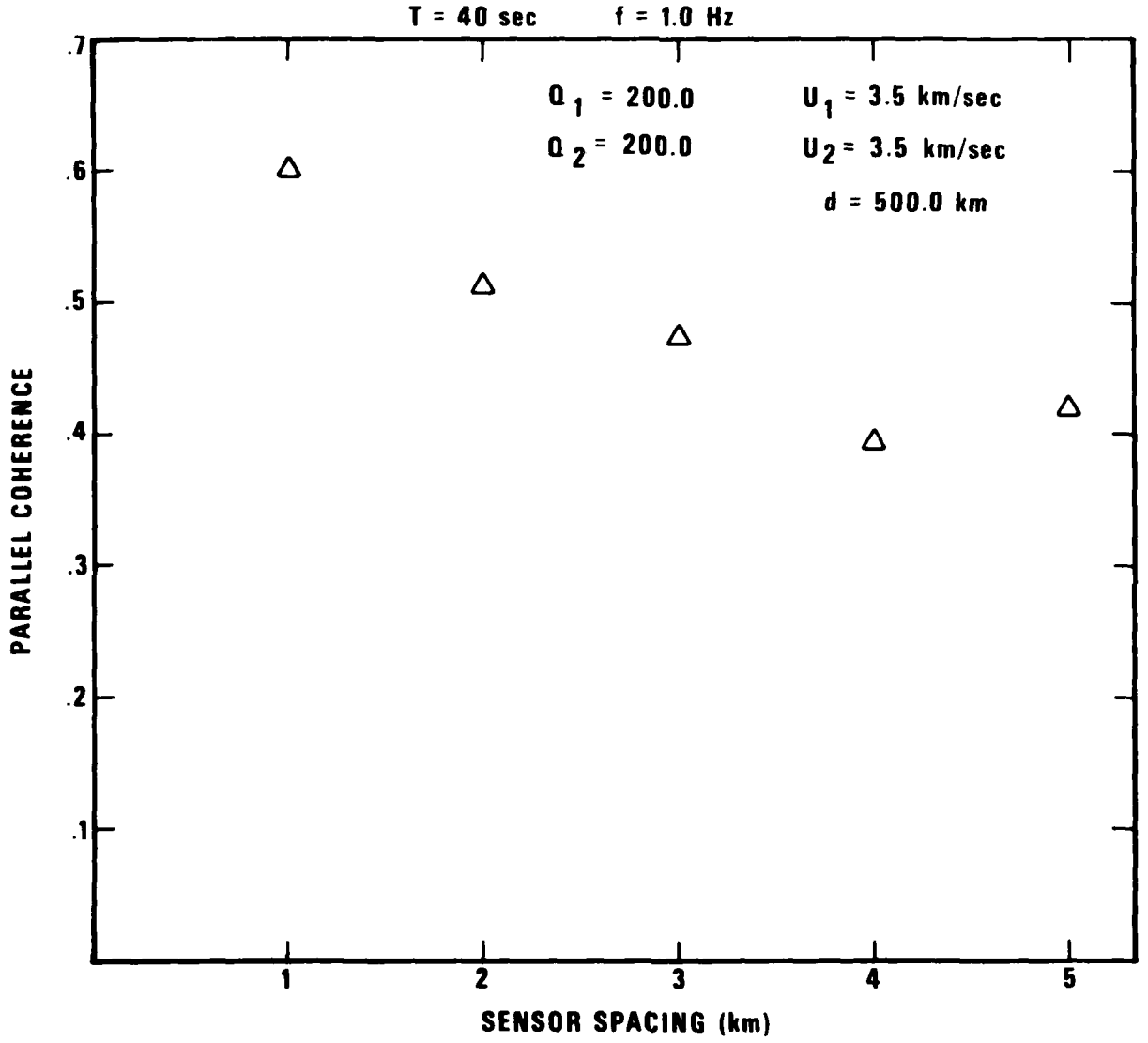

Figure 19 Intersensor coherences in the direction of propagation as functions of sensor spacing for the case of unequal velocities and Q's at T = 10 sec. Note that these coherences are lower than in *Figure 18*.

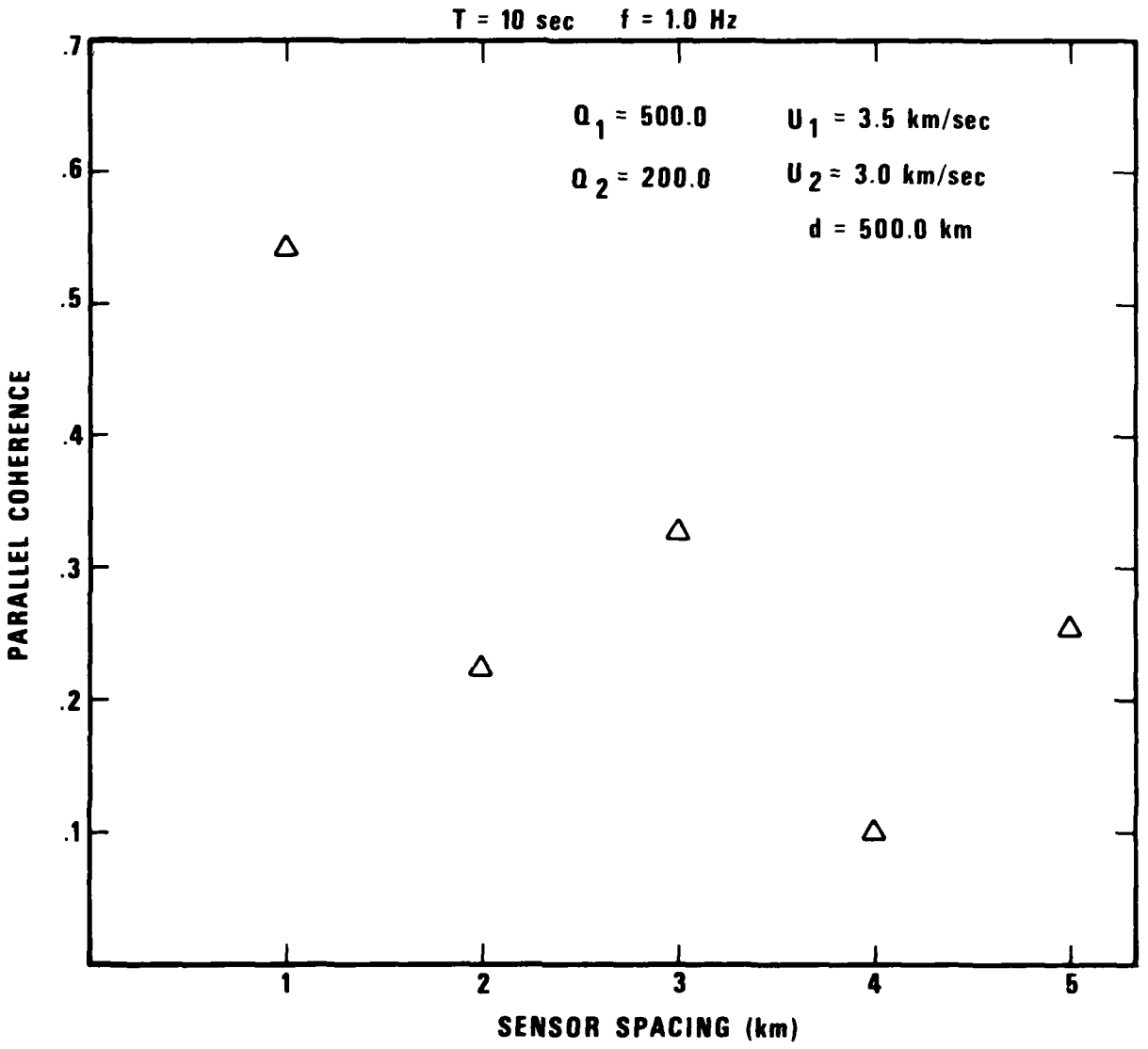

Figure 20 Intersensor coherences in the direction of propagation as functions of sensor spacing for the case of equal velocities and Q's at T = 40 sec.

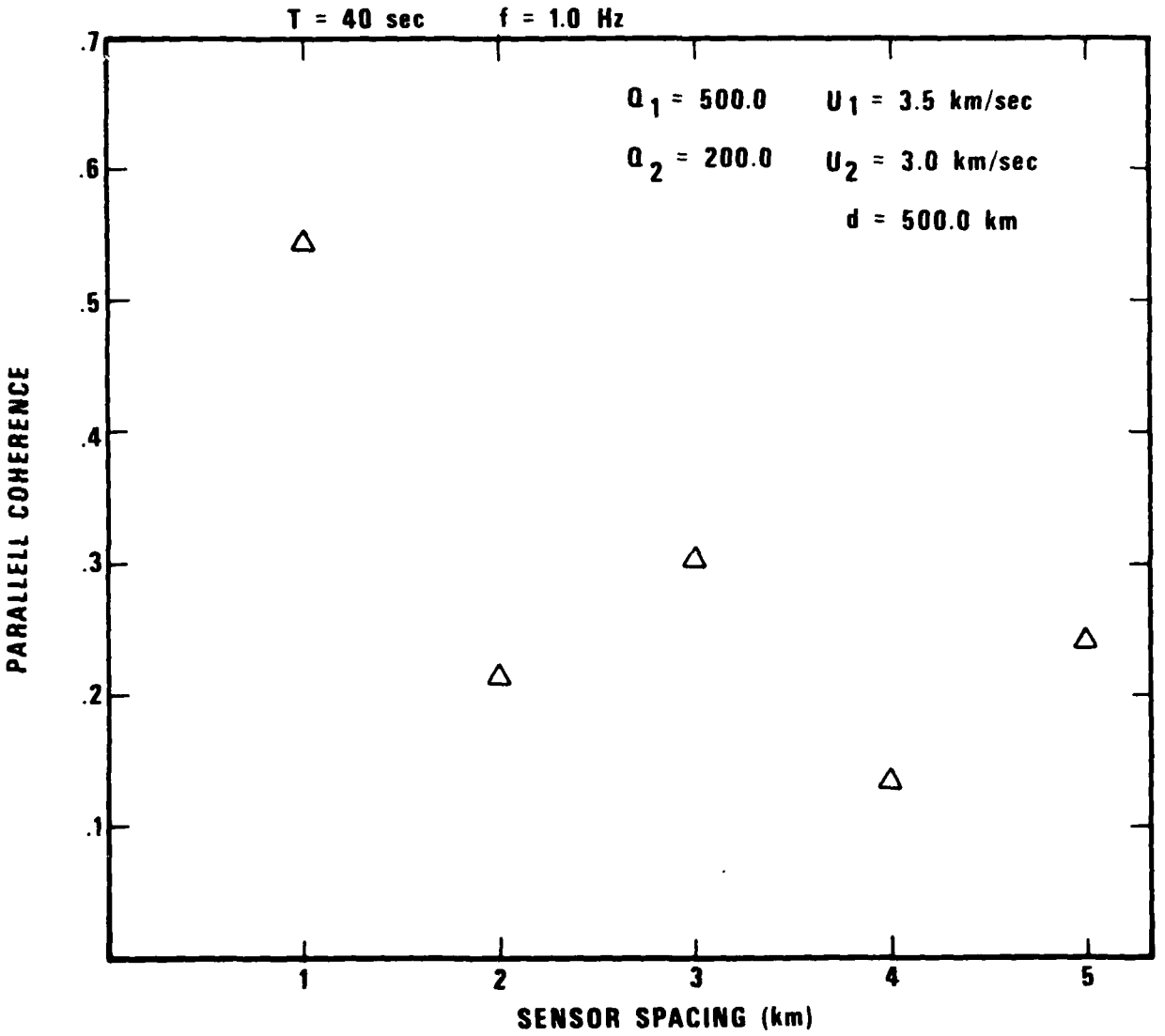

Figure 21 Intersensor coherences in the direction of propagation as functions of sensor spacing for the case of unequal velocities and Q's at T = 40 sec. Note that these coherences are lower than in Figure 19.

small for the late coda, but are applicable to the main part of the L_g wavetrain. A mixture of any appreciable amount of scattered waves with the main part of L_g can easily degrade the coherence to the levels that were observed at many sites.

Study of the L_g Coda

While the main wavetrain of L_g and the early coda may consist to a large degree of low order scattered modes, later in the record the contribution from such waves must diminish with increasing time due to the lower effective Q of such waves. It is likely therefore that the later coda has a modal composition that is closer to that of the primary wave. If the coda analysis as proposed by Aki (1969), Aki and Chouet (1975) and Herrmann (1980) is used for measuring the effective crustal Q, this is an essential condition for the validity of the results. Let us first investigate the structure of the main L_g wavetrain by passing the record through some narrow band pass filters. Figure 22 shows a band pass filtered record of an event at RKON, a presumably high Q station. The length of the L_g wavetrain varies with frequency; at low frequencies, it is longer than at high frequencies. This is in accordance with the expectations of Aki's (1969) theory. A similarly filtered signal at the same station, however, reveals that much of this is due to the presence of the fundamental mode R_0 buried in the coda of L_g (Figure 23). This wavetrain of R_0 is quite distinct in the .5 - 1.5 and the 1.0 - 2.0 Hz bands. It has a retrograde particle motion and a radial to vertical amplitude ratio of about .6 as appropriate to the fundamental mode. If we had interpreted this in terms of a crustal Q, our conclusions would have been in error. It is thus necessary to go to the late parts of the record where even the coda of the fundamental mode is negligible. Unfortunately, this is not easy to do, and we believe that much of the time domain work done by Herrmann may be biased by such effects. In such work it is necessary to remain below a certain magnitude threshold such that the corner frequency is above the highest frequencies picked, but this requirement conflicts with the need for high signal to noise ratio in the late coda. The only solution of the problem is to use digital or analog data with high dynamic range, drop the magnitude limitations and use band pass filtering as was done by Aki and Chouet (1975). If this method is used large events with high S/N ratios can be used and the dependence

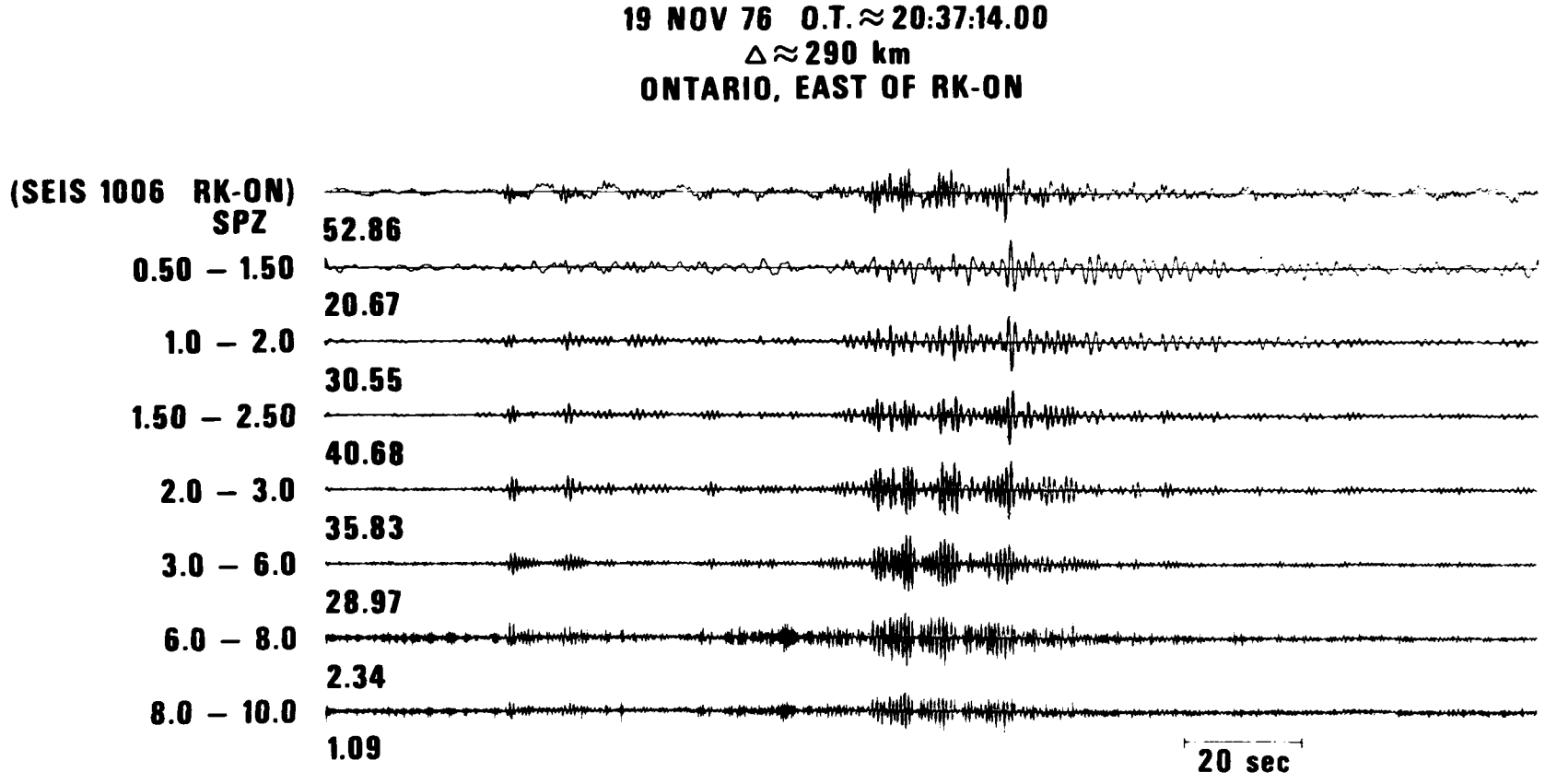

Figure 22 Band pass filtered records of an event in Ontario recorded at RKON.

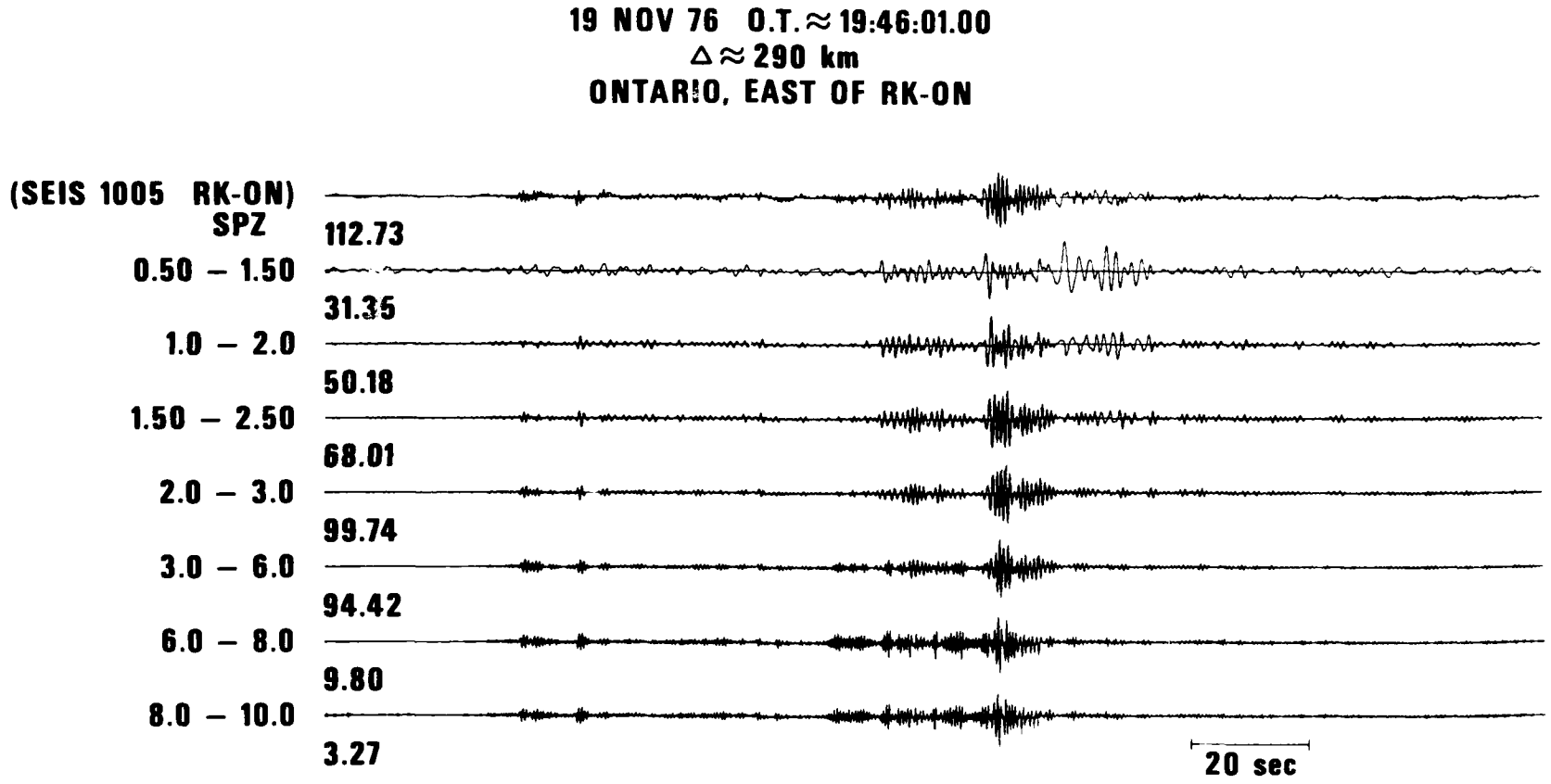

Figure 23 Band pass filtered records of an event in Ontario recorded at RKON. A wavetrain, presumably R_0, is seen in the coda of L_g.

of Q on frequency can be investigated since the S/N ratio remains high in most frequency bands. Another interesting and revealing example is a pair of recordings on SPT at the NTS stations OB2NV granite, the station YFNV on the sedimentary basin at Yucca Flats and NT2NV on the Pahute Mesa. The band pass filtered traces (Figures 24, 25, 26) at OB2NV show a short L_g wavetrain followed by a recognizable L_o contribution. If we disregard this, L_g itself has about the same lengths in all bands. The YFNV recording in sharp contrast shows a prolongation of the wavetrain in all bands. This has been observed before (Barker et al, 1980), but this analysis also shows that while the prolongation of the wavetrain is minor at high frequencies, it is the greatest in the .5 - 1.5 Hz band. The distance between the stations at Yucca Flats and OB2NV is only about 17 miles and the seismic velocities are not much different below depths of 500 meters. The differences in the visible wavetrains must thus be confined to those depths shallower than this, and this implies that the long codas at Yucca Flats must be due to low order modes confined to the vicinity of the stations at Yucca Flats. Aside from our finite difference simulations as described by Barker et al (1980), other researchers also reported similar findings, (Boore et al, 1971; Bard and Bouchon, 1980a,b). These figures illustrate vividly how dangerous it is to interpret codas without any regard to site geology.

Analysis of the intersensor coherence of stations at Yucca Flats showed that the long wavetrain acquired by the L_g phase by passing through the sedimentary valley is not propagating energy, since there is no measurable coherence between even the closest of the stations. Coherences and cross correlation functions are below the significance level, and thus no velocity measurement is possible.

Let us proceed now to analyze the late coda of some events after the arrival of the fundamental mode. Starting with the shield station RKON, we show the coda of two events in Figures 27a and 27b. The unfiltered trace is on the top, followed by the band pass filter outputs. The bars at the end of the traces show the background noise level. Unfortunately, for most of the traces, the background level is too high to make any conclusions about Q values. The superposed solid and dashed lines show the coda decay functions computed by the algorithm described above for the Q values of 600 and 1000

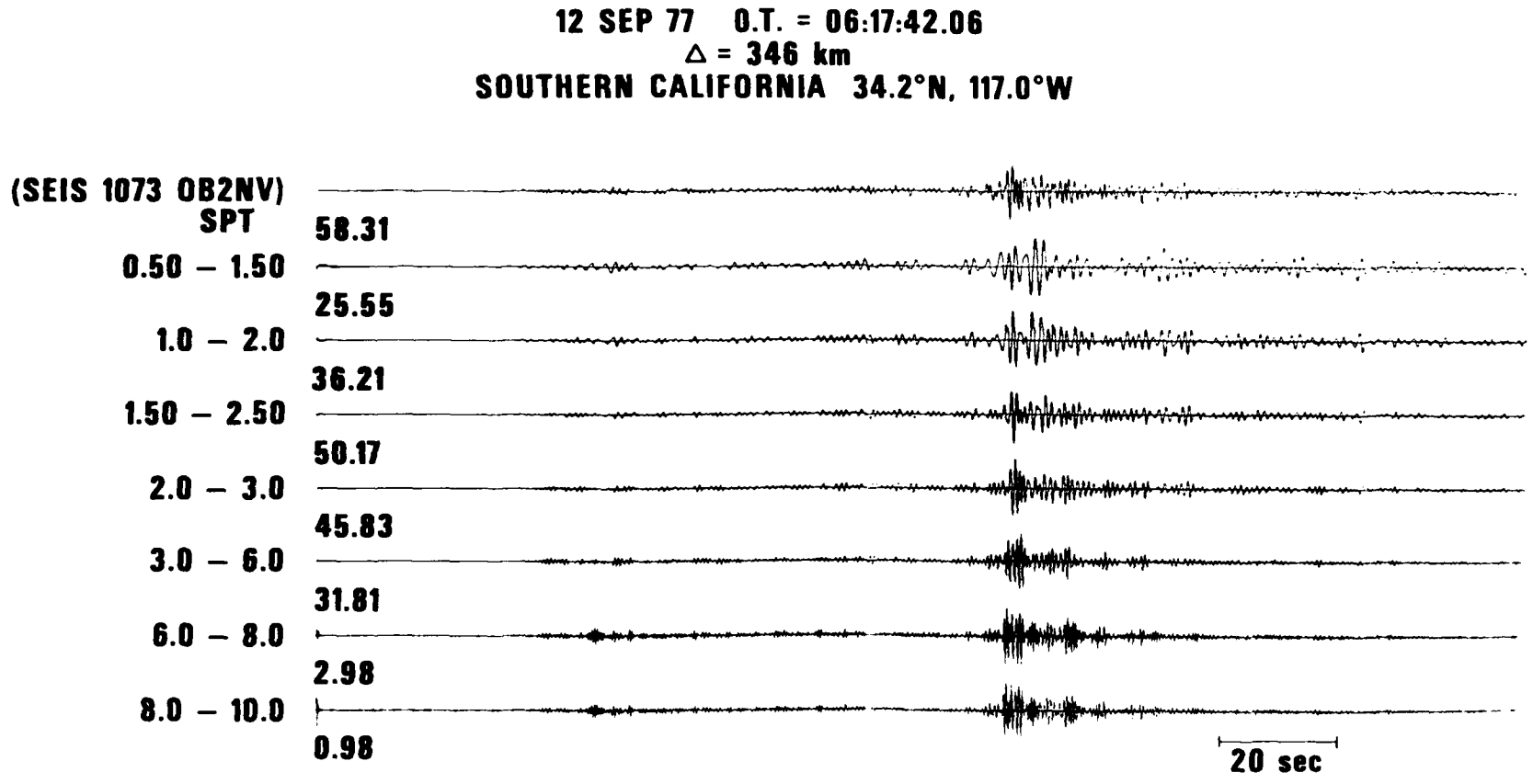

Figure 24 Band pass filtered records at OB2NV showing a L_o mode buried in the coda of L_g.

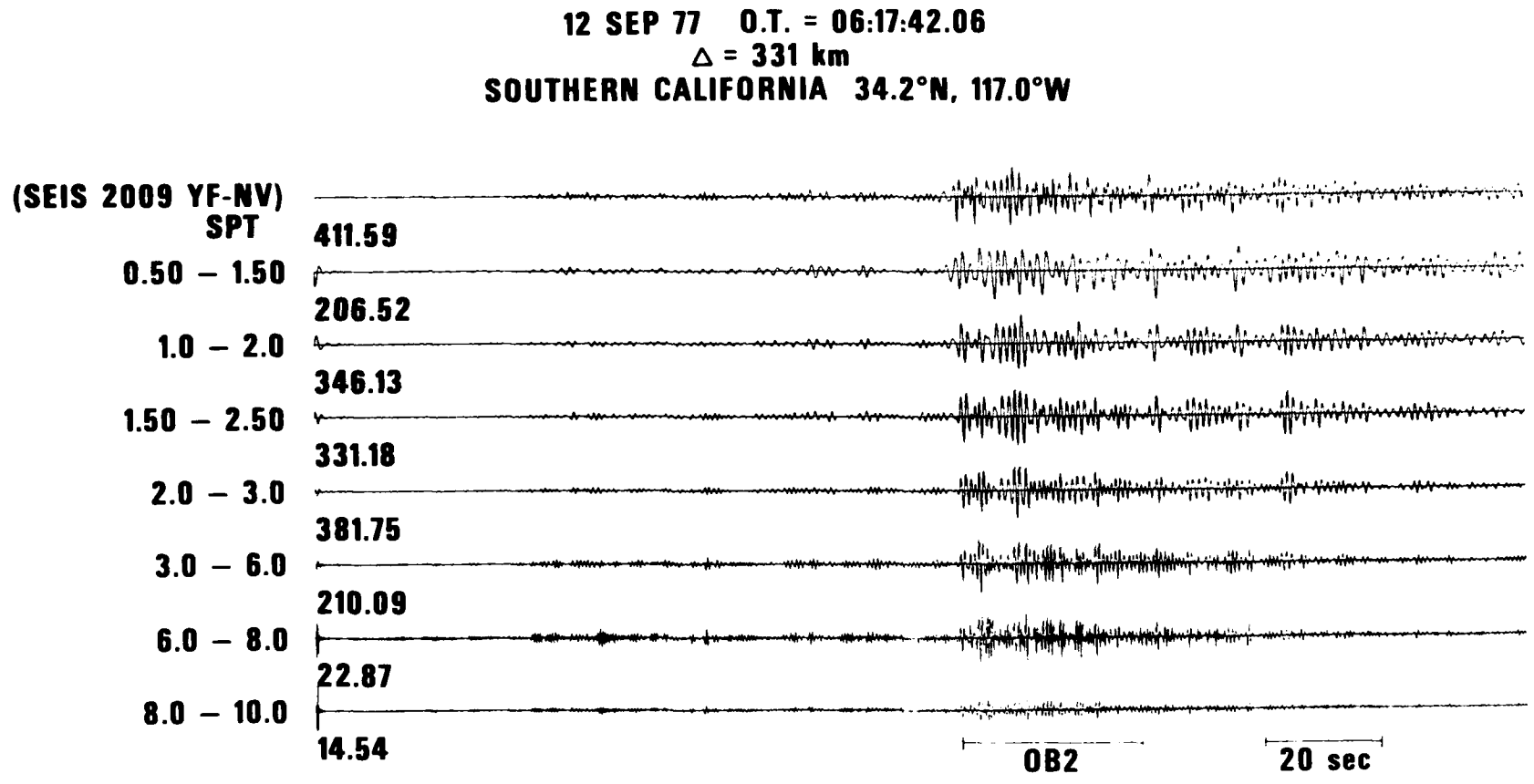

Figure 25 Band pass filtered seismograms of an event in southern California as observed at YFNV and OB2NV. Most of the site resonance occurs at the low frequencies. The time interval marked with OB2 shows the length of the $L_g + L_o$ wavetrain at OB2NV, L_o marks the location of L_o wavetrain at OB2NV if present.

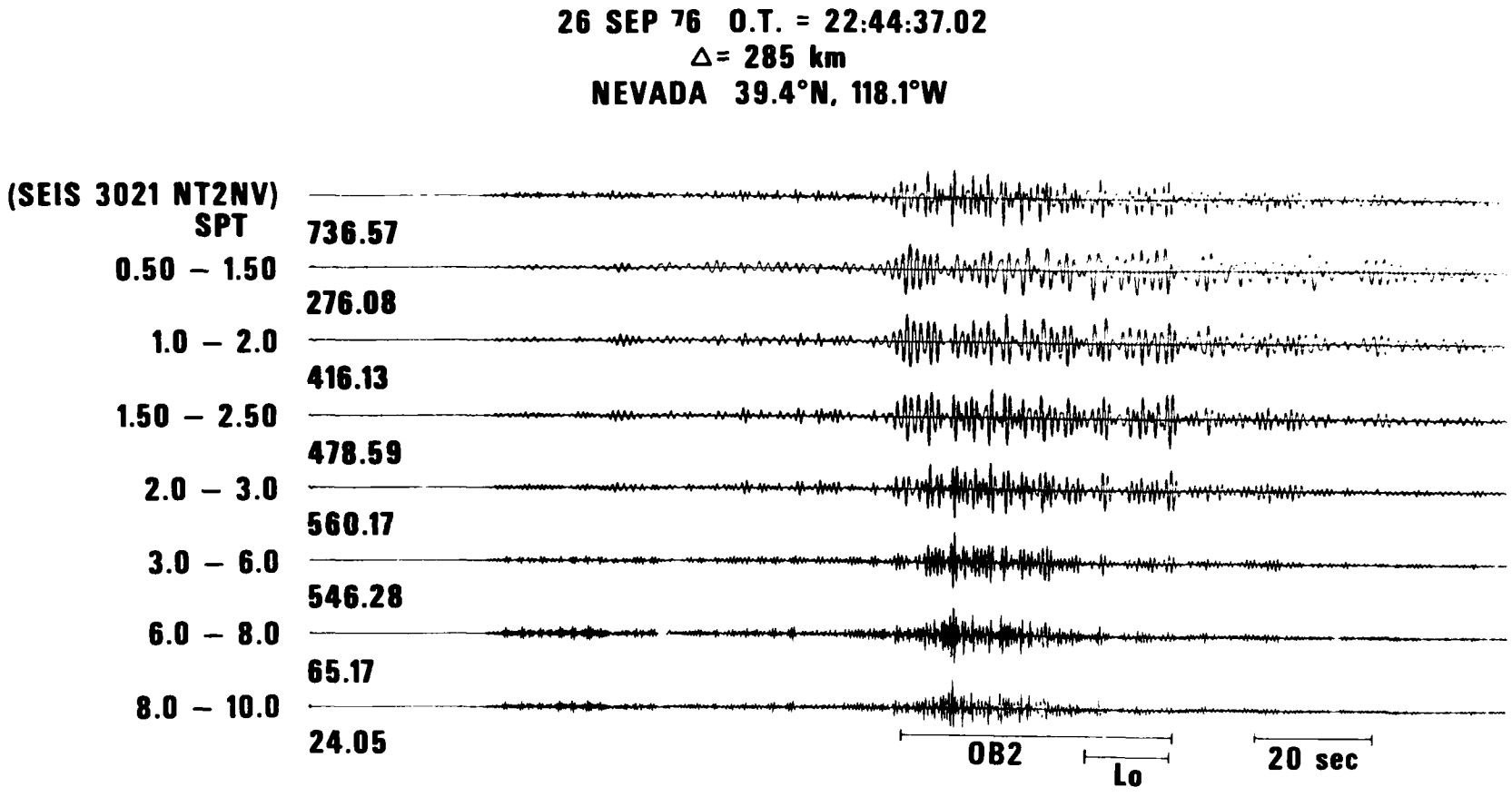

Figure 26 Band pass filtered seismograms of an event in southern California as observed at YFNV and OB2NV. Most of the site resonance occurs at the low frequencies. The time interval marked with OB2 shows the length of the $L_g + L_o$ wavetrain at OB2NV, L_o marks the location of L_o wavetrain at OB2NV if present.

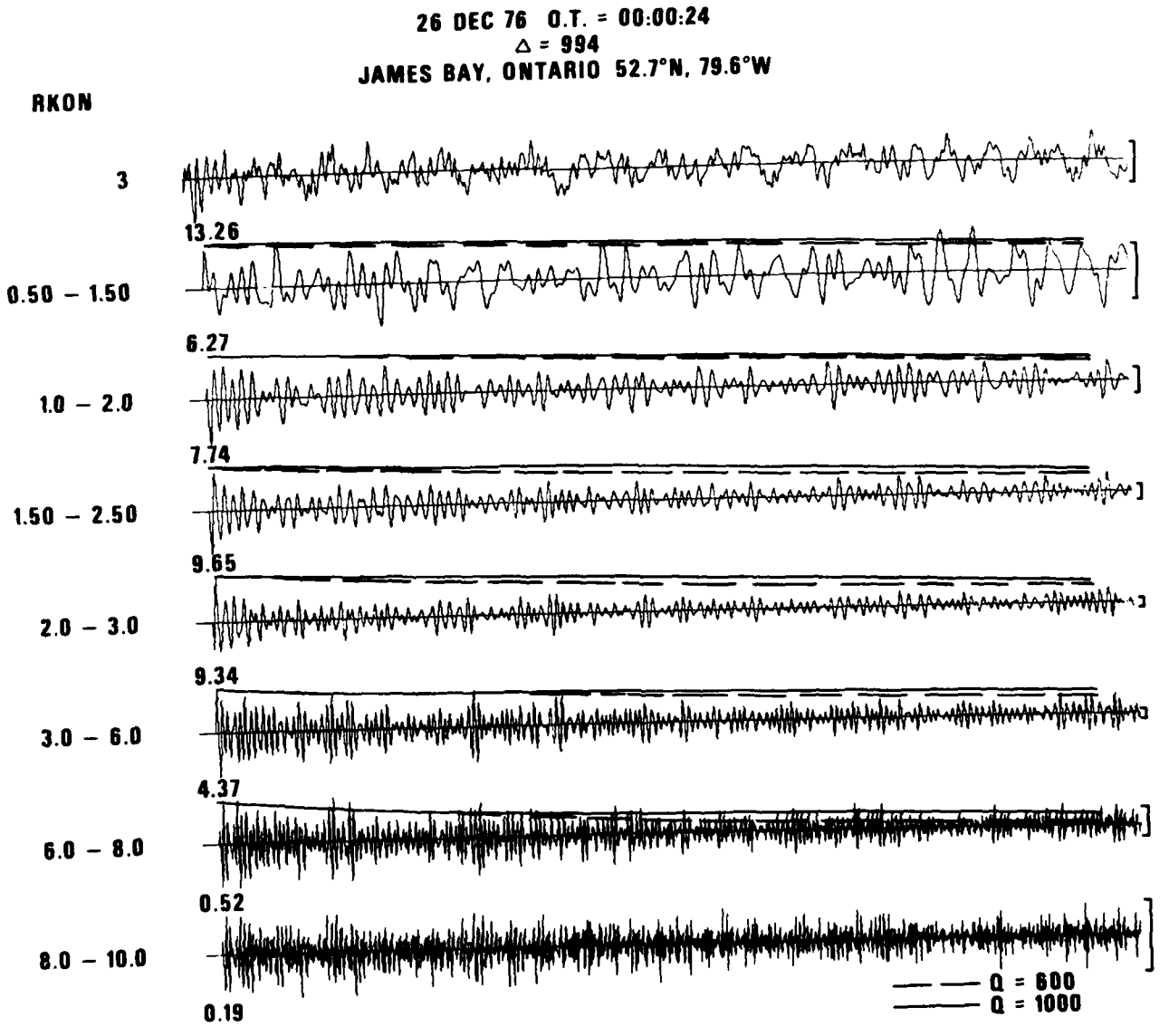

Figure 27a Band pass filtered codas of L_g at RKON with the theoretical coda shapes for Q = 600 and Q^g= 1000. Bars show background noise levels.

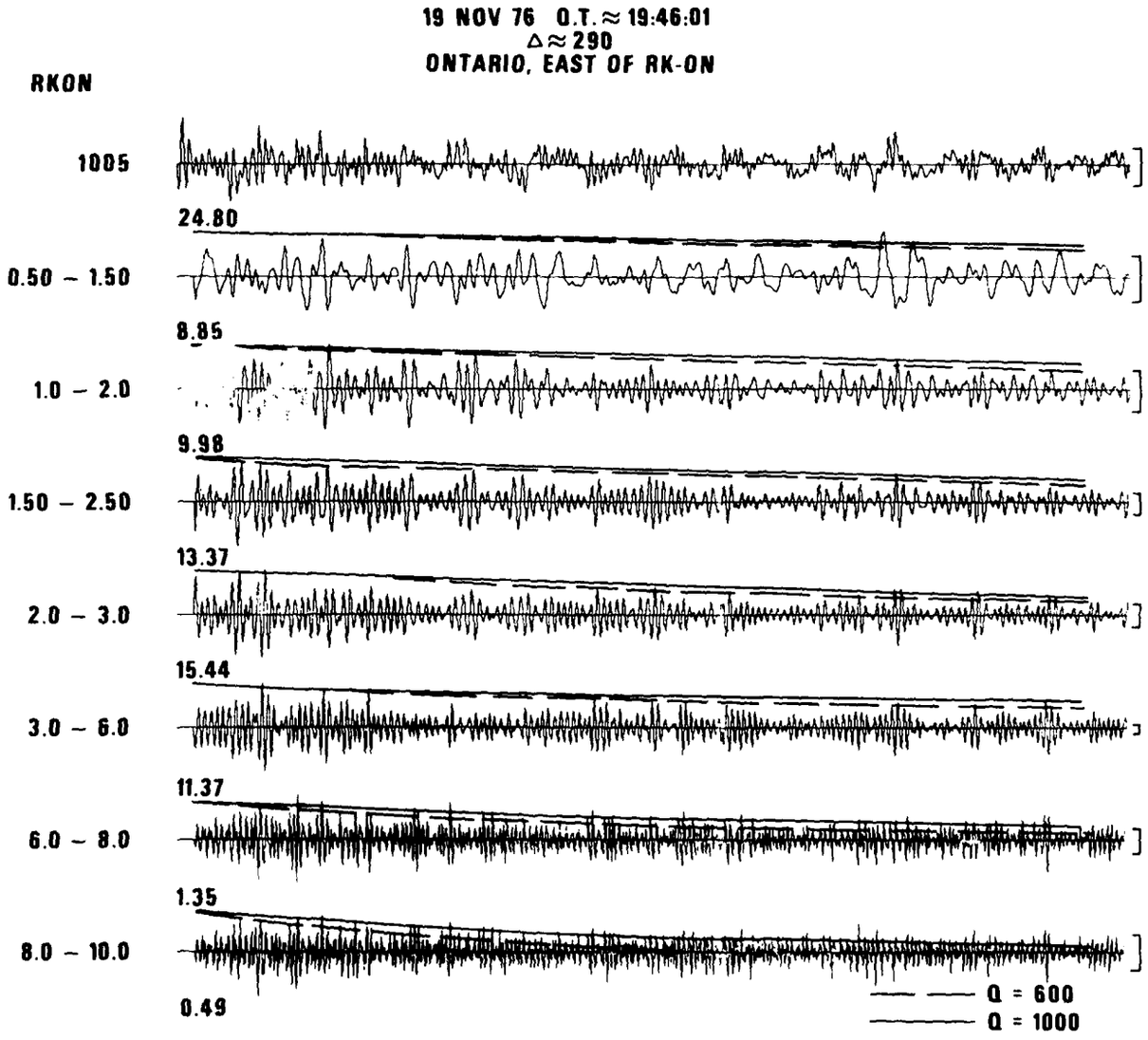

Figure 27b Band pass filtered codas of L_g at RKON with the theoretical coda shapes for Q = 600 and Q^g= 1000. Bars show background noise levels.

respectively. Since only the traces in the 1.5 to 6 Hz band have an acceptable S/N ratio, the only conclusion that can be made is that the Q is high, being in the 600 - 1000 range, and in agreement with the studies of others studying this region. In these fits the decay rate with time is being matched. On some of the traces, the absolute amplitude of the filtered trace is low due to normalization to the largest peak in the plot routine used. Nevertheless, the decay rates match if one makes allowance for this. In the new improved version of the programs this defect has been corrected by smoothing the envelope of the filtered traces.

Examining the similar recordings at OB2NV, the NTS station on granite (Figures 28a and 28b), and superposing the lines for Q = 200 and Q = 600, we find that Q = 200 fits the low frequencies quite well, but the high frequency codas are fitted better with Q = 600. This is unmistakable since the noise levels are relatively low. This is a confirmation of the observations of Chouet (1976), Rautina and Khalturin (1978), Mitchell (1980) and others indicating the frequency dependence of the apparent Q in the crust. This observation is of great importance for the detection of decoupled shots. If the Q in the crust did not depend on frequency there would be no hope of seeing decoupled shots at high frequencies in tectonic regions (Murphy, 1980). The indicated increase of Q with frequency implies that Q at the high frequency end of the spectrum may not be as different in regions of various tectonic regimes as some studies (such as Herrmann's, 1980) indicate. Aki (1980) puts the limit of convergence at 25 Hz, beyond which the crustal Q would be the same in most regions. Since our data do not extend to such high frequencies, we cannot confirm this.

Investigation of the crustal Q is not only of academic interest. Since regional phases are propagating in the crust and the uppermost part of the mantle, the detectability of such phases is severely affected by any regional variation of the crustal Q (Murphy, 1980). It has also been found by some investigators that cavity decoupling at high frequencies may be less effective relative to lower frequencies (Terhune et al, 1979; Rodean, 1979). Any increase of Q with frequency would be extremely favorable for the detection of small and decoupled events. It is thus not only the regional variations of the average Q that are important (Herrmann, 1980) but also the precise form of frequency dependence, if any. Using analog or digital recordings with dynamic range, as was done here, is necessary for such studies.

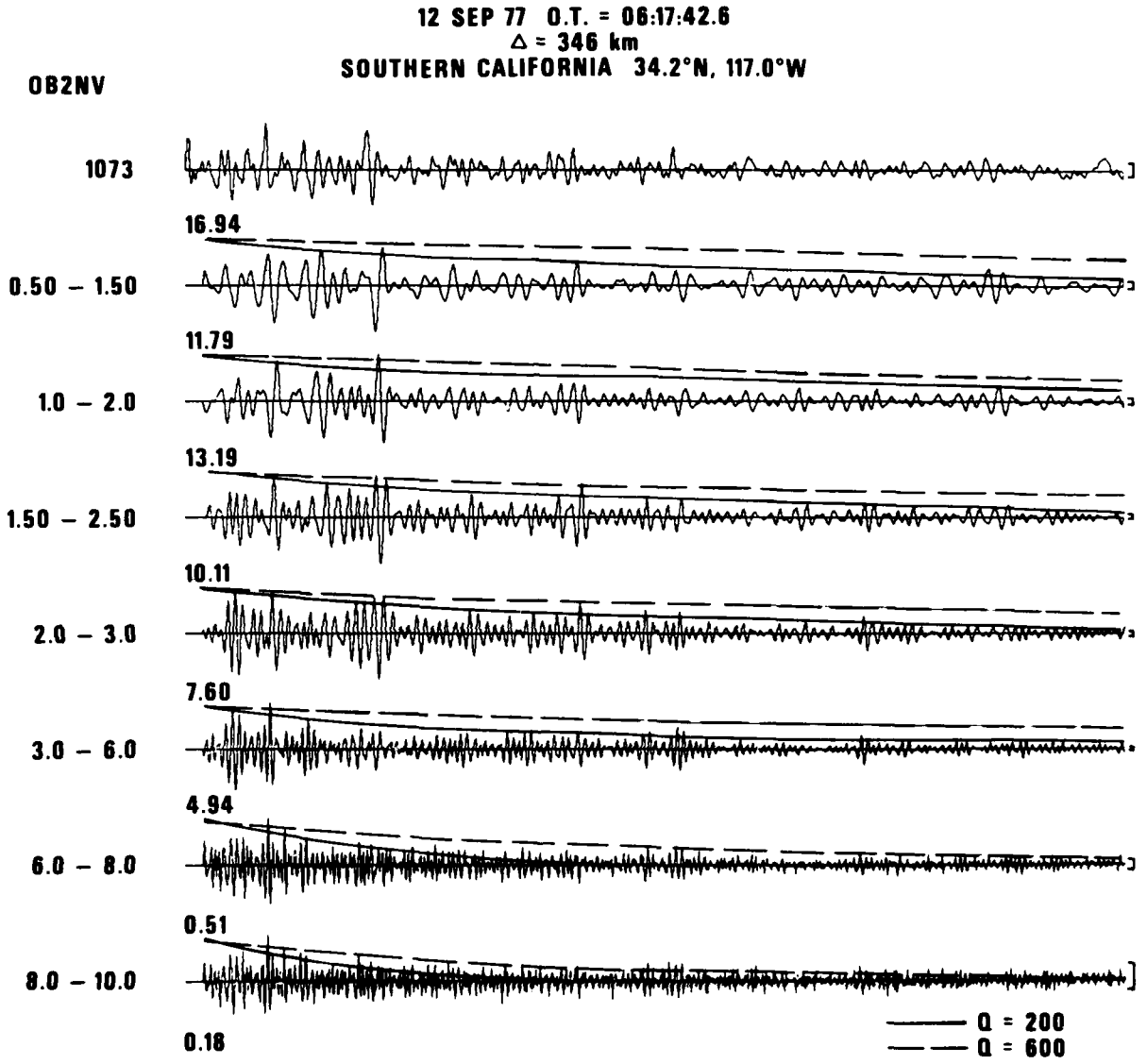

Figure 28a Band pass filtered codas of L_g at RKON with the theoretical coda shapes for Q = 200 and Q = 600. There are indications of an increase of Q with frequency. The low Q = 200 that fits at low frequencies does not fit at high frequencies where the Q = 600 fits better. Bars show background noise levels.

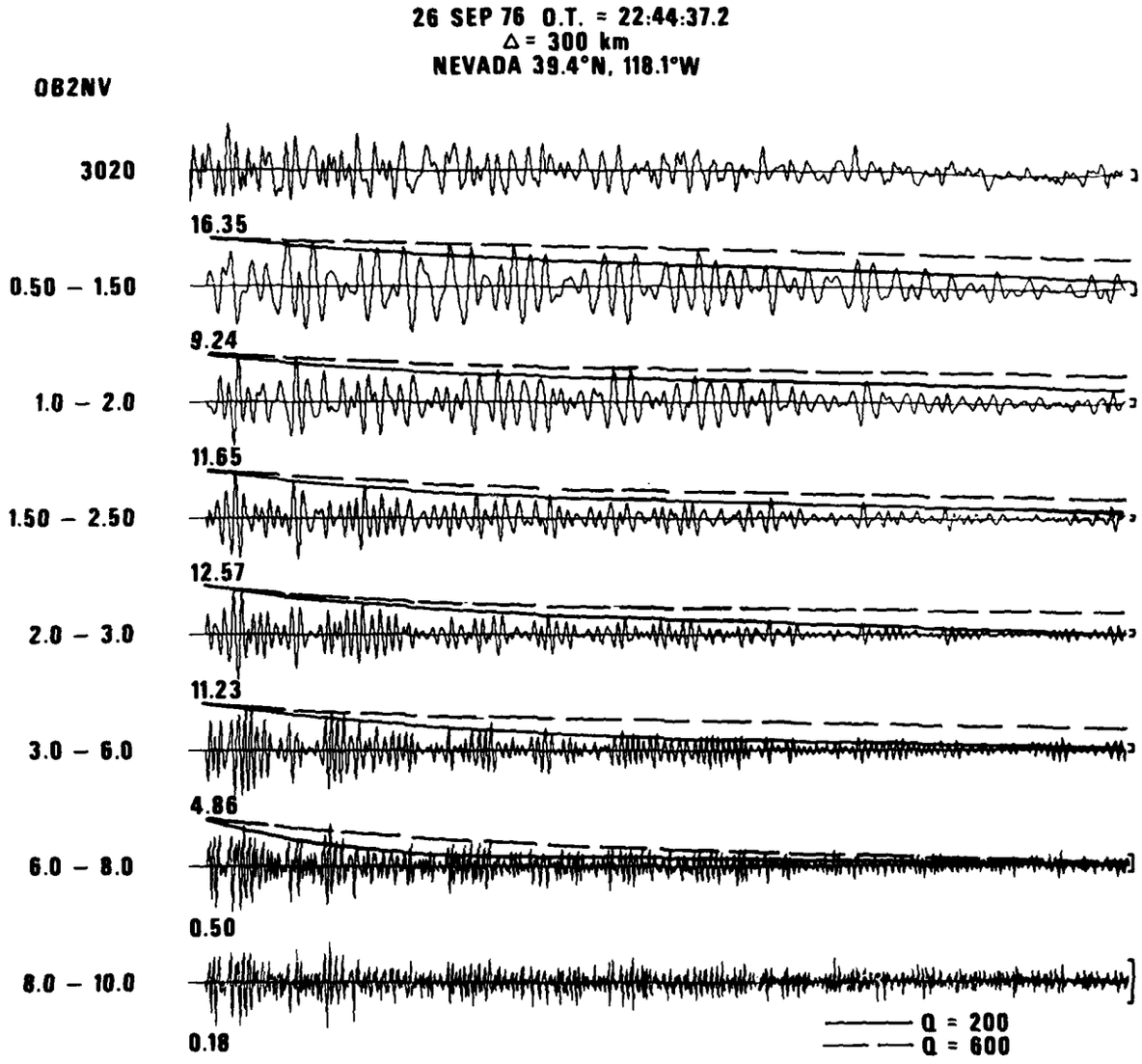

Figure 28b Band pass filtered codas of L_g at RKON with the theoretical coda shapes for Q = 200 and Q = 600. There are indications of an increase of Q with frequency. The low Q = 200 that fits at low frequencies does not fit at high frequencies where the Q = 600 fits better. Bars show background noise levels.

CONCLUSIONS

Amplitudes of the regional phases P_n, P_g and L_g are significantly increased by local sedimentary structures. The general shapes of the L_g wavetrains are also altered; on sedimentary sites the maximum in L_g arrives later and there is a tendency for ringing, prolonging the wavetrains. These effects must be considered if L_g wave envelopes or group arrival velocities (Pomeroy and Chen, 1980) are to be used for discrimination.

L_g wave envelope characteristics and intersensor coherence structures cannot be explained in terms of simple normal mode propagation from the source to the receiver. Such theory would predict spatial coherences much higher than observed.

Concentration of lateral inhomogeneities with large velocity contrasts near the surface facilitates the scattering of primary energy in L_g and other regional phases into lower order modes, with special facility to conversion into the fundamental mode. Such scattered low order modes, that incidentally have a low effective Q_β also can explain the low coherences in L_g and other regional phases. The presence of these low order modes is indicated directly by observations at Yucca Flats.

Analysis of the codas of regional events at RKON by band pass filtering and fitting of coda envelopes gave a crustal Q_β in the 600 to 1000 range. Similar analysis of data at OB2NV showed a fit of Q = 200 at low frequencies (.5 - 2.5 Hz) range and 600 at frequencies in the 3 - 8 Hz range. These observations tend to confirm the frequency dependence of the crustal Q_β also noted by other workers. Such variations in the crustal attenuation are of great importance in detecting small and decoupled explosions at regional distances.

ACKNOWLEDGEMENT

The authors wish to thank Ms. Peggy Marshall, Ms. Liz Tobin and Mr. Tom McElfresh for their help in this report.

REFERENCES

Aki, K. (1980). Scattering and attenuation of shear waves in the lithosphere, J. Geophys. Res., 85, 6496-6504.

Aki, K. (1969). Analysis of the seismic coda of local earthquakes as scattered waves, J. Geophys. Res., 74, 615.

Aki, K. and B. Chouet (1975). Origin of coda waves, source attenuation and scattering effects, J. Geophys. Res., 80, 3322.

Aki, K. and P. G. Richards (1980). Quantitative Seismology-Theory and Methods, W. H. Freeman and Company, San Francisco, 721-759.

Alsup, S. A. (1972). Estimation of upper mantle Q beneath the United States from P_n amplitudes, Ph.D. Thesis, George Washington University, Washington, D.C.

Bard, P. Y. and M. Bouchon (1980a). The seismic response of sediment filled valleys; Part 1. The case of incident SH waves, Bull. Seism. Soc. Am., 70, 1263-1286.

Bard, P. Y. and M. Bouchon (1980b). The seismic response of sediment filled valleys; Part 2, The case of incident P and SV waves, Bull. Seism. Soc. Am., 70, 1921-1941.

Barker, B. W., Z. A. Der and C. P. Mrazek (1980). The effect of crustal structure on the regional phases P_g and L_g at NTS, Studies of Seismic Wave Characteristics at Regional Distances, AL-80-1, Teledyne Geotech, Alexandria, Virginia.

Blandford, R. R. and R. A. Hartenberger (1978). Regional Discrimination Between Earthquakes and Explosions, Paper presented at the 1978 Fall American Geophysical Union Meeting.

Boore, D. M., K. L. Larner and K. Aki (1971). Comparison of two independent methods for the solution of wave scattering problem, response of a sedimentary basin to vertically incident SH waves, J. Geophys. Res., 76, 558-569.

Brune, J. N. (1964). Travel time, body waves and normal modes of the earth, Bull. Seism. Soc. Am., 54, 2099-2128.

Chernov, L. A. (1960). Wave propagation in a random medium, (translated by R. A. Silverman), McGraw Hill Book Company.

Chouet, B. (1976). Source, scattering and attenuation effects in high frequency seismic waves, Ph.D. Thesis, Massachusetts Institute of Technology, Cambridge, Massachusetts.

Gilbert, F. and L. Knopoff (1960). Seismic scattering from topographic irregularities, J. Geophys. Res., 65, 3437-3444.

Gupta, I. N. and J. A. Burnetti (1981). An investigation of discriminants for events in western USSR based on regional phases recorded at station Kabul, Bull. Seism. Soc. Am., 71, no. 1.

Gupta, I. N., B. W. Barker, J. A. Burnetti and Z. A. Der (1980). A study of regional phases from earthquakes and explosions in western Russia, Bull. Seism. Soc. Am., 70, 851-872.

Haddon, R. A. W. (1978). Scattering of seismic body waves by small random inhomogeneities in the Earth, NORSAR Scientific Report No. 3-77/78.

Harkrider, D. G. (1964). Surface waves in multilayered elastic media. I. Rayleigh and Love waves from buried sources in a multilayered elastic half-space, Bull. Seism. Soc. Am., 54, 627-679.

Harvey, D. J. (1980). High frequency normal seismogram synthesis-the P_g phase at near-regional distances, paper presented at the 1980 Spring Meeting of the American Geophysical Union.

Haskell, N. A. (1964). Radiation patterns of surface waves from point sources in a multilayered medium, Bull. Seism. Soc. Am., 54, 377-393.

Herrmann, R. B. (1980). Q estimates using the coda of local earthquakes, Bull. Seism. Soc. Am., 70, 447-468.

Hudson, J. A. (1977). Scattered waves in the coda of P, J. Geophys. Res., 43, 359-374.

Hudson, J. A. (1967). Scattered surface waves from a surface obstacle, Geophys. J., 13, 441-458.

Hudson, J. A. and L. Knopoff (1967). Statistical properties of Rayleigh waves due to scattering by topography, Bull. Seism. Soc. Am., 57, 83-90.

Knopoff, L. and J. A. Hudson (1966). Frequency dependence of amplitudes of scattered elastic waves, J. Acoust. Soc. Am., 42, 18-20.

Knopoff, L. and J. A. Hudson (1964). Scattering of elastic waves by small inhomogeneities, J. Acoust. Soc. Am., 36, 338-343.

Knopoff, L., F. Schwab and E. Kausel (1973). Interpretation of L_g, Geophys. J., 33, 389-404.

Malin, P. E. (1979). First order scattering solution for modeling elastic wave codas, Dept. of Geological and Geophysical Sciences, Princeton, New Jersey.

Malin, P. E. (1978). A first order scattering solution for modeling lunar and terrestrial seismic codas, Ph.D. dissertation, Princeton University, Princeton, New Jersey.

Miles, J. W. (1960). Scattering of elastic waves by small inhomogeneities, Geophysics, 25, 642-648.

Mitchell, B. J. (1980). Frequency dependence of shear wave internal friction in the continental crust of Eastern North America, J. Geophys. Res., 85, 5212-5218.

Mrazek, C. P., Z. A. Der, B. W. Barker and A. O'Donnell (1980). Seismic array design for regional phases, in Studies of Seismic Wave Characteristics at Regional Distances, AL-80-1, Teledyne Geotech, Alexandria, Virginia.

Murphy, J. R. (1980). An evaluation of the factors influencing the seismic detection of decoupled explosions at regional distances, Systems, Science and Software, Inc., SSS-R-80-4579.

Mukkeltveit, S., F. Ringdal and H. Bungum (1980). An experimental small subarray within the NORSAR array: Crustal phase velocities and azimuths from local and regional events, AFTAC-TR-80-37.

Nuttli, O. W. (1980). Talk given at AFOSR research conference, Grand Island, New York, May 1980.

Oliver, J. and M. Ewing (1957). Higher modes of continental Rayleigh waves, Bull. Seism. Soc. Am., 47, 187-204.

Panza, G. F. and G. Calcagnile (1975). L_g, L_i and R_g from Rayleigh modes, Geophys. J. R. Astr. Soc., 30, 475-482.

Press, F. and M. Ewing (1952). Two slow surface waves across North America, Bull. Seism. Soc. Am., 42, 219-228.

Pomeroy, P. W. (1980). Regional seismic wave propagation, Semiannual Technical Report, Rondout Associates, Inc., Stone Ridge, New York, F49620-78-C-0043.

Pomeroy, P. W. (1978a). An investigation of seismic wave propagation in Eastern North America, Rondout Associates, Semiannual Technical Report under contract F49620-78-C-0043.

Pomeroy, P. W. (1978b). An investigation of seismic wave propagation in Western U.S.S.R., Semiannual Technical Report No. 2 under contract F49620-78-C-0043.

Pomeroy, P. W. and T. C. Chen (1980). Regional seismic wave propagation (Final Report for the AFOSR), Rondout Associates, Inc., Stone Ridge, New York.

Rautian, T. G. and V. Khalturin (1978). The use of coda for determination of the earthquake source spectra, Bull. Seism. Soc. Am., 68, 923-948.

Rodean, H. C. (1979). Optimum frequencies for regional detection of cavity-decoupled explosions, Lawrence Livermore Laboratory, University of California, UCRL-52690.

Terhume, R. W., C. M. Snell and H. C. Rodean (1979). Enhanced coupling and decoupling of underground nuclear explosions, Lawrence Livermore Laboratory, University of California, UCRL-52806.

Tolstoy, I. and C. S. Clay (1966). Ocean Acoustics, McGraw-Hill Book Co., New York.

Tsujiura, M. (1978). Spectral analysis of the coda waves from local earthquakes, Bull. Earthquake Res. Inst., Tokyo University, 53, 1-48.

Tsujiura, M. (1966). Frequency analysis of seismic waves 1, Bull. Earthquake Res. Inst., Tokyo University, 44, 873-891.

von Seggern, D. (1980). Source, path and station effects on L_g propagation in North America, Trans. Am. Geophys. Union (EOS), 61, 307.

Werth, G., and P. Randolph (1966). The SALMON experiment, J. Geophys. Res., 71, 3405-3414.

APPENDIX

L_g Envelope Lengths for Various Events

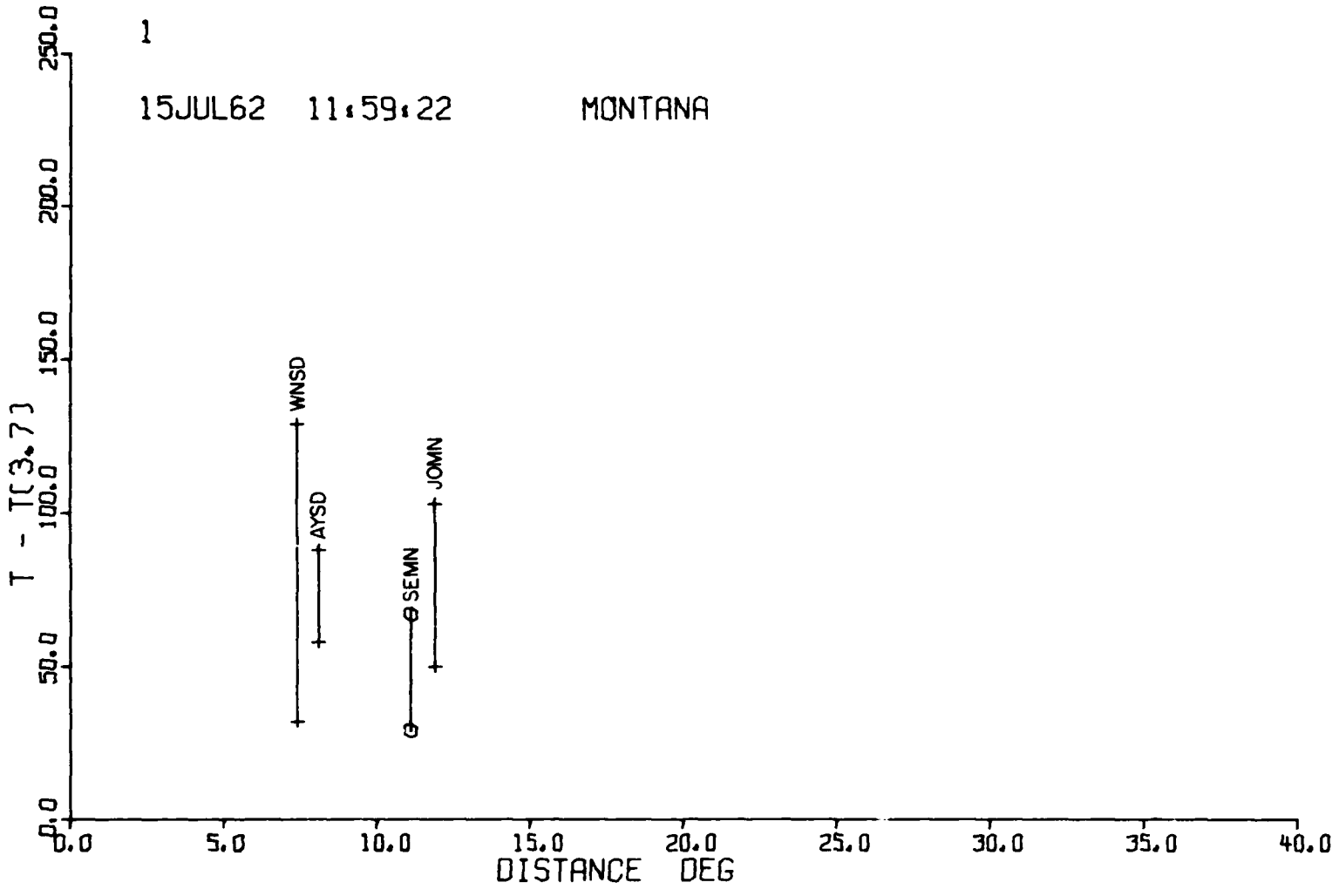
1
15JUL62 11:59:22
MONTANA
T - T[3.7]
250.0
200.0
150.0
100.0
50.0
0.0
WNSD
AYSD
SEMN
JOMN
0.0
5.0
10.0
15.0
20.0
25.0
30.0
35.0
40.0
DISTANCE DEG

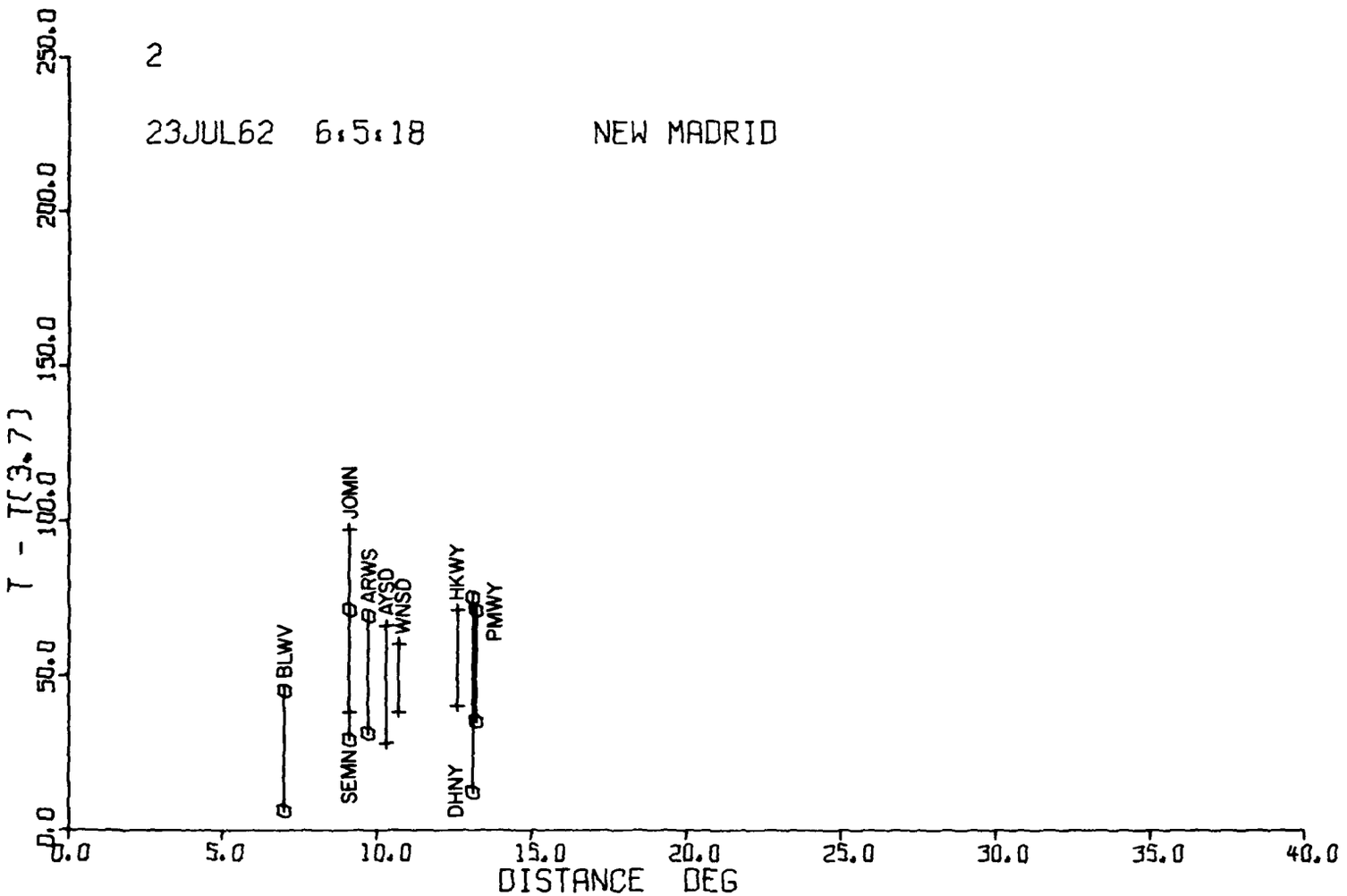
2
23JUL62 6:5:18
NEW MADRID
T - T[3.7]
250.0
200.0
150.0
100.0
50.0
0.0
0.0
5.0
10.0
15.0
20.0
25.0
30.0
35.0
40.0
DISTANCE DEG
BLWV
SEMN
JOMN
ARWS
AYSD
WNSD
DHNY
HKWY
PMWY

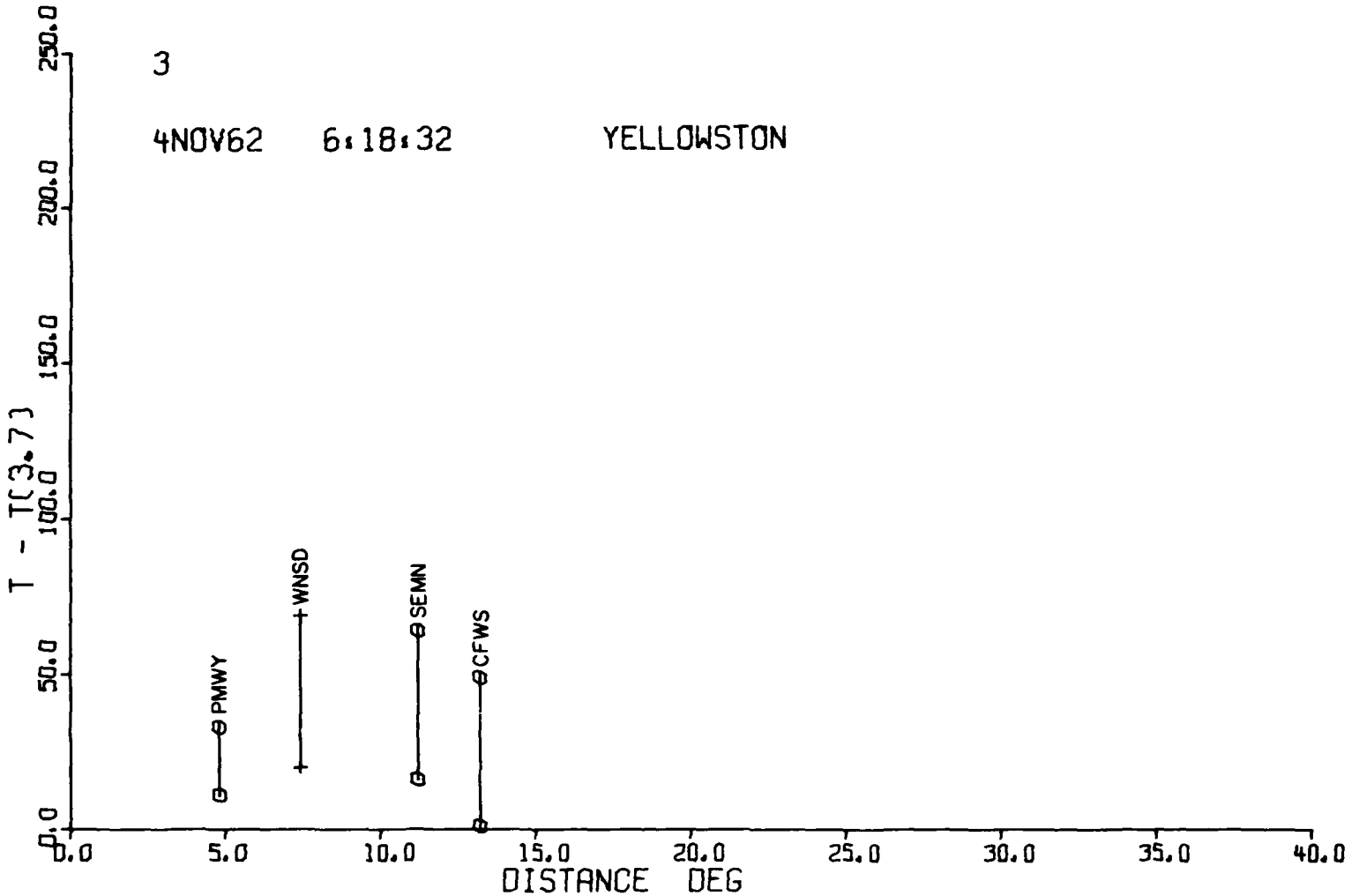
3
4NOV62 6:18:32 YELLOWSTON
T - T(3.7)
250.0
200.0
150.0
100.0
50.0
0.0
PMWY
WNSD
SEMN
CFWS
0.0
5.0
10.0
15.0
20.0
25.0
30.0
35.0
40.0
DISTANCE DEG

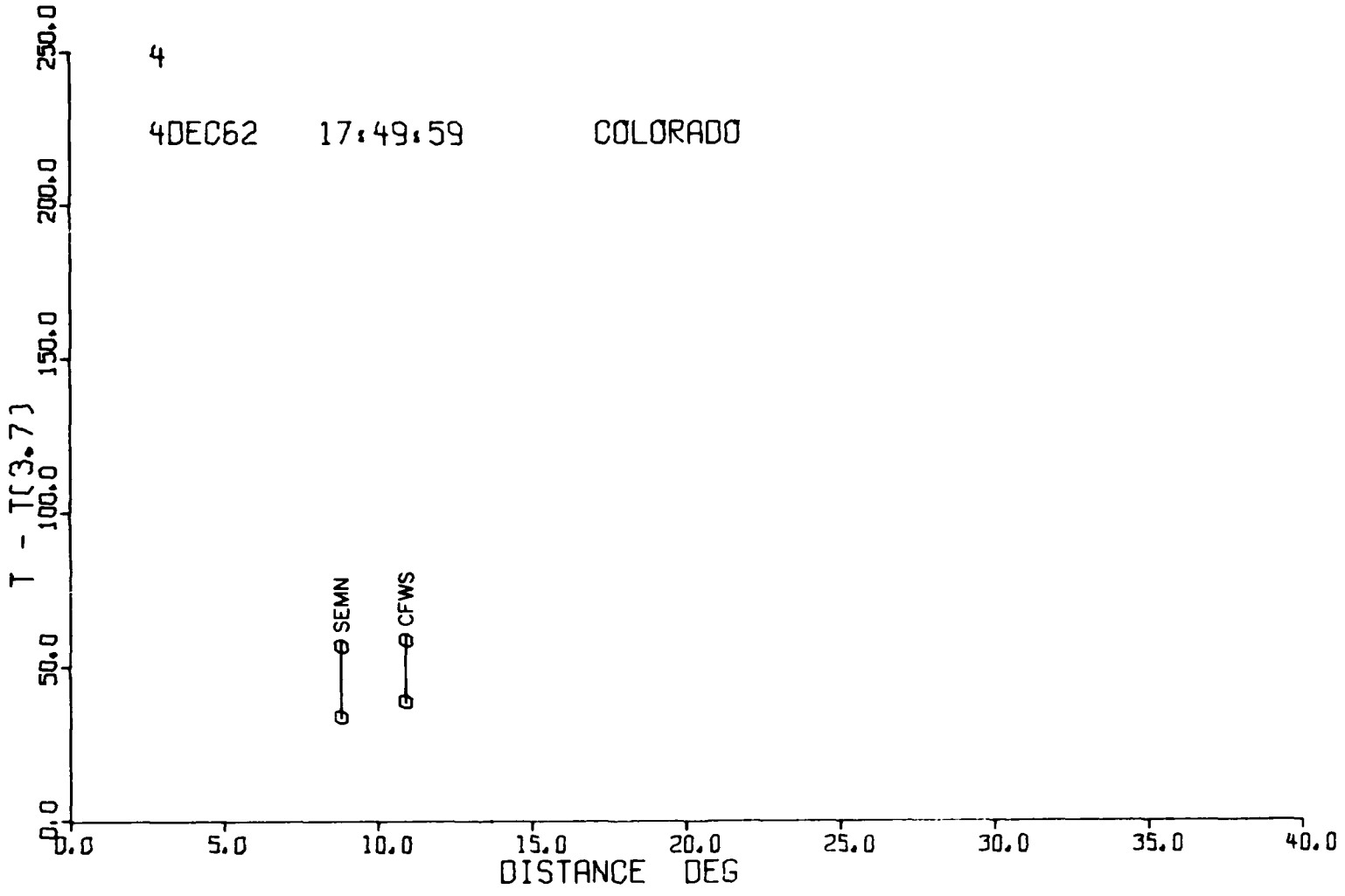
4
4DEC62 17:49:59 COLORADO
T - T[3.7]
250.0
200.0
150.0
100.0
50.0
0.0
SEMN
CFWS
0.0
5.0
10.0
15.0
20.0
25.0
30.0
35.0
40.0
DISTANCE DEG

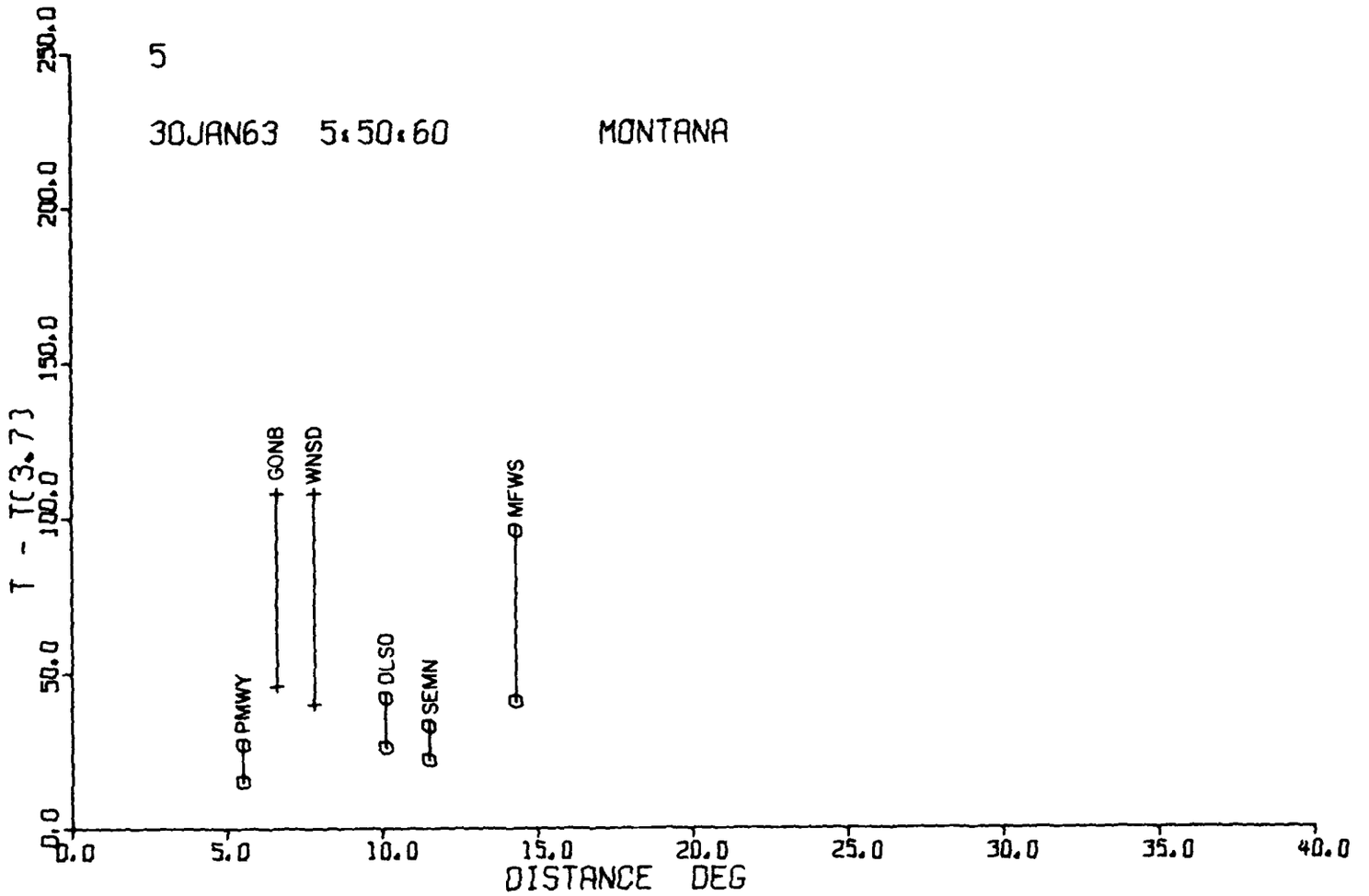
5
30JAN63 5:50:60
MONTANA
T - T(3.73)
250.0
200.0
150.0
100.0
50.0
0.0
PMWY
GONB
WNSD
OLSO
SEMN
MFWS
0.0
5.0
10.0
15.0
20.0
25.0
30.0
35.0
40.0
DISTANCE DEG

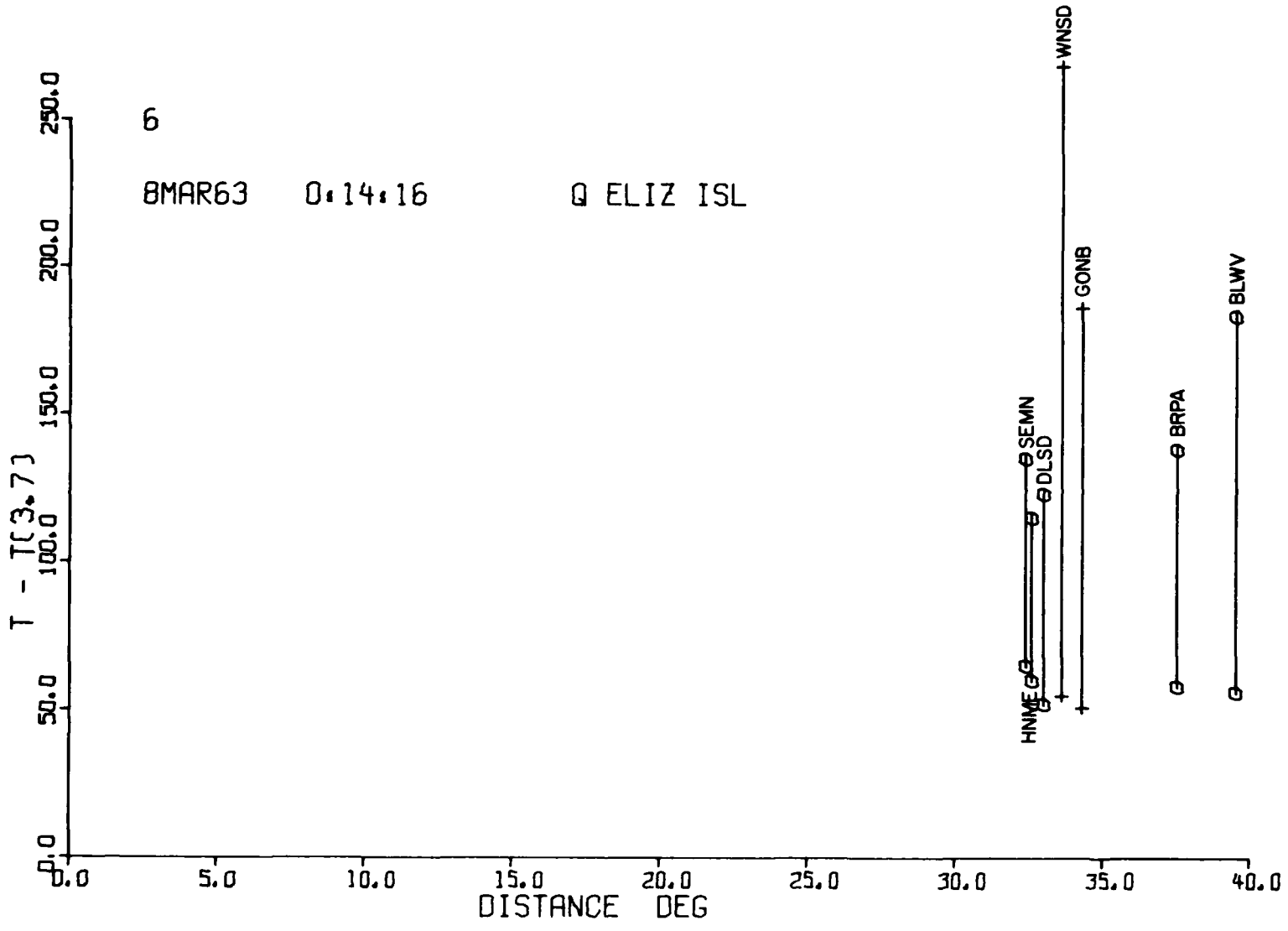
6
8MAR63 0:14:16
Q ELIZ ISL
T - T[3.7]
DISTANCE DEG
0.0
50.0
100.0
150.0
200.0
250.0
0.0
5.0
10.0
15.0
20.0
25.0
30.0
35.0
40.0
WNSD
GONB
BLWV
BRPA
SEMN
DLSD
HNME

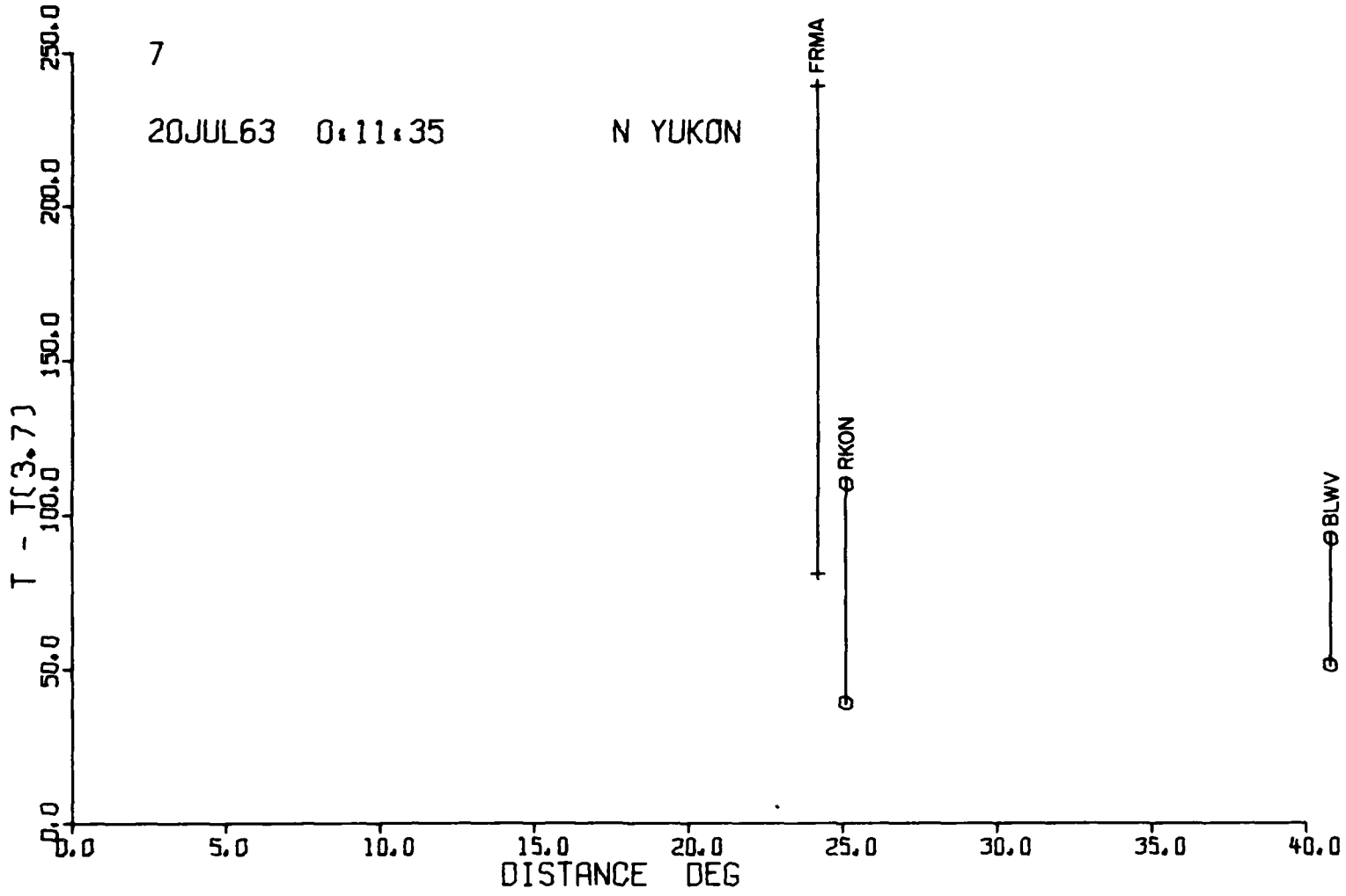
7
20JUL63 0:11:35
N YUKON
FRMA
RKON
BLWV
T - T[3.7]
250.0
200.0
150.0
100.0
50.0
0.0
0.0
5.0
10.0
15.0
20.0
25.0
30.0
35.0
40.0
DISTANCE DEG

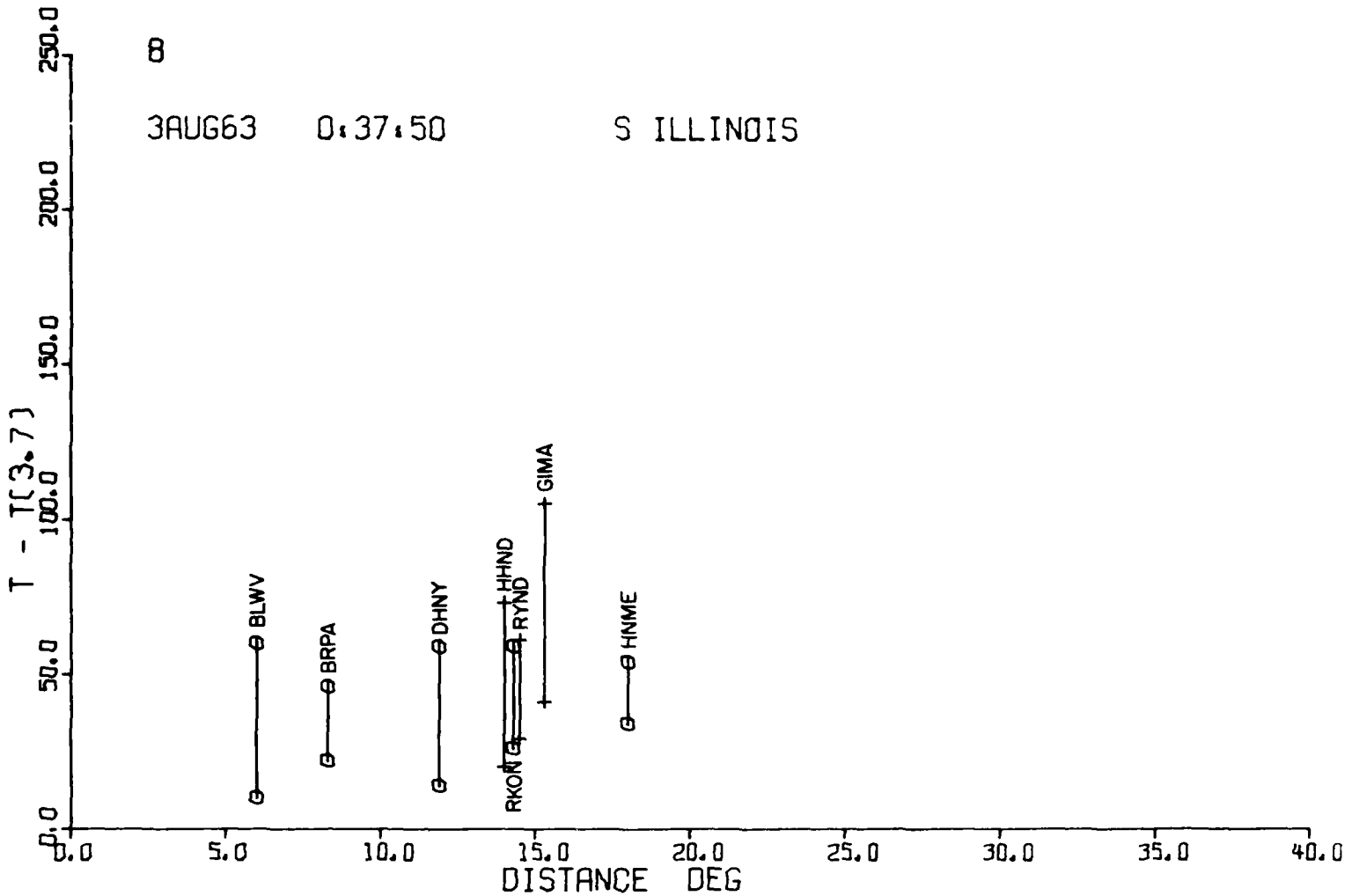
8
3AUG63 0:37:50
S ILLINOIS
T - T[3.7]
250.0
200.0
150.0
100.0
50.0
0.0
BLWV
BRPA
DHNY
RKON
HHND
RYND
GIMA
HNME
0.0
5.0
10.0
15.0
20.0
25.0
30.0
35.0
40.0
DISTANCE DEG

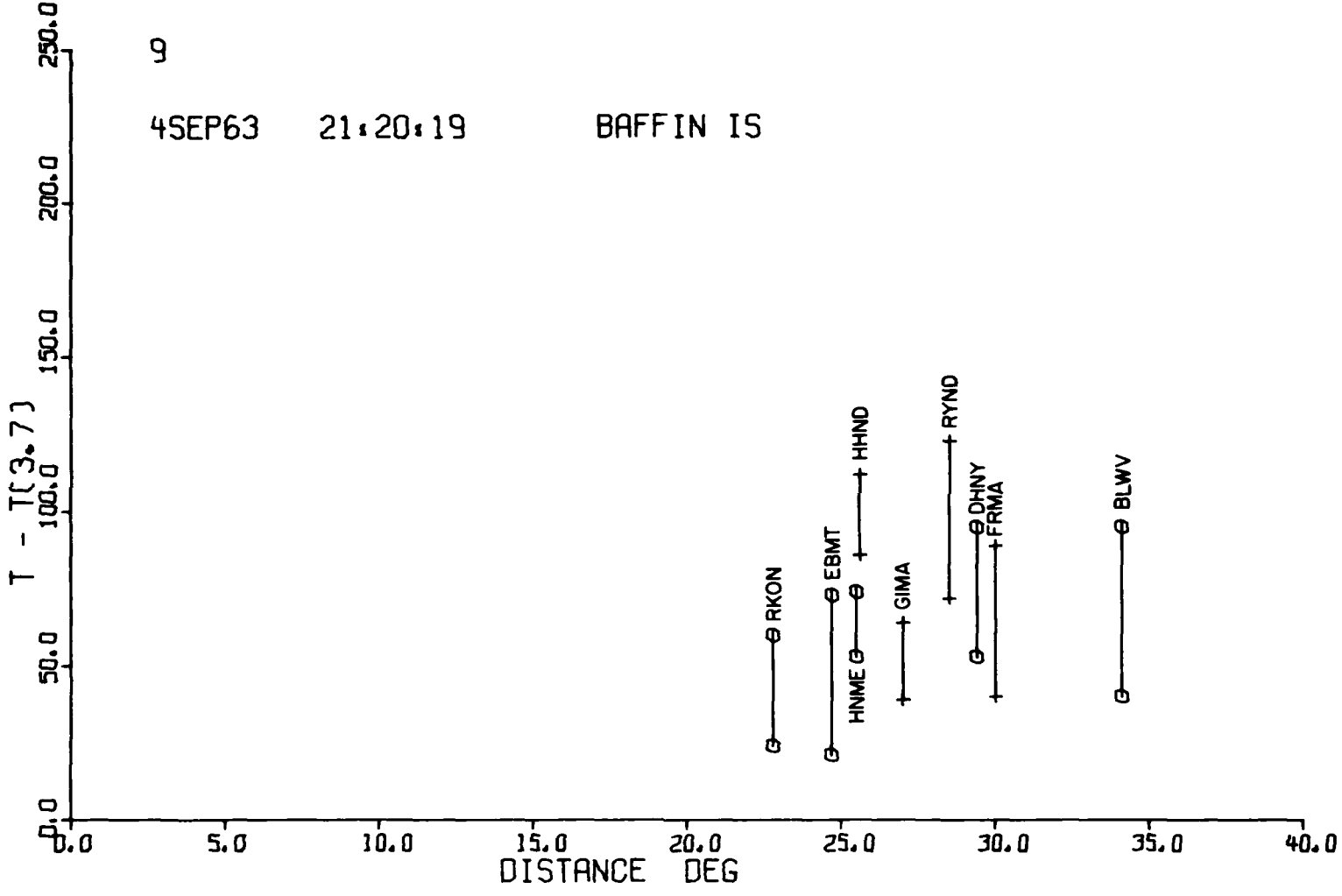
9
4SEP63 21:20:19 BAFFIN IS
T - T[3.7]
250.0
200.0
150.0
100.0
50.0
0.0
0.0
5.0
10.0
15.0
20.0
25.0
30.0
35.0
40.0
DISTANCE DEG
RKON
EBMT
HNME
HHND
GIMA
RYND
DHNY
FRMA
BLWV

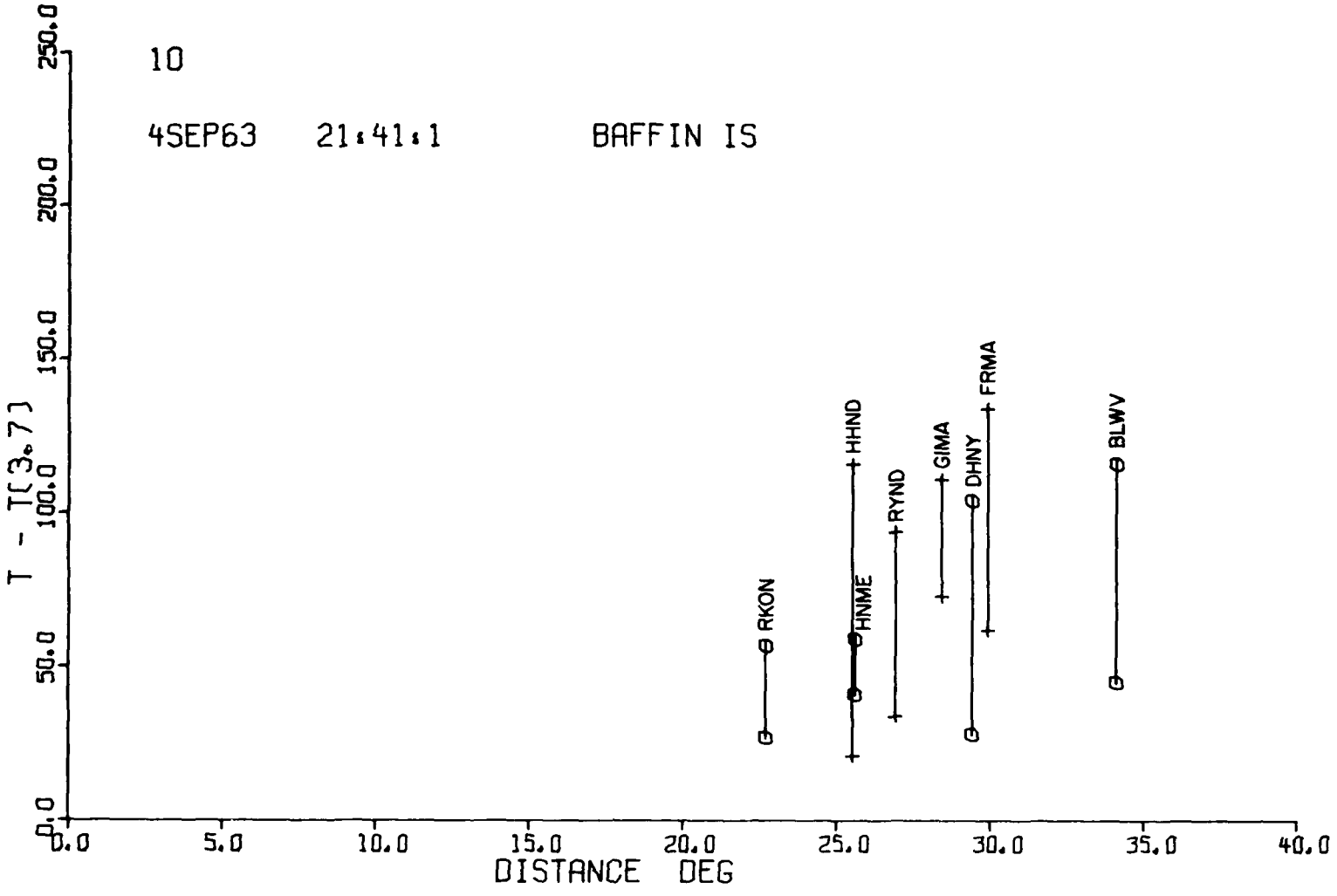
10
4SEP63 21:41:1
BAFFIN IS
T - T[3.7]
250.0
200.0
150.0
100.0
50.0
0.0
0.0
5.0
10.0
15.0
20.0
25.0
30.0
35.0
40.0
DISTANCE DEG
RKON
HNME
HHND
RYND
GIMA
DHNY
FRMA
BLWV

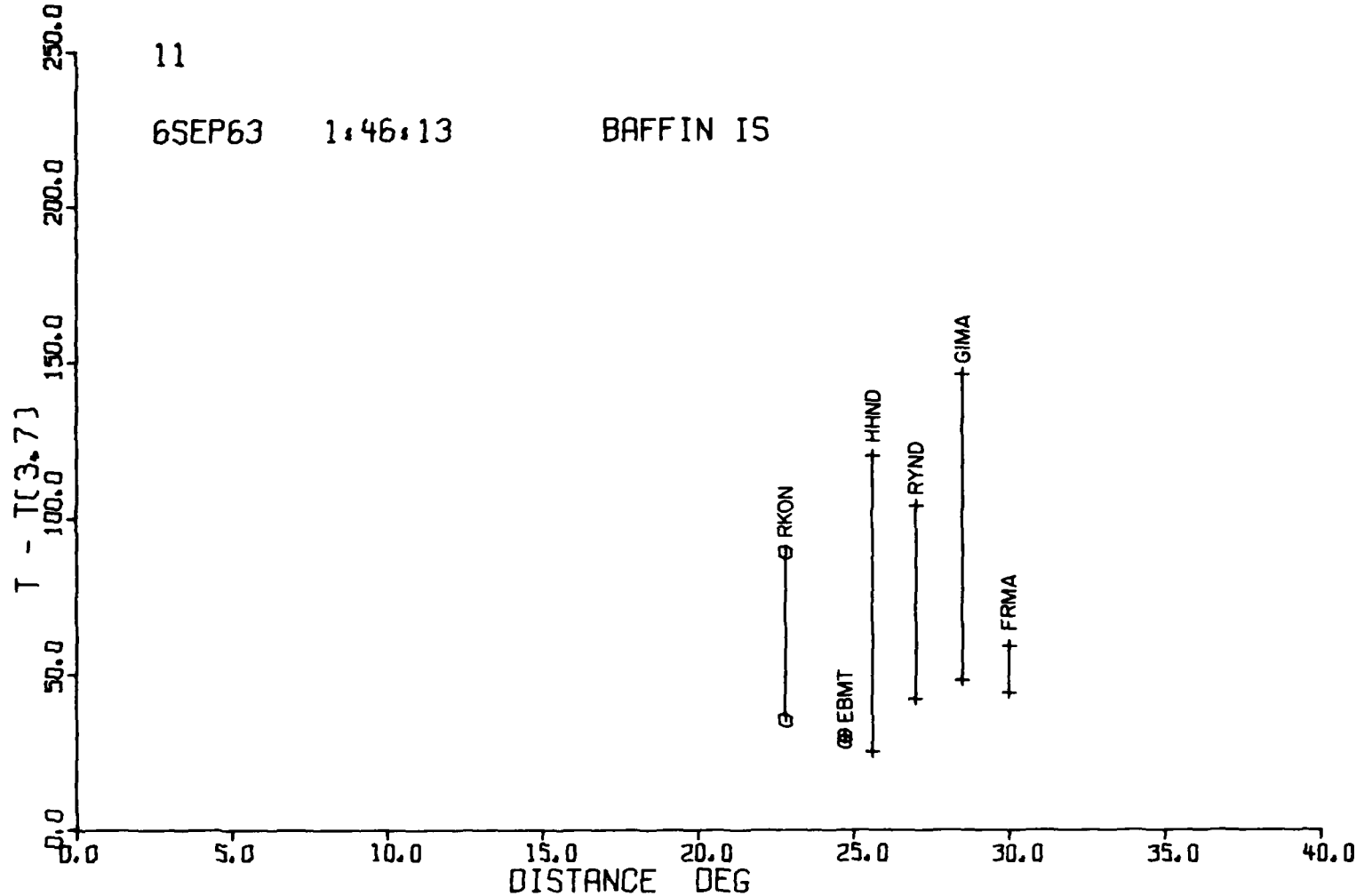
11
6SEP63 1:46:13
BAFFIN IS
T - T[3.7]
250.0
200.0
150.0
100.0
50.0
0.0
0.0
5.0
10.0
15.0
20.0
25.0
30.0
35.0
40.0
DISTANCE DEG
RKON
EBMT
HHND
RYND
GIMA
FRMA

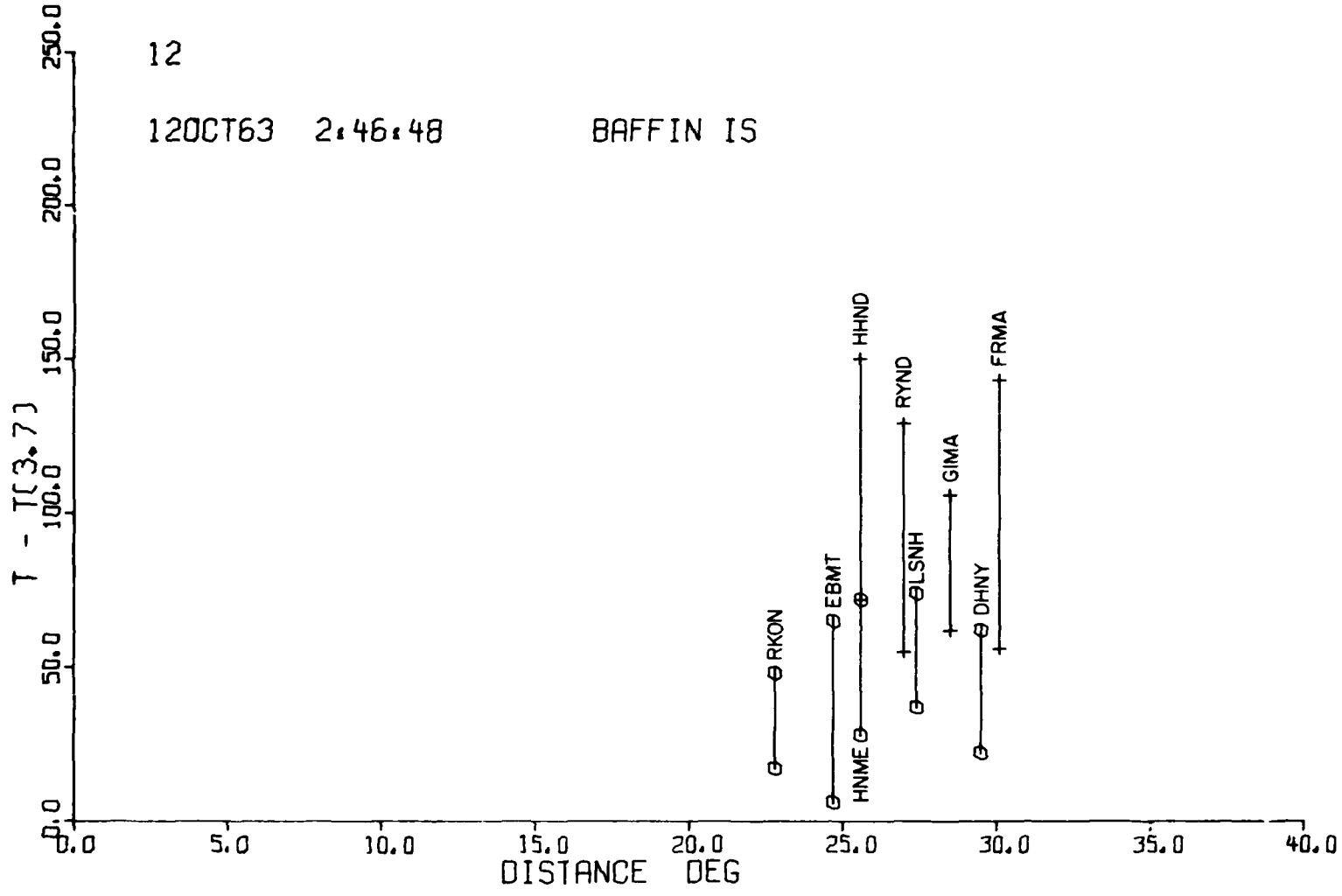
12
12OCT63 2:46:48
BAFFIN IS
T - T[3.7]
250.0
200.0
150.0
100.0
50.0
0.0
0.0
5.0
10.0
15.0
20.0
25.0
30.0
35.0
40.0
DISTANCE DEG
RKON
EBMT
HNME
HHND
LSNH
RYND
GIMA
DHNY
FRMA

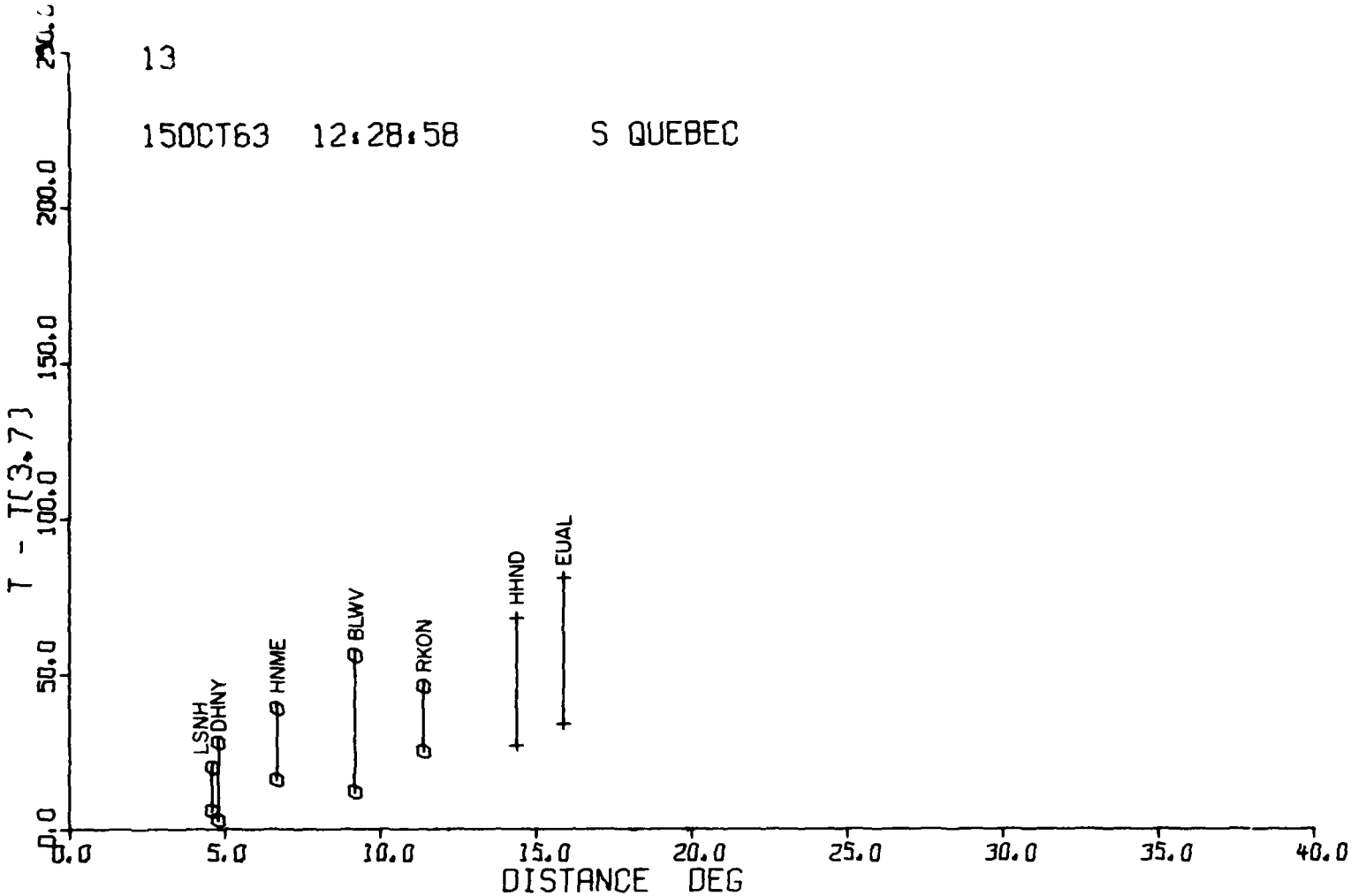
13
150CT63 12:28:58 S QUEBEC
T - T[3.7]
0.0
50.0
100.0
150.0
200.0
LSNH
DHNY
HNME
BLWV
RKON
HHND
EUAL
0.0
5.0
10.0
15.0
20.0
25.0
30.0
35.0
40.0
DISTANCE DEG

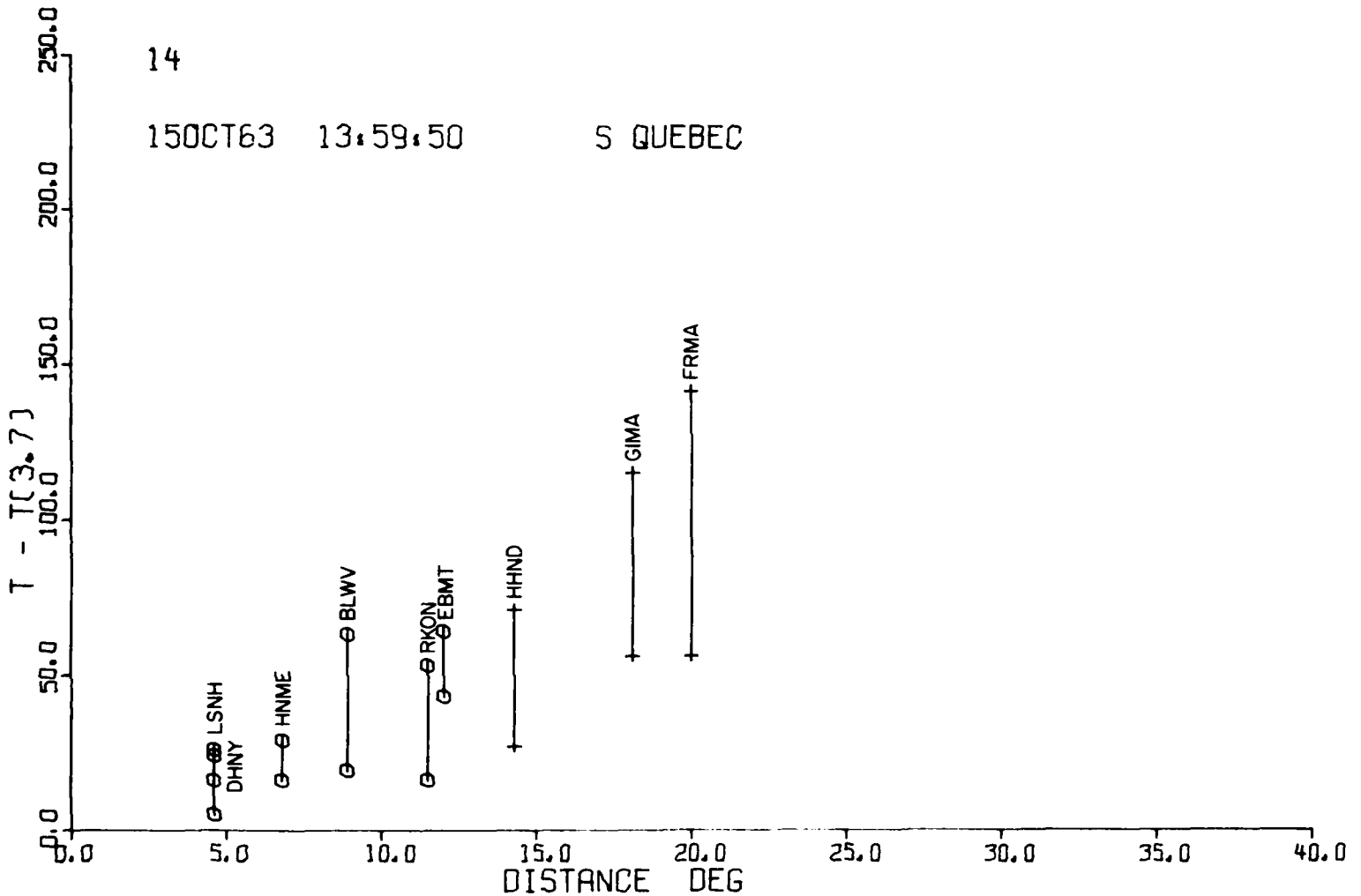
14
15OCT63 13:59:50 S QUEBEC
T - T[3.7]
250.0
200.0
150.0
100.0
50.0
0.0
0.0
5.0
10.0
15.0
20.0
25.0
30.0
35.0
40.0
DISTANCE DEG
DHNY
LSNH
HNME
BLWV
RKON
EBMT
HHND
GIMA
FRMA

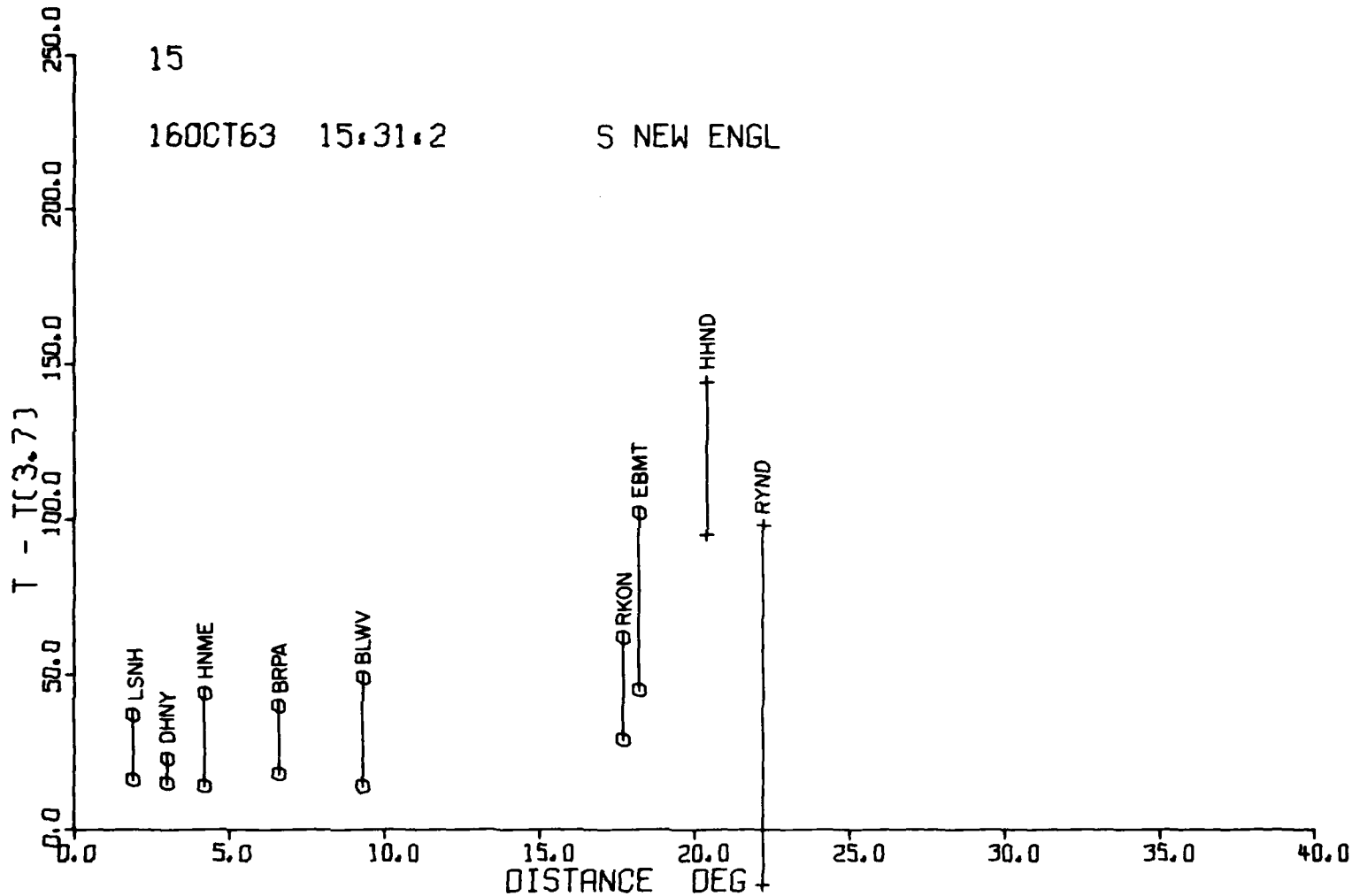
15
160CT63 15:31:2
S NEW ENGL
T - T[3.7]
250.0
200.0
150.0
100.0
50.0
0.0
LSNH
DHNY
HNME
BRPA
BLWV
RKON
EBMT
HHND
RYND
0.0
5.0
10.0
15.0
20.0
25.0
30.0
35.0
40.0
DISTANCE DEG

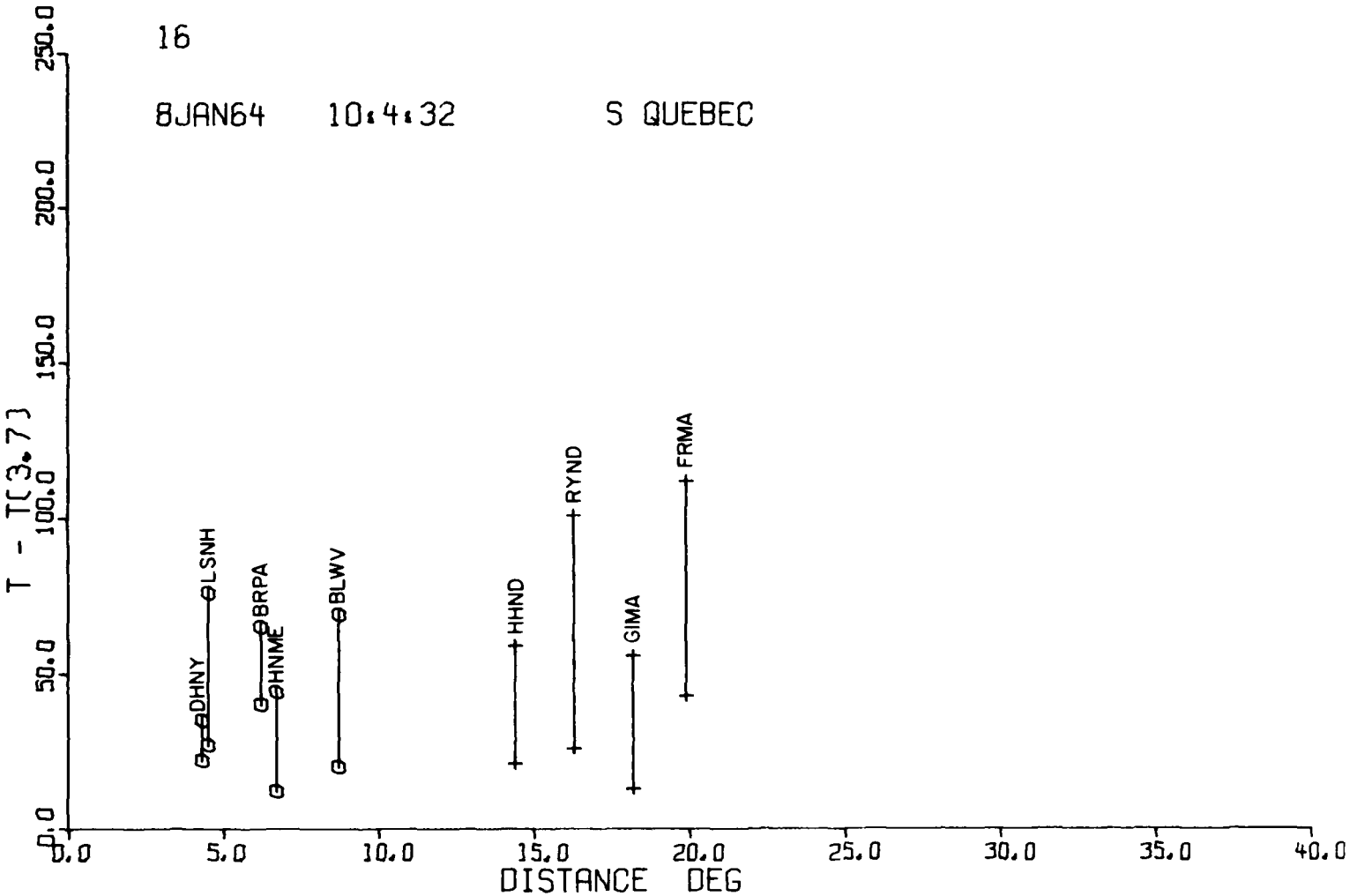
16
8JAN64 10:4:32 S QUEBEC
T - T[3.73]
250.0
200.0
150.0
100.0
50.0
0.0
DHNY
LSNH
BRPA
HNME
BLWV
HHND
RYND
GIMA
FRMA
0.0
5.0
10.0
15.0
20.0
25.0
30.0
35.0
40.0
DISTANCE DEG

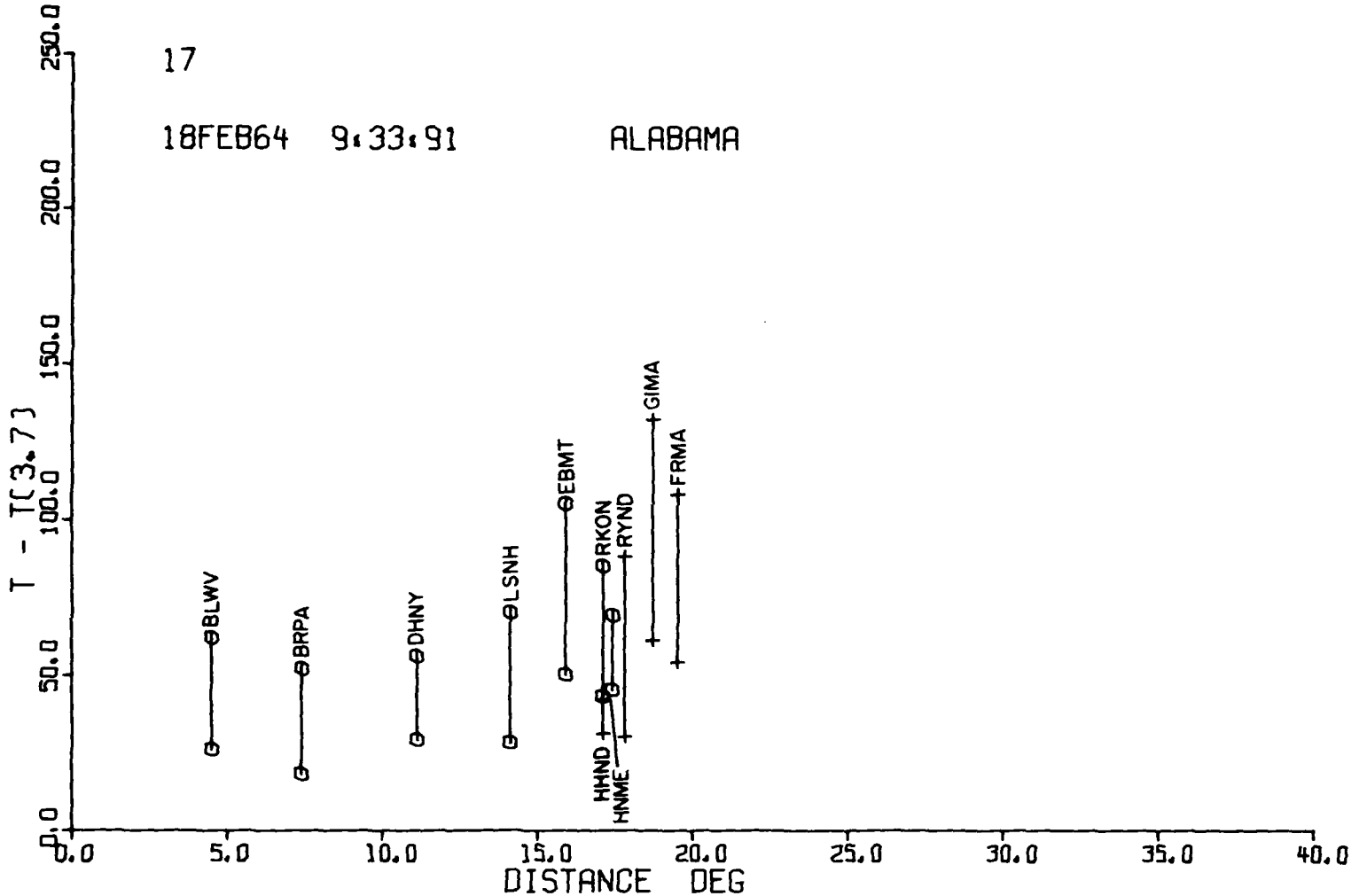
17
18FEB64 9:33:91
ALABAMA
T - T[3.7]
250.0
200.0
150.0
100.0
50.0
0.0
BLWV
BRPA
DHNY
LSNH
EBMT
RKON
RYND
GIMA
FRMA
HHND
HNME
0.0
5.0
10.0
15.0
20.0
25.0
30.0
35.0
40.0
DISTANCE DEG

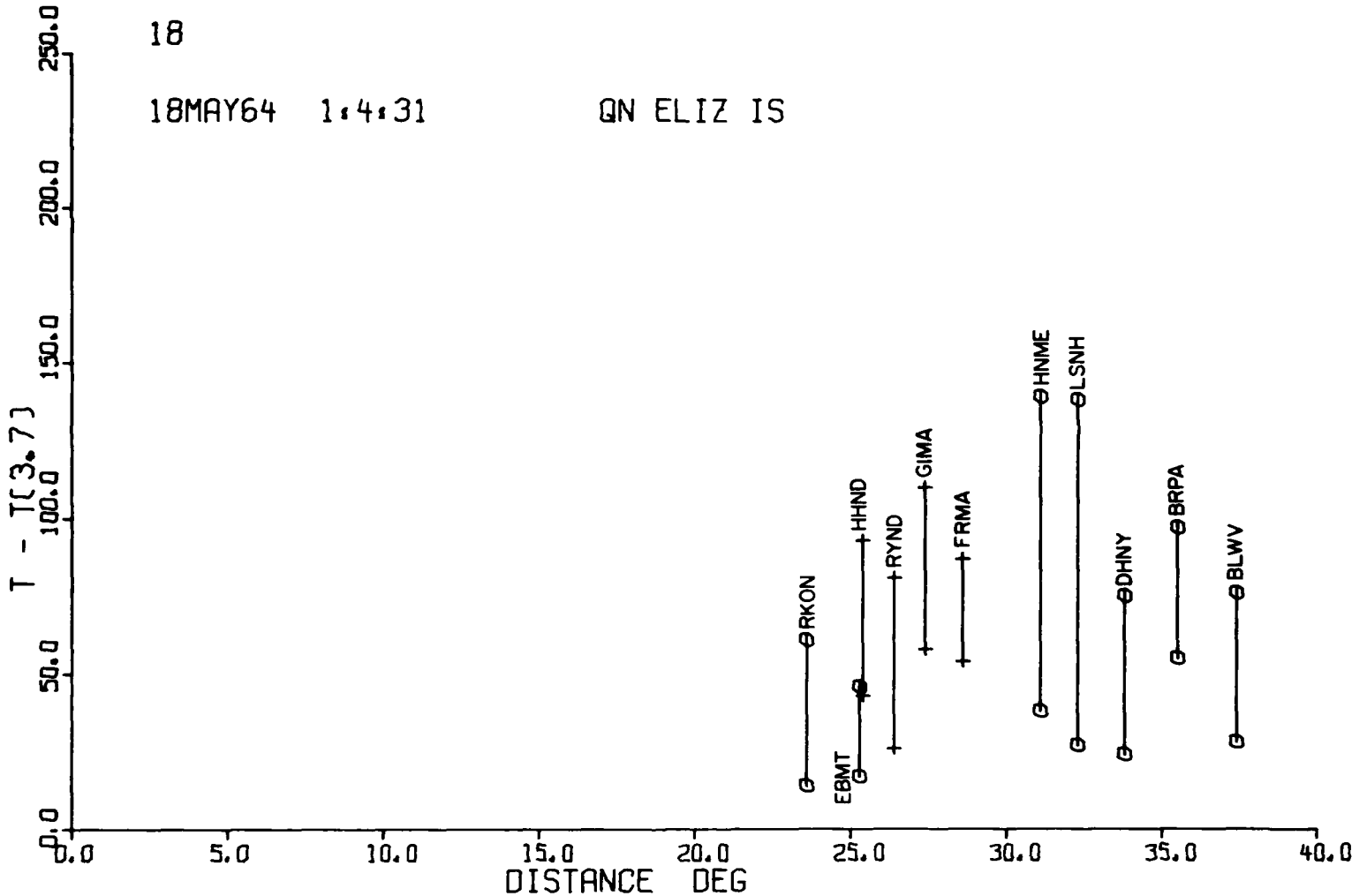
18
18MAY64 1:4:31
QN ELIZ IS
T - T[3.7]
250.0
200.0
150.0
100.0
50.0
0.0
0.0
5.0
10.0
15.0
20.0
25.0
30.0
35.0
40.0
DISTANCE DEG
RKON
EBMT
HHND
RYND
GIMA
FRMA
HNME
LSNH
DHNY
BRPA
BLWV

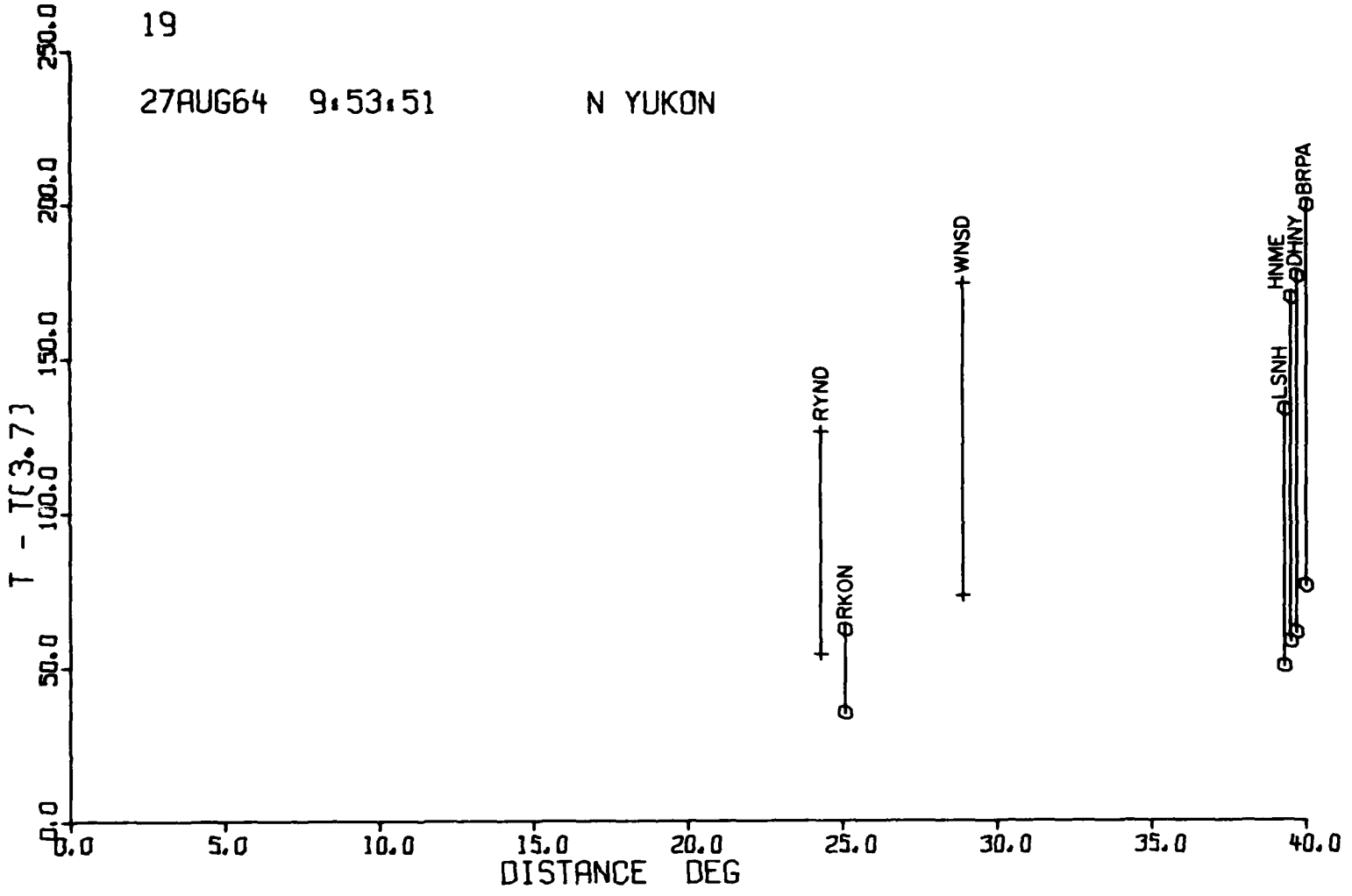
19
27AUG64 9:53:51
N YUKON
T - T(3.7)
250.0
200.0
150.0
100.0
50.0
0.0
0.0
5.0
10.0
15.0
20.0
25.0
30.0
35.0
40.0
DISTANCE DEG
RYND
RKON
WNSD
LSNH
HNME
HNY
BRPA

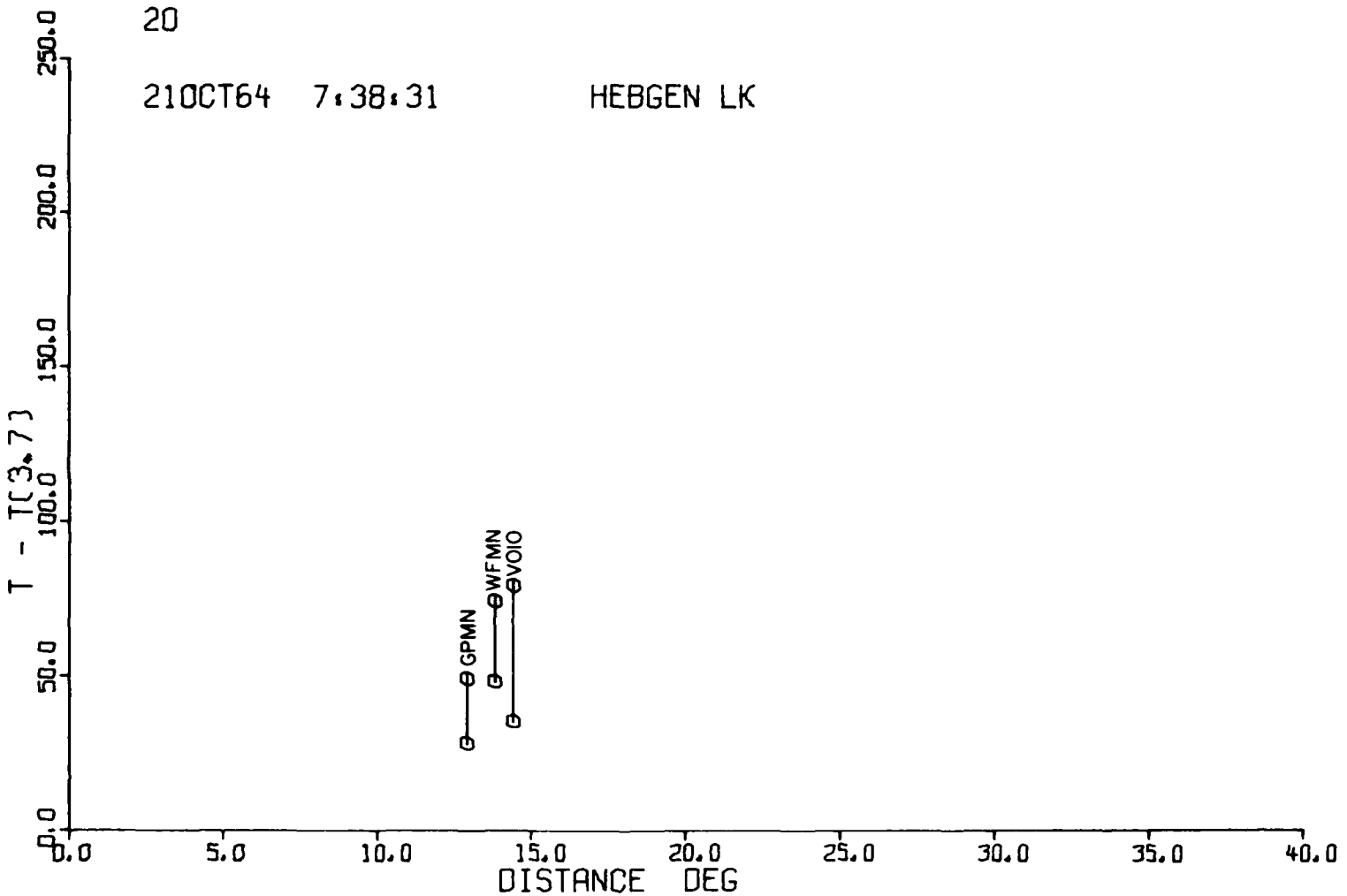
20
21OCT64 7:38:31
HEBGEN LK
T - T[3.7]
250.0
200.0
150.0
100.0
50.0
0.0
GPMN
WFMN
VOIO
0.0
5.0
10.0
15.0
20.0
25.0
30.0
35.0
40.0
DISTANCE DEG

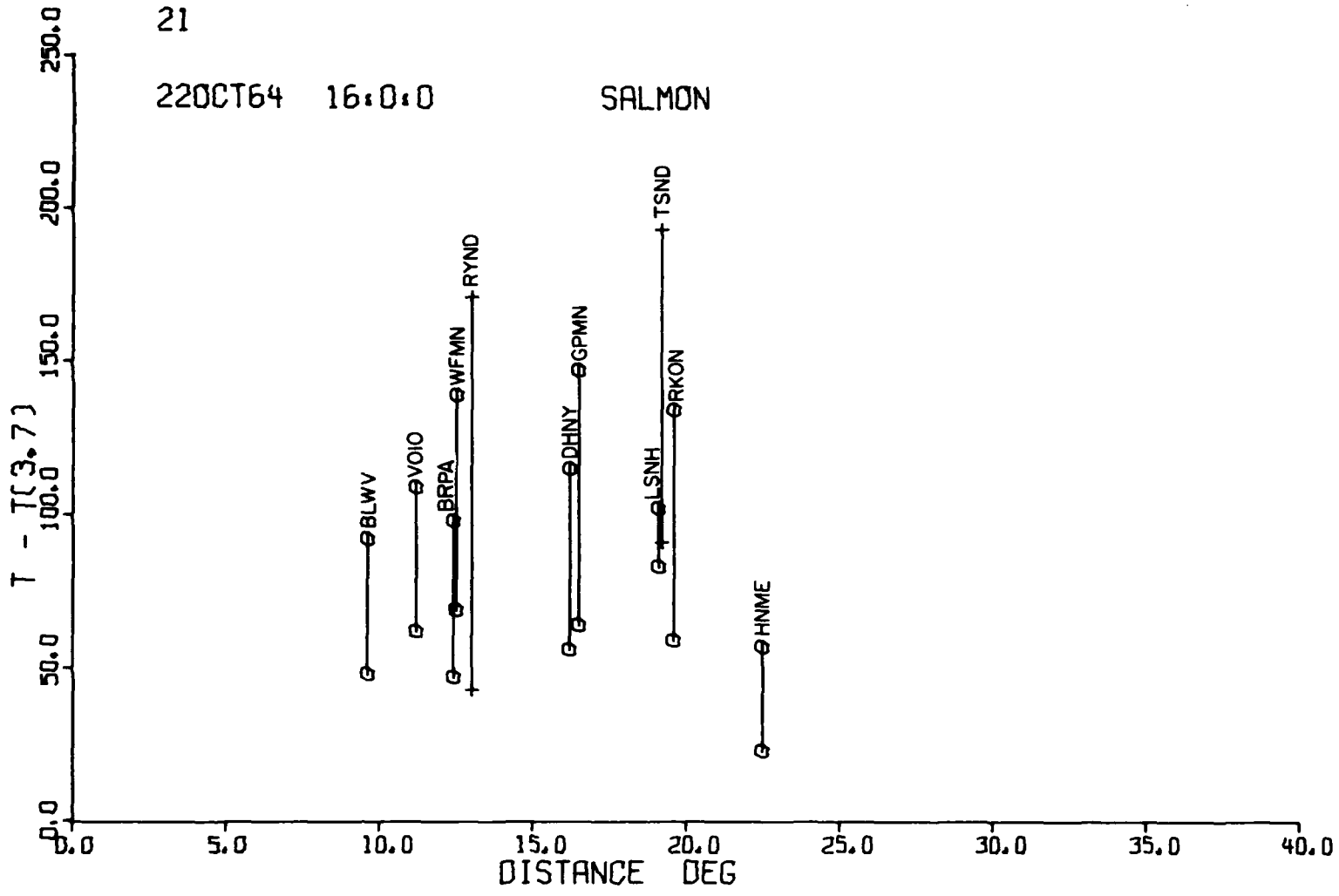
21
220CT64 16:0:0
SALMON
T - T(3.7)
250.0
200.0
150.0
100.0
50.0
0.0
BLWV
VOIO
BRPA
WFMN
RYND
DHNY
GPMN
LSNH
RKON
TSND
HNME
0.0
5.0
10.0
15.0
20.0
25.0
30.0
35.0
40.0
DISTANCE DEG

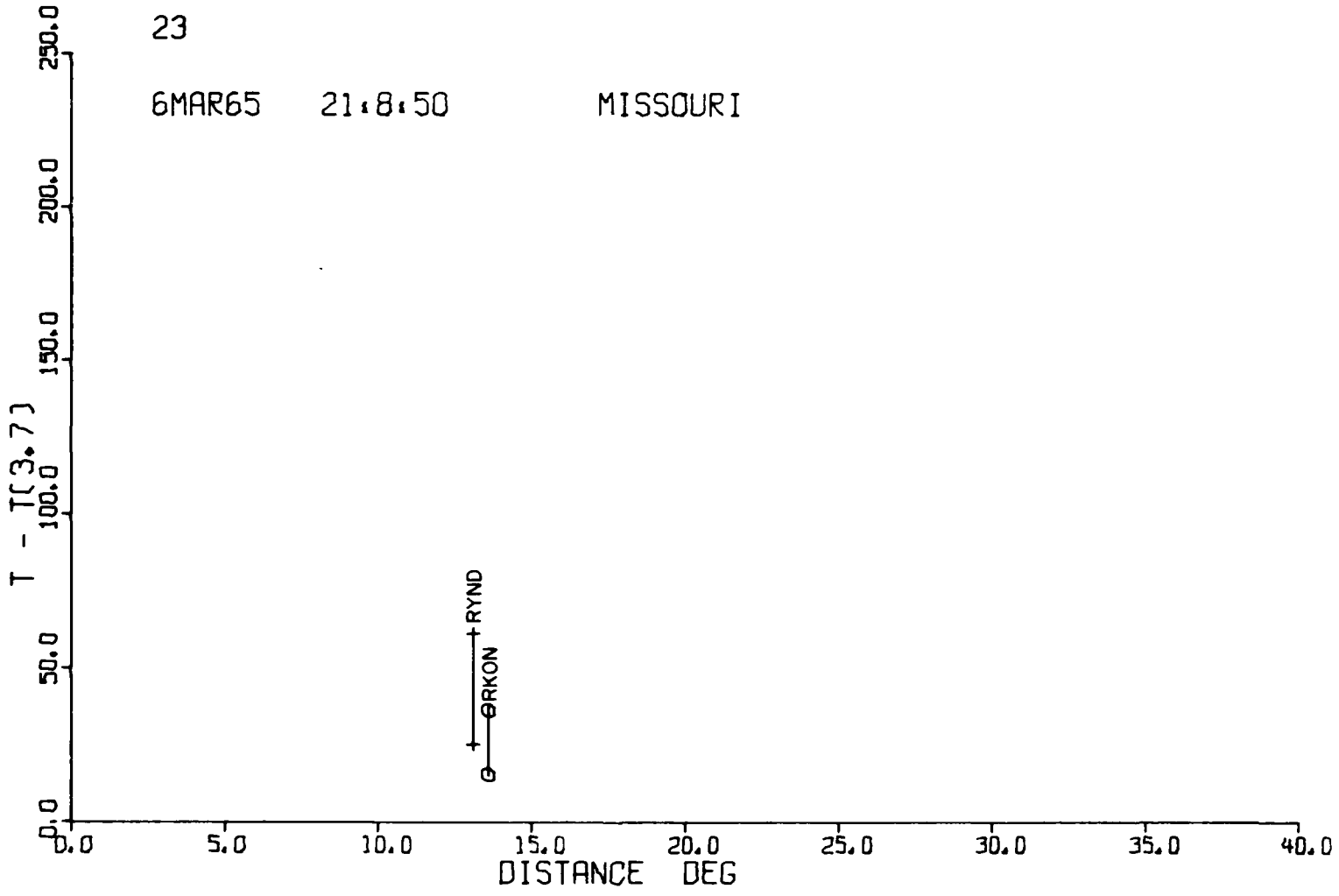
23
6MAR65 21:8:50 MISSOURI
T - T[3.7]
250.0
200.0
150.0
100.0
50.0
0.0
0.0
5.0
10.0
15.0
20.0
25.0
30.0
35.0
40.0
DISTANCE DEG
RYND
ØRKON

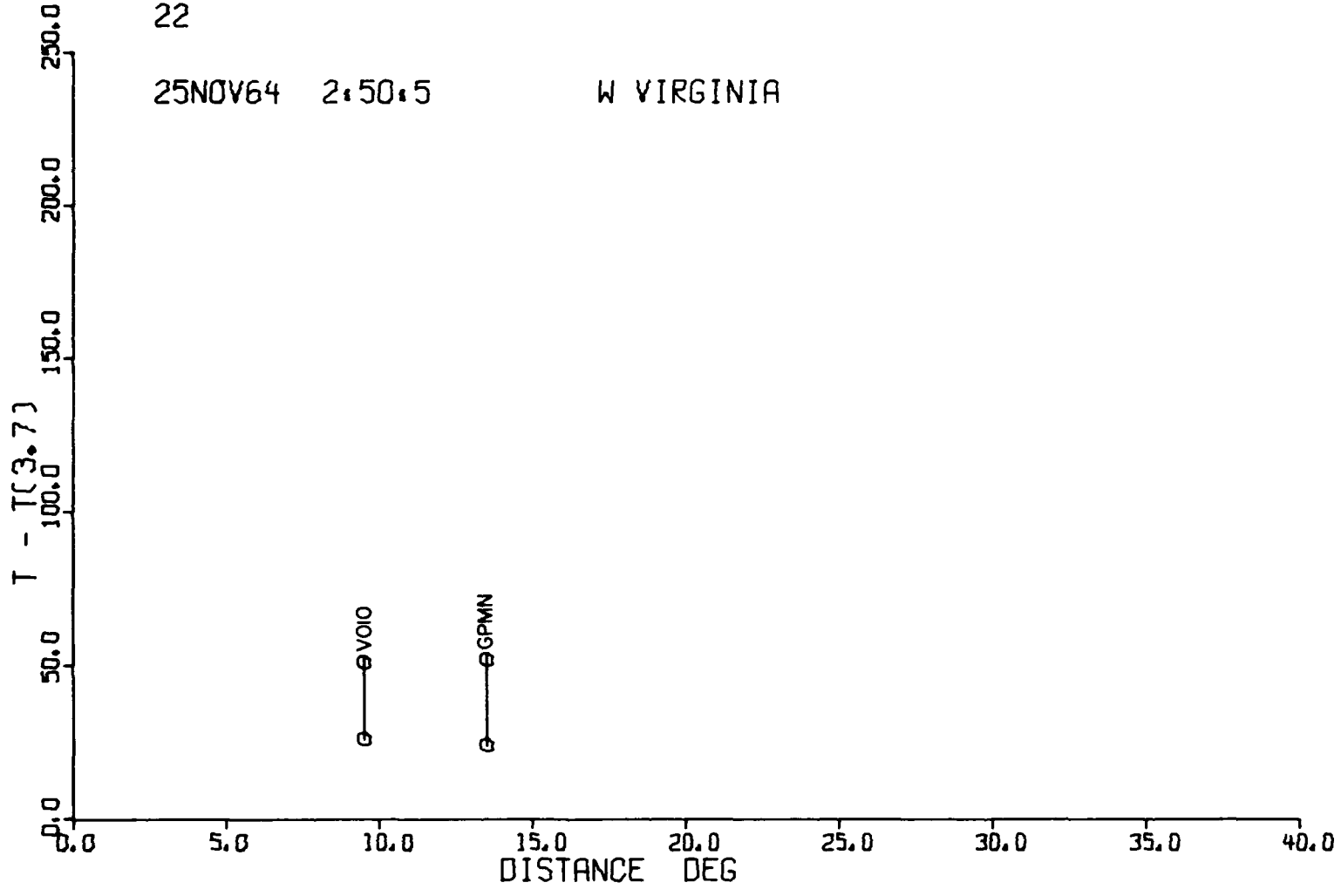
22
25NOV64 2:50:5
W VIRGINIA
T - T[3.7]
250.0
200.0
150.0
100.0
50.0
0.0
VOIO
GPMN
0.0
5.0
10.0
15.0
20.0
25.0
30.0
35.0
40.0
DISTANCE DEG

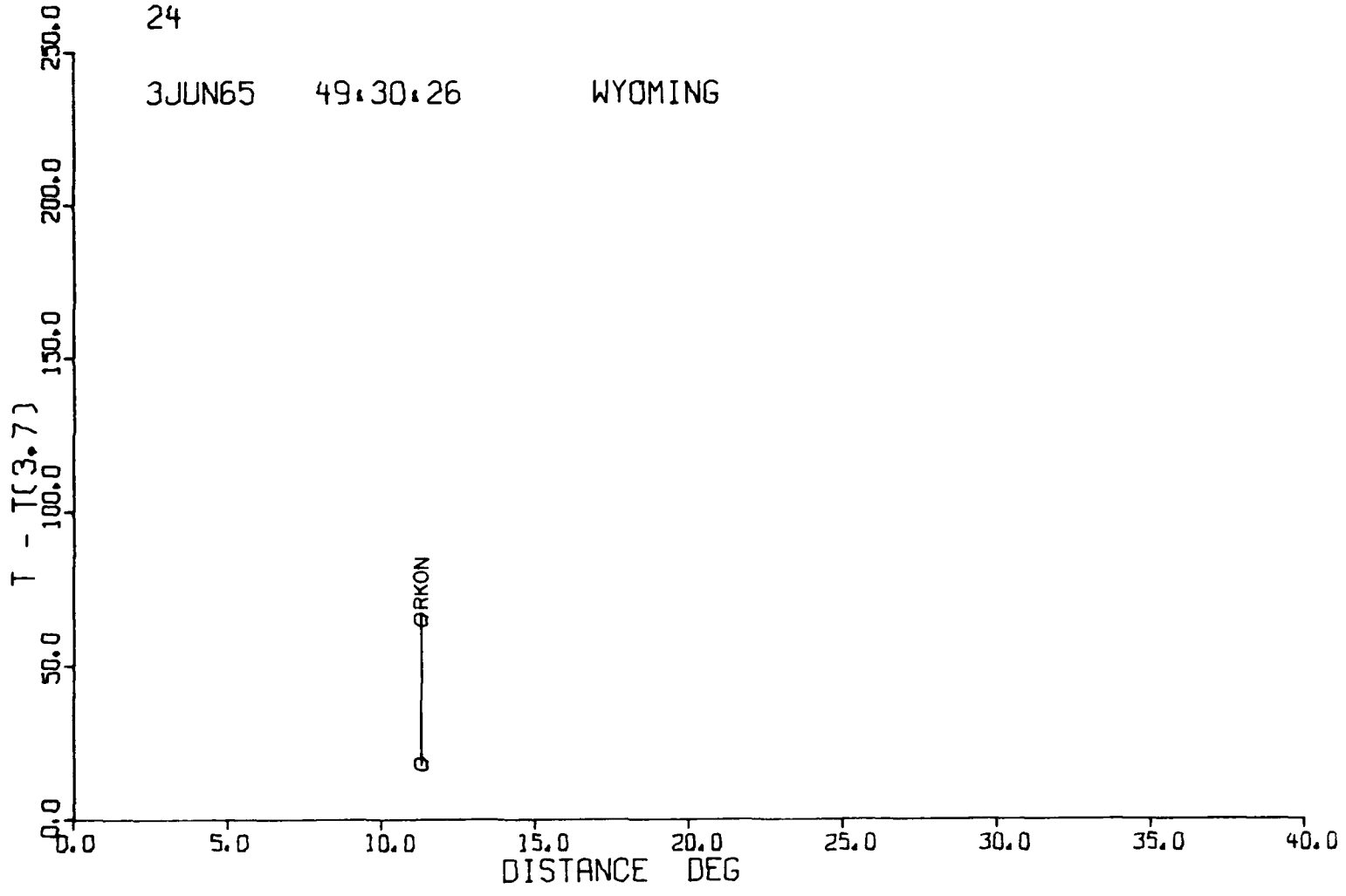
24
3JUN65 49:30:26 WYOMING
T - T(3.7)
250.0
200.0
150.0
100.0
50.0
0.0
RKON
0.0
5.0
10.0
15.0
20.0
25.0
30.0
35.0
40.0
DISTANCE DEG

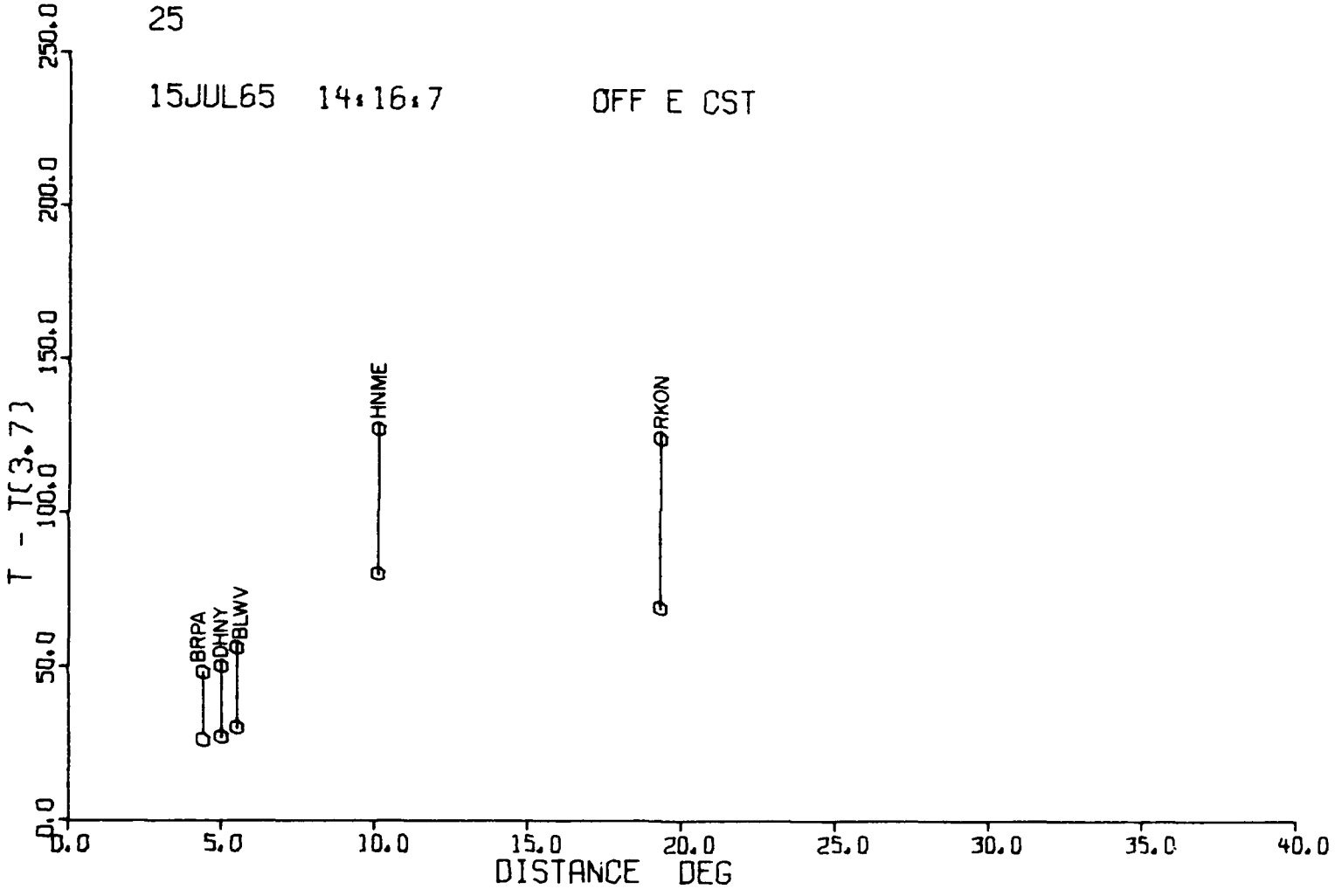
25
15JUL65 14:16:7
OFF E CST
T - T[3.7]
250.0
200.0
150.0
100.0
50.0
0.0
BRPA
OHNY
BLWV
HNME
RKON
0.0
5.0
10.0
15.0
20.0
25.0
30.0
35.0
40.0
DISTANCE DEG

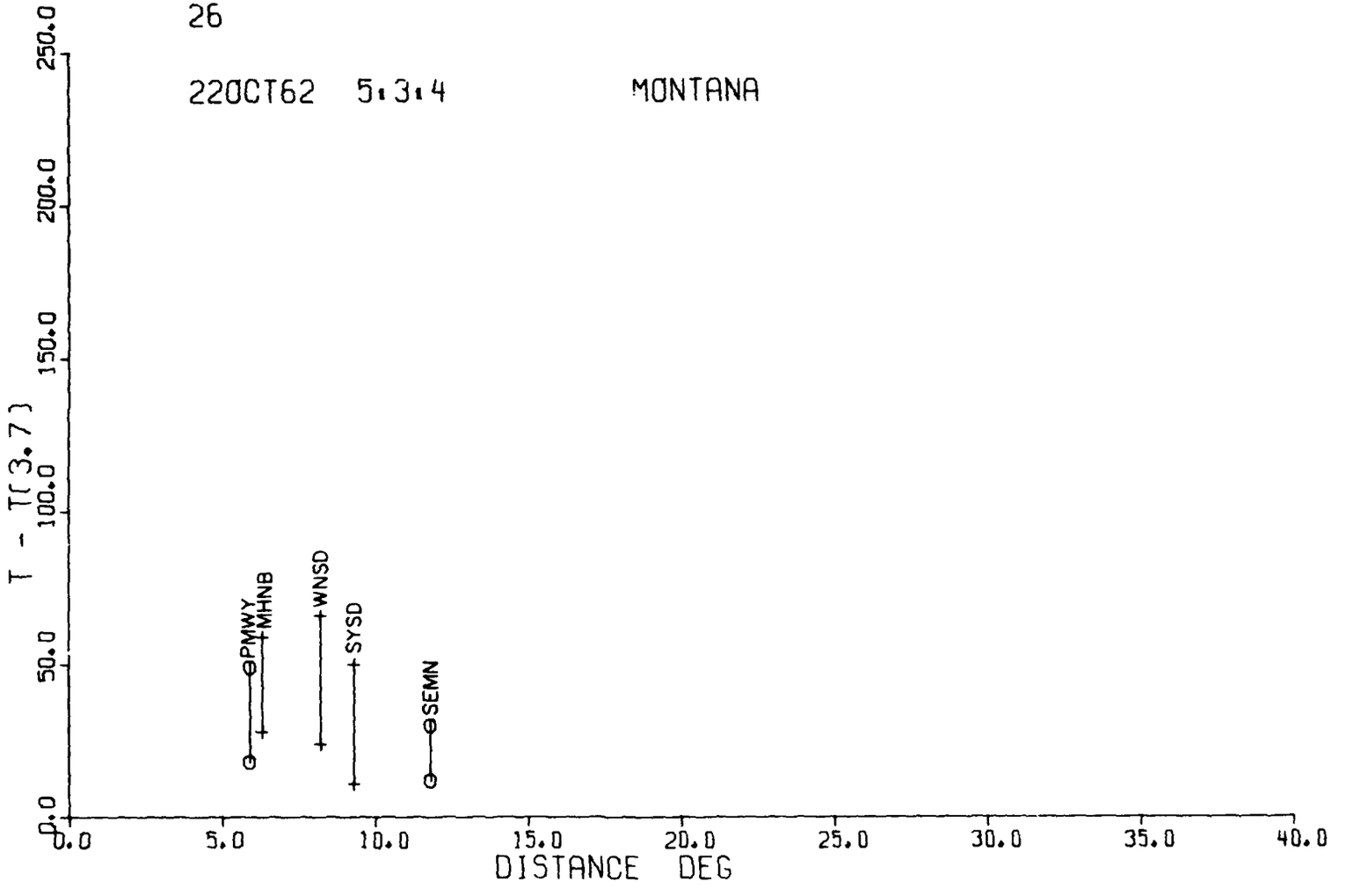
26
22OCT62 5:3:4
MONTANA
T - T(3.7)
250.0
200.0
150.0
100.0
50.0
0.0
PMWY
MHNB
WNSD
SYSD
SEMN
0.0
5.0
10.0
15.0
20.0
25.0
30.0
35.0
40.0
DISTANCE DEG

AD-A105 995 TELEDYNE GEOTECH ALEXANDRIA VA SEISMIC DATA LAB F/6 17/10
AN INVESTIGATION OF ATTENUATION, SCATTERING AND SITE EFFECTS ON--ETC(U)
MAR 81 Z A DER, A O'DONNELL, P J KLOUDA F08606-79-C-0007
UNCLASSIFIED SDAC-TR-81-4 VSC-TR-81-11 NL

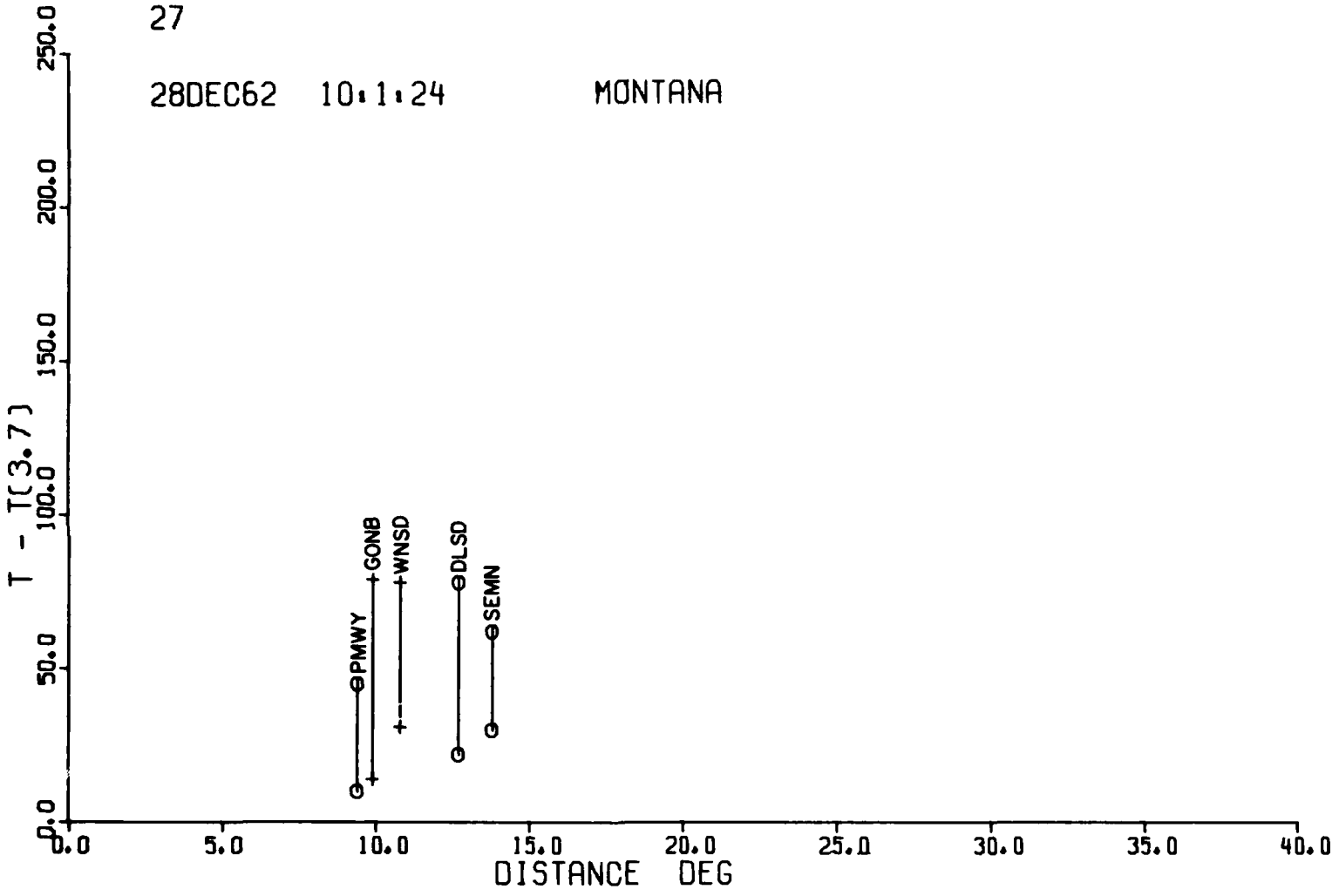
27
28DEC62 10:1:24
MONTANA
T - T(3.7)
250.0
200.0
150.0
100.0
50.0
0.0
PMWY
GONB
WNSD
DLSD
SEMN
0.0
5.0
10.0
15.0
20.0
25.0
30.0
35.0
40.0
DISTANCE DEG

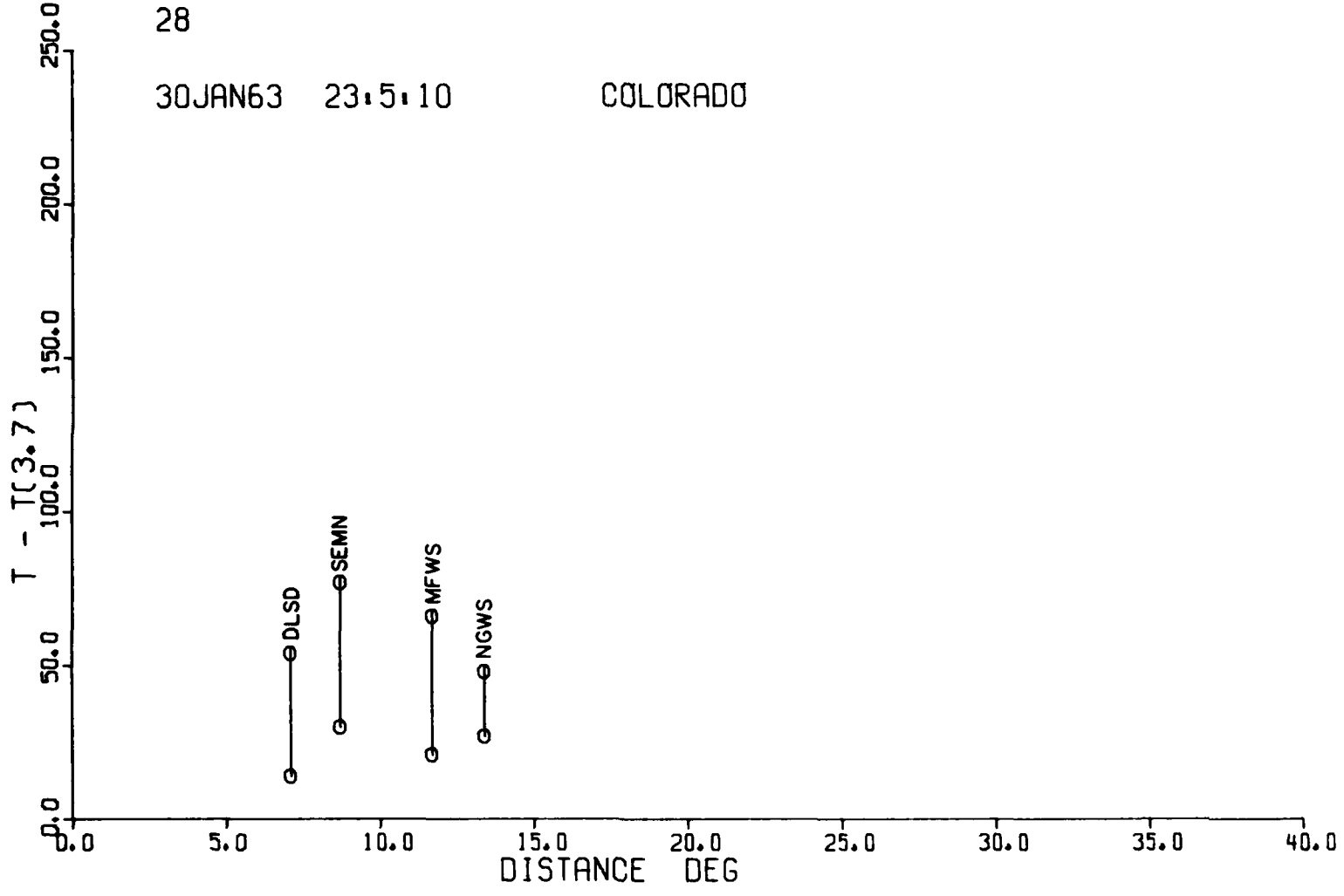
28
30JAN63 23:5:10
COLORADO
T - T(3.7)
250.0
200.0
150.0
100.0
50.0
0.0
DLSD
SEMN
MFWS
NGWS
0.0
5.0
10.0
15.0
20.0
25.0
30.0
35.0
40.0
DISTANCE DEG

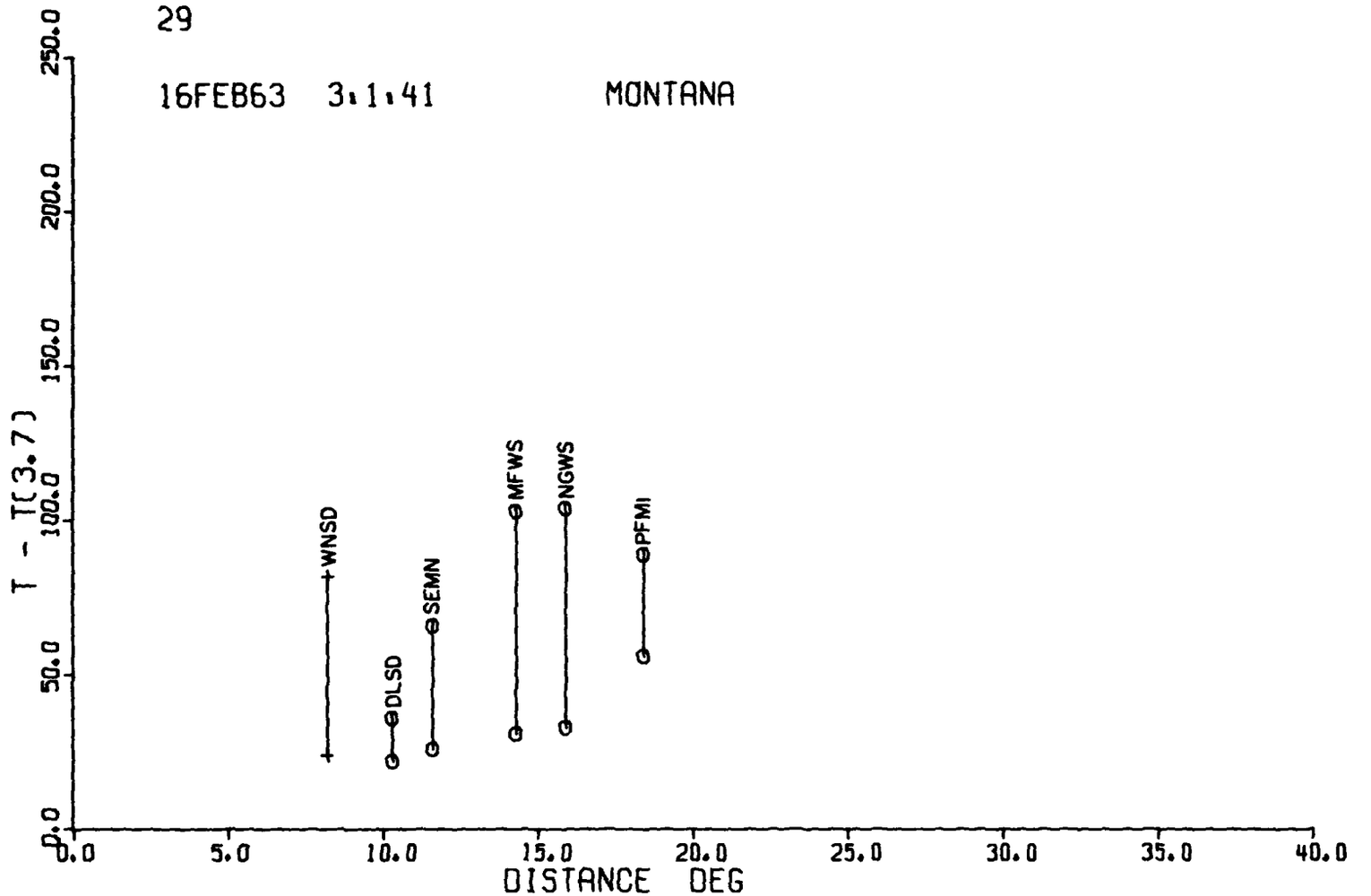
29
16FEB63 3:1:41
MONTANA
T - T(3.7)
250.0
200.0
150.0
100.0
50.0
0.0
WNSD
DLSD
SEMN
MFWS
NGWS
PFMI
0.0
5.0
10.0
15.0
20.0
25.0
30.0
35.0
40.0
DISTANCE DEG

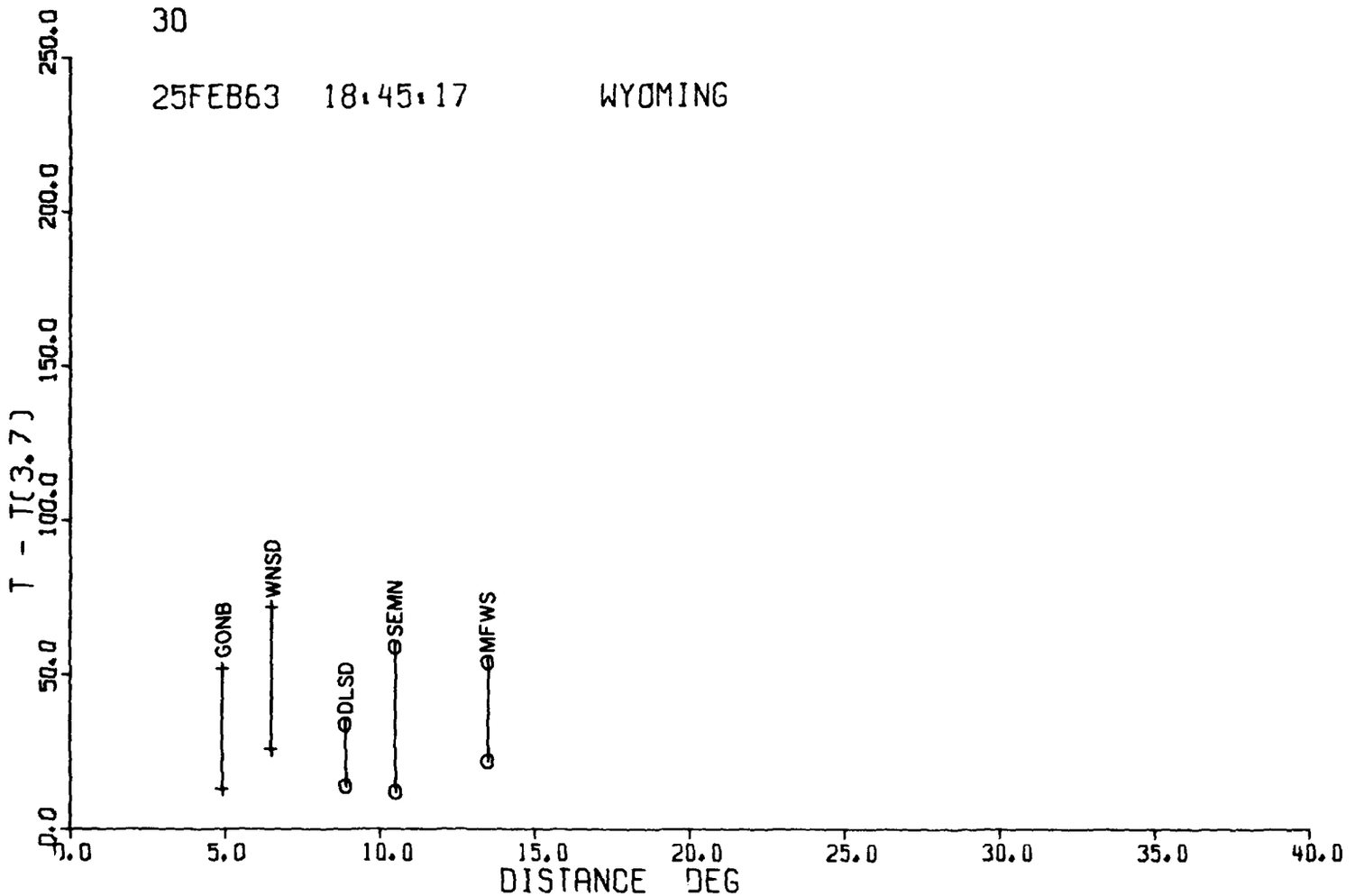
30
25FEB63 18:45:17 WYOMING
T - T[3.7]
250.0
200.0
150.0
100.0
50.0
0.0
GONB
WNSD
DLSD
SEMN
MFWS
0.0
5.0
10.0
15.0
20.0
25.0
30.0
35.0
40.0
DISTANCE DEG


DATE
ILME